MONO- AND MULTINUCLEAR PGM COMPLEXES CONTAINING THIOSEMICARBAZONES: SYNTHESIS, CHARACTERIZATION AND ANTIPLASMODIAL EVALUATION

Muneebah Adams

UNIVERSITY OF CAPE TOWN
2012

Mono- and multinuclear PGM complexes containing thiosemicarbazones: Synthesis, characterization and antiplasmodial evaluation

Muneebah Adams

Dissertation presented for the degree
Master of Science in Chemistry

University of Cape Town
Department of Chemistry

Supervisor: Dr. G. S. Smith
Co-supervisor: Prof. K. Chibale

August 2012

Declaration

I know the meaning of plagiarism and declare that all of the work in the dissertation "**Mono- and multinuclear PGM complexes containing thiosemicarbazones: Synthesis, characterization and antiplasmodial evaluation**", save for that which is properly acknowledged, is my own.

Ms Muneebah Adams	Date of signature

Acknowledgements

I would like to extend my thanks to my supervisors:
Dr G.S. Smith for his continued guidance and advice throughout the project, particularly during the write-up of this dissertation. Prof K. Chibale for the helpful advice on synthetic methods, as well as the biological studies.

I would also like to acknowledge the following people for their assistance during this project: Mr P. Roberts for recording all NMR spectra. Mr G. Benincasa for microanalytical analyses and mass spectral analyses, Dr M. Stander and Mr. F. Hiten (University of Stellenbosch) for mass spectral analyses and Dr H. Su for Single-crystal X-ray diffraction analyses. Prof P.J. Smith, Dr. C. de Kock and Mr D. Taylor (UCT Department of Clinical Pharmacology) for antiplasmodial screenings. Peter Malatji for assistance with cyclic voltammetry studies.

Special thanks go to my friends, Ms Ashleigh Maart, Ms Shakeela Sayed, Ms Shankari Nair, Ms. Saajidah Fakier, Ms Gaynor Manuel, Ms Heena Khot and Ms Gadijah Akleker for all their support. A heartfelt thanks to Tameryn Stringer and the rest the Organometallic Research group for proof reading my dissertation and their assistance in and out of the lab.

For funding, I thank the University of Cape Town and the National Research Foundation.

My greatest thanks go to my parents for their continued support throughout my tertiary education, for reading through drafts and sitting through mock presentations.

Abstract

Four aryl- and ferrocenyl-derived thiosemicarbazone ligands have been synthesized and characterized using NMR, infrared (IR) spectroscopy and mass spectrometry. These ligands were used towards the synthesis of three series of mono- and multinuclear complexes, in which the thiosemicarbazone ligands chelate in either a bidentate (*N,S*) or tridentate (*C,N,S*) mode.

The first series focuses on aryl-derived cyclopalladated thiosemicarbazone complexes. Two [C,N,S] tetranuclear complexes were prepared by reacting the thiosemicarbazone ligands with $K_2[PdCl_4]$/$Na_2[PdCl_4]$, and were used in subsequent reactions with P- and N-donor ligands. Three mononuclear complexes containing P-donor ligands, and one mononuclear and two binuclear complexes containing N-donor ligands were synthesized. These complexes were characterized using NMR and IR spectroscopies, and mass spectrometry. The complexes containing the P-donor ligands were synthesized more readily than those containing the N-donor ligands, where reactions occurred more sluggishly and required harsher conditions. Further to their spectroscopic and analytical characterization, molecular structures of two mononuclear cyclopalladated complexes, containing P-donor ligands, have been solved using single-crystal X-ray diffraction, and the palladium atoms were found to have slightly distorted square-planar geometries.

A second series based on *N,S*-chelated ferrocenylthiosemicarbazone ruthenium(II) complexes was also synthesized. Three ruthenium(II)-arene dimers (Ar = *p*-$^{i}PrC_6H_4CH_3$, $C_6H_5O(CH_2)_2OH$, C_6H_6) were reacted with ferrocenyl-derived thiosemicarbazones to prepare three binuclear and two tetranuclear ruthenium(II)-arene complexes. These complexes were characterized using NMR and IR spectroscopies, and mass spectrometry.

The third series centres around the synthesis of ferrocenyl-derived [N,S] palladium(II) complexes. This series proceeds via a binuclear chloro-bridged complex, prepared by reacting the monomeric ferrocenyl-derived thiosemicarbazone with $K_2[PdCl_4]$. Subsequent reactions were carried out using the binuclear chloro-bridged complex to prepare heterobimetallic complexes containing P-donor ligands. Two binuclear complexes, two tetranuclear complexes and one pentanuclear complex were synthesized and characterized using NMR and IR spectroscopies, and mass spectrometry. The molecular structure for the a binuclear complex,

containing the water-soluble P-donor ligand 1,3,5-triaza-7-phosphaadamantane, was solved using single-crystal X-ray diffraction.

Selected ligands and metal complexes were evaluated for antiplasmodial activity against *Plasmodium falciparum*. The ligands and complexes exhibited moderate inhibitory effects. In certain cases, an enhancement of activity was observed for the complexes relative to that of the free ligand.

List of abbreviations and symbols

%	Percent
˚C	Degree Celsius
br s	Broad signal (NMR)
$CDCl_3$	Deuterated chloroform
cm^{-1}	Reciprocal centimetres (IR)
COSY	Correlation Spectroscopy
CQR	Chloroquine-resistant
CQS	Chloroquine-sensitive
d	Doublet (NMR)
dd	Doublet of doublets (NMR)
Decomp.	Decomposition
DMSO-d_6	Deuterated dimethyl sulfoxide
dppf	1,1'-Bis(diphenylphosphino)ferrocene
EI	Electron impact
ESI	Electrospray ionisation
HSQC	Heteronuclear Single Quantum Coherence
Hz	Hertz (NMR)
IR	Infrared
J	Coupling constant (NMR)
Lit.	Literature
m	Multiplet (NMR); Medium intensity (IR)
MeOH	Methanol
MHz	Megahertz (NMR)
m.p.	Melting point
MS	Mass spectrometry

m/z	Mass to charge ratio (MS)
NMR	Nuclear Magnetic Resonance
PPh_3	Triphenylphosphine
ppm	Parts per million (NMR)
PTA	1,3,5-Triaza-7-phosphaadamantane
q	Quartet (NMR)
s	Singlet (NMR); Strong intensity (IR)
t	Triplet (NMR)
w	Weak intensity (IR)

Table of Contents

CHAPTER 1

The role of thiosemicarbazones and its metal complexes as biological agents.

1. Introduction

Malaria is one of the leading parasitic diseases in the world, and the second major infectious disease in Africa. It is estimated that in 2010, there were 216 million clinical cases, which led to nearly 655 000 deaths.[1] The disease affects mainly the tropical and subtropical regions, where Africa is the most affected with 81% of the cases, as illustrated in Fig. 1.1.

There are five species affecting humans, namely *Plasmodium falciparum*, *P. vivax*, *P. malariae*, *P. ovale* and *P. knowlesi*. However, *P. knowlesi* has only recently been affecting humans, as it is originally an ape strain. *P. falciparum* is the most prevalent and deadly species.[2] Therefore, a majority of drug discovery research is focused on the treatment of *P. falciparum*.

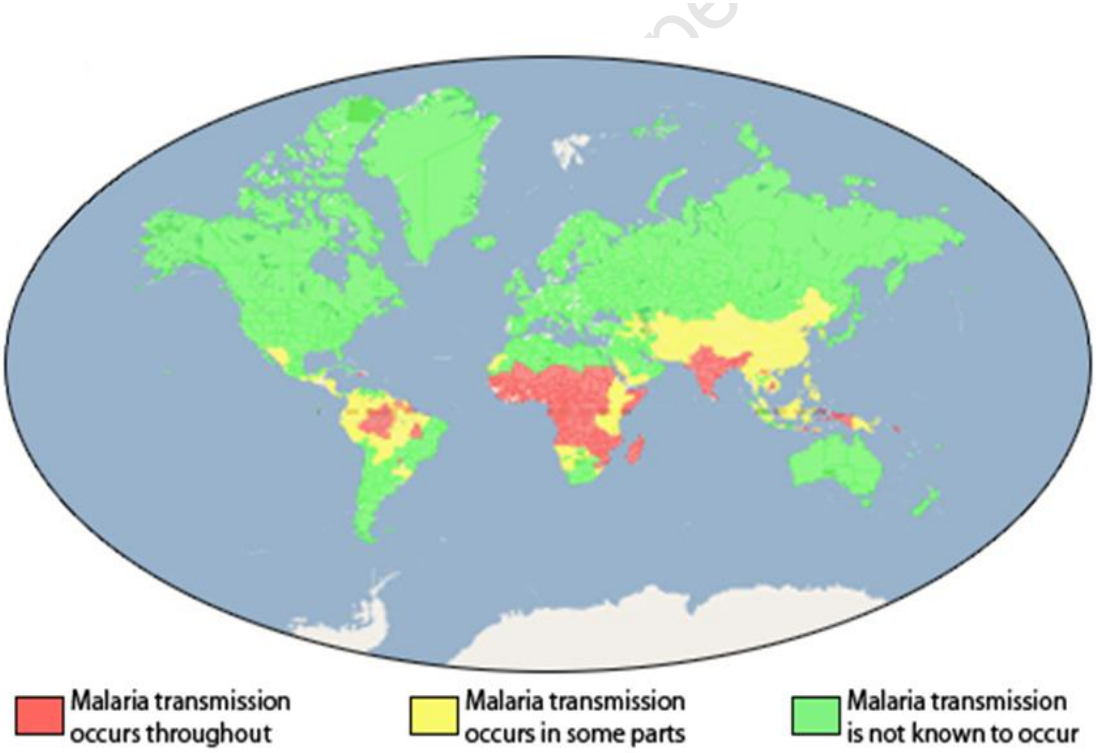

Figure 1.1: A world map illustrating the different regions affected by malaria.[3]

1.1. Defence mechanism of the malaria parasite

After infection, the red blood cell cytoplasm is ingested and transported to the digestive vacuole of the parasite (Fig. 1.2.a.). The haemoglobin is digested by cysteine proteases (falcipains 2 and 3),[4] metalloprotease falcilysin[5] and aspartic proteases plasmepsin (I-III, Fig.

1.2.b.),[6-7] to generate short peptides (Fig. 1.2.c.). After being transported out of the digestive vacuole (Fig. 1.2.d.), the peptides are converted to amino acids.[8] Upon the degradation of haemoglobin (Fig. 1.2.d.), free haem (Fe(III)PPIX) is released. The iron in the haem is then oxidised, from Fe(II) to Fe(III), by molecular dioxygen to produce reactive oxygen species, namely hydroxyl radicals (Fig. 1.2.f.). The hydroxyl radicals produced are known to be disruptive to lipid membranes; leading to the death of the parasites.[9] However, the parasite does have a defence mechanism to protect itself against the cytotoxicity of α-haematin. In an aqueous environment, haem dimerizes (Fig. 1.2.g.) and is transported to a lipid body (Fig. 1.2.h.) where biomineralization (haemozoin formation) occurs (Fig. 1.2. i-l).

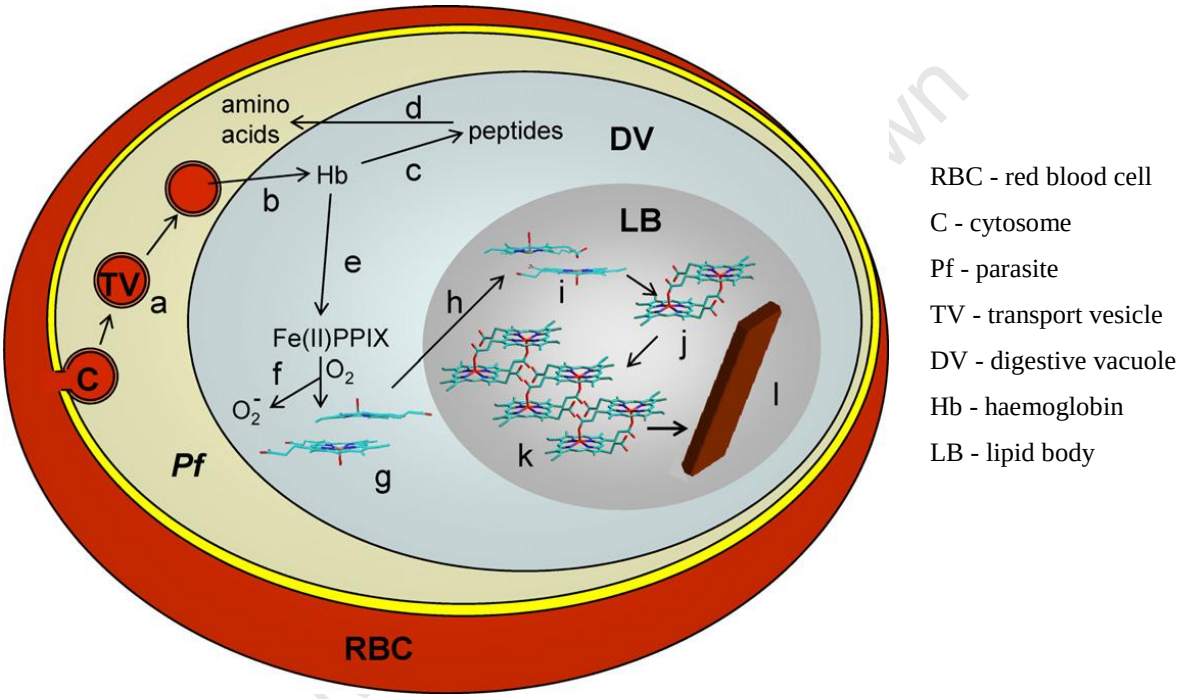

Figure 1.2: The proposed sequence of events which leads to the formation of haemozoin.[10]

Alpha-haematin dimers, linked via hydrogen bonds between the iron in the haem and the propionic acid side chain of the adjacent haem, are able to form chains. The chains, which exist due to the hydrogen bonded propionic acid side chains, form low solubility haemozoin crystals which accumulate in the food vacuole.[10]

Therefore, a number of antimalarial drug candidates are designed with the intent of either inhibiting the above mentioned proteases or preventing the conversion of α-haematin to haemozoin (or β-haematin).

1.2. Drugs administered for the treatment of malaria

1.2.1. The use of quinoline-based compounds as antimalarial agents

Antimalarial drugs synthesized with a quinoline base became a popular choice with the success of quinine, **I** (Fig. 1.3). Quinine has a variety of medical uses, including anti-inflammatory effects, and it was the first effective antimalarial treatment. The use of quinine as an antimalarial treatment originated in the 17th century and was used up until the 1940's.[11]

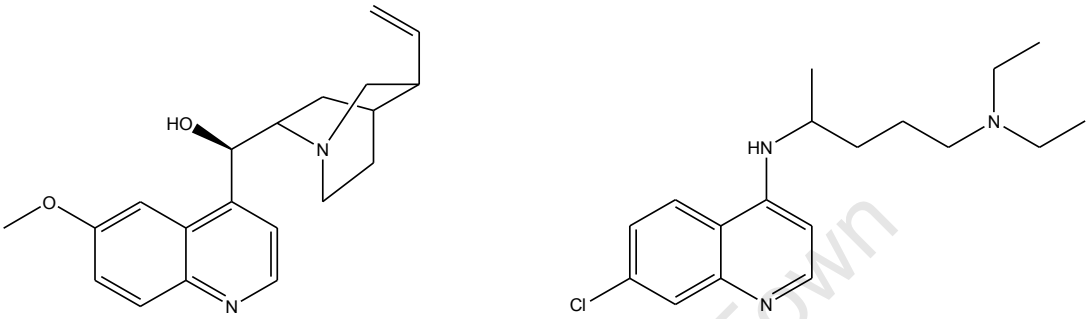

I **II**

Figure 1.3: The antimalarial compounds quinine (**I**) and chloroquine (**II**).[11-12]

Chloroquine, **II** (Fig. 1.3), was one of the most widely used antimalarial drugs, due to its low cost. Studies have shown that the mode of action of chloroquine involves binding to the α-haematin through π - π complexation in an attempt to inhibit the parasites' defence mechanism by slowing the rate of conversion to haemozoin.[12] An accumulation of α-haematin leads to parasite cell death. However, as chloroquine-resistance increases, quinine is being reintroduced.[12]

With the development of resistance to chloroquine, drugs such as mefloquine (**III**) and piperaquine (**IV**, Fig. 1.4) were developed for areas affected by chloroquine-resistant strains. The mode of action of mefloquine is not known but it is believed to play a role in the transport of the parasites' nutrient source to the food vacuole.[13] When piperaquine is used in conjunction with chloroquine, it is believed that the bulky structure of piperaquine may act by preventing an efflux of chloroquine out of the digestive vacuole, by blocking the membrane transporters. However, the drugs started losing effectiveness as the parasite developed resistance.[14-17]

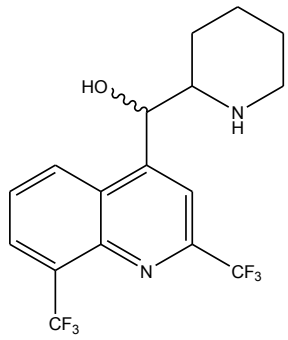

III

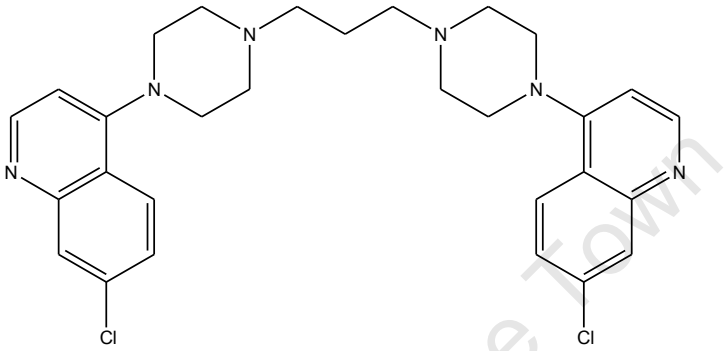

IV

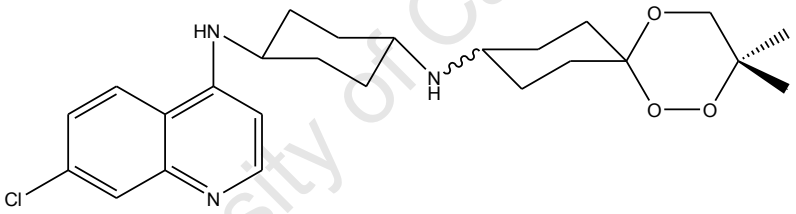

V

Figure 1.4: The antimalarial compounds mefloquine (**III**), piperaquine (**IV**) and trioxaquine (**V**).[13-14,18]

This has led to the synthesis of compounds such as trioxaquine (PA1103/SAR116242), **V** (Fig. 1.4) by Cosledan *et al.*, which has a dual mode of action.[18] The compound contains a 1,2,4-trioxane motif, along with the attached cyclohexyl ring, is required for haem alkylation.[18] The 7-chloro-4-aminoquinoline base allows for haem stacking, which prevents haemozoin formation while the stability of the compound is enhanced by the linker cyclohexyl ring. Trioxaquine exhibited the best activity against D6 (CQS) and FcM29 (CQR) malaria strains *in vitro* with IC_{50} values of 7 nM and 10 nM respectively.[18] *In vivo* studies carried out on mice infected with rodent strains *P. vinckei petteri* (CQS strain) and *P. vinckei vinckei* (CQR strain) demonstrated that the antimalarial activity was similar. Therefore, due to the high antimalarial activity of compound **V**, as well as the low toxicity of the compound, trioxaquine was entered into clinical trials.[18]

1.2.2. The use of artemisinin-derivatives, antifolates and cysteine protease inhibitors as antimalarial agents

There have been successful antimalarial drugs which do not contain a quinoline base. Artemisinin, **VI**, (Fig. 1.5) is an antimalarial drug used against chloroquine-resistant strains of *P. falciparum*. The drug has a 1,2,4-trioxane core that contains a peroxide bond whose cleavage is required for the compounds' activity.[19]

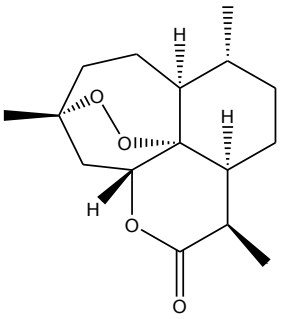

VI

Figure 1.5: The antimalarial drug artemisinin (**VI**).[19]

Artemisinin exhibits antimalarial activity against chloroquine-sensitive (D10) and chloroquine-resistant K1 strains, with IC_{50} values 0.013 µM and 0.011 µM respectively. These IC_{50} values are lower than those observed for chloroquine at 0.03 µM and 0.66 µM for D10 and K1 respectively.[20] However, in an attempt to slow down the emergence of resistance artemisinin-based combination therapies (ACTs) were developed.

ACTs, in which two antimalarial drugs are used in combination to overcome drug resistance, are being used worldwide to combat resistant strains. One such combination is marketed as Coartem™, artemether/lumefantrine (Fig. 1.6), where artemisinin derivatives are fast acting drugs with a short half-life (artemether (**VII**), $t_{1/2}$ = ~ 4hr), which kills off parasitaemia very quickly.[21] These fast acting drugs are used in combination with a drug which has a longer half-life. Lumefantrine (**VIII**), has a half-life of approximately 4.5 days, and thus remains in the body long after artemether, to remove any remaining parasites.[22-23]

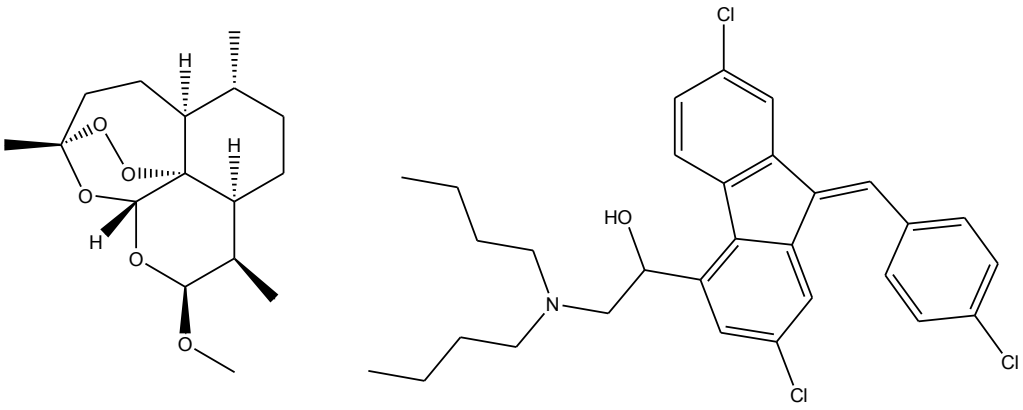

VII **VIII**

Figure 1.6: The artemether (**VII**) and lumefantrine (**VIII**) ACT, Coartem™.[21]

Another target for antimalarial agents is the folic acid cycle. The folic acid cycle involves the transfer of one-carbon units during the synthesis of DNA components such as amino acids, nucleotides and other biomolecules. Therefore antifolates inhibit enzymes, such as dihydrofolate reductase (DHFR) and dihydropteroate synthase (DHPS), which are involved in parasite folate biosynthesis.[24]

Proguanil, **IX** (Fig. 1.7) an antifolate discovered in 1945, functions as a prodrug (i.e. a drug administered in its inactive form which activates upon metabolism) with its active form being chlorcycloguanil (**X**). Chlorcycloguanil, an inhibitor of DHFR, attracted attention after exhibiting better activity against avian malaria than quinine.[25-26] Due to the activity exhibited by chlorcycloguanil, prodrug derivatives such as chlorproguanil (**XI**), clociguanil (**XII**) and the dihydrotriazine BRL 6231 (**XIII**), were synthesized. An increase in activity has been observed upon chlorination of the aryl group or an increase in the length of the linker chain.[27]

However, the most widely used antimalarial antifolate would be pyrimethamine (**XIV**), which is used in combination with sulfadoxine (**XV**).[28] Pyrimethamine, inhibits DHFR whereas sulfadoxine inhibits DHPS. However, as mutations in DHFR and DHPS genes develop, antifolates start to lose their efficacy.[29-30]

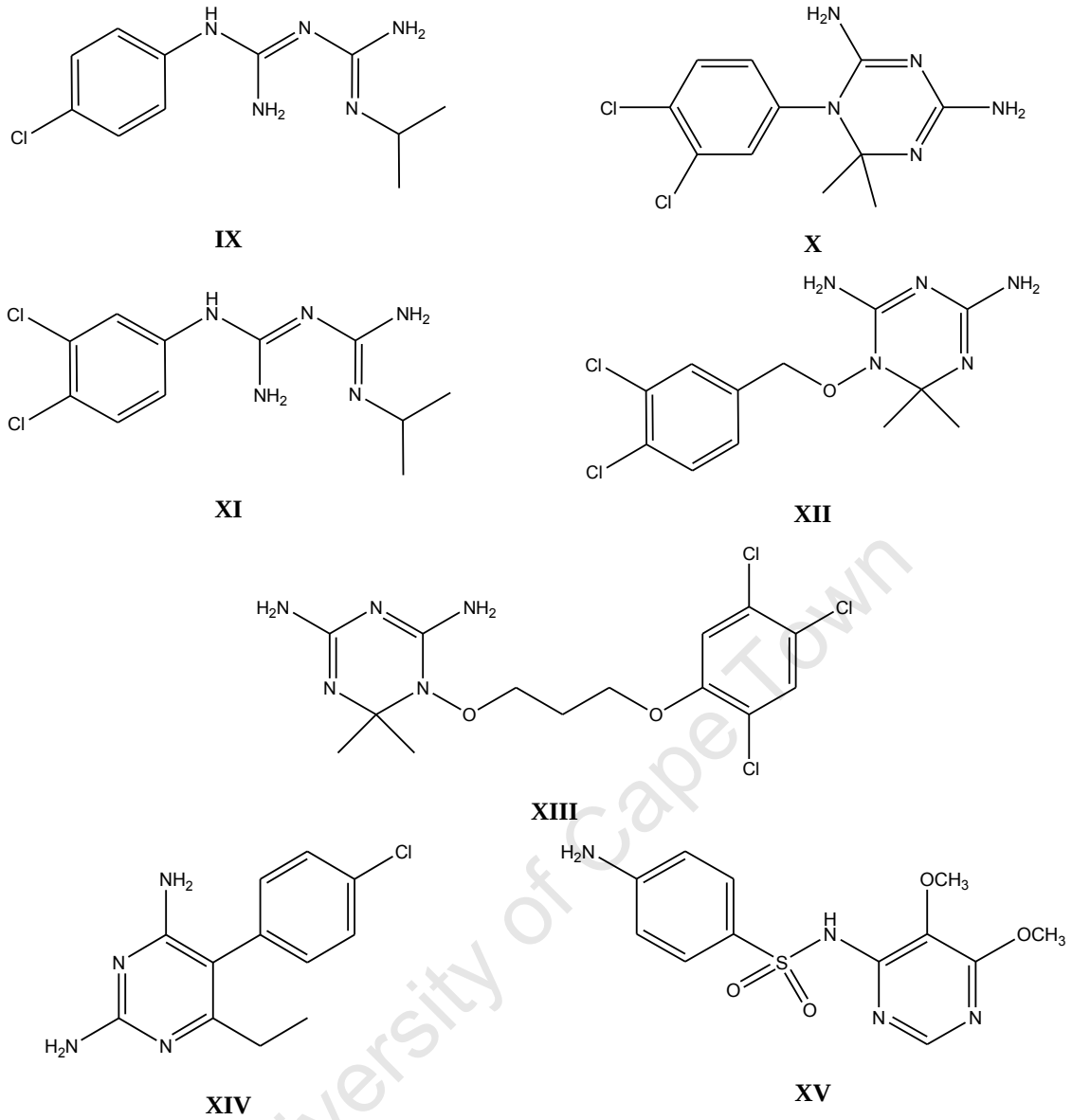

Figure 1.7: The antimalarial compounds proguanil (**IX**), chlorcycloguanil (**X**), chlorproguanil (**XI**), clociguanil (**XII**), BRL 6231 (**XIII**), pyrimethamine (**XIV**) and sulfadoxine (**XV**).[25-27]

As previously mentioned, cysteine proteases play a role in the degradation of haemoglobin.[31] Inhibition of these proteases has also been a target of interest.[31] Peptide structures such as fluoromethyl ketones (**XVI**) and vinyl sulfones (**XVII**), as well as nonpeptide structures such as isoquinolines (**XVIII**) and chalcones (**XVIX**) have been tested as protease inhibitors (Fig. 1.8).[31-35] The fluoromethyl ketone, *Z*-Phe-Arg-CH_2F, and the vinyl sulfone, Mu-Phe-homoPhe-VSPh, exhibited good activity when tested against the cysteine protease FP-2. The fluoromethyl ketone exhibited activity with values of IC_{50} values of 0.36 nM and 64 nM against FP-2 and cultured malaria parasites respectively.[32] The vinyl sulfone was active against the *P. falciparum* and *vinckei* FP-2 cysteine proteases with IC_{50} values of 0.08 μM and 0.1 μM respectively.[33]

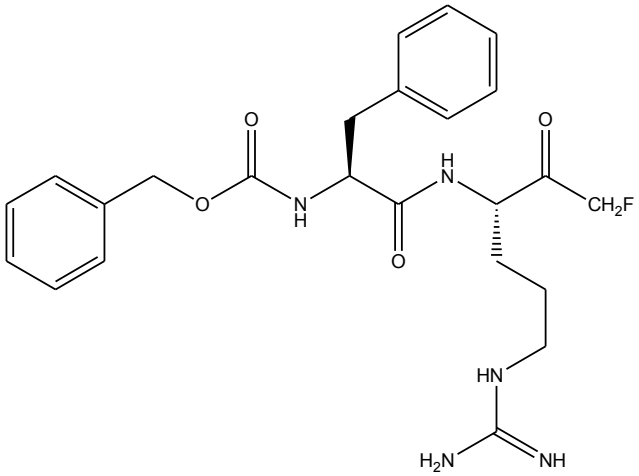

XVI

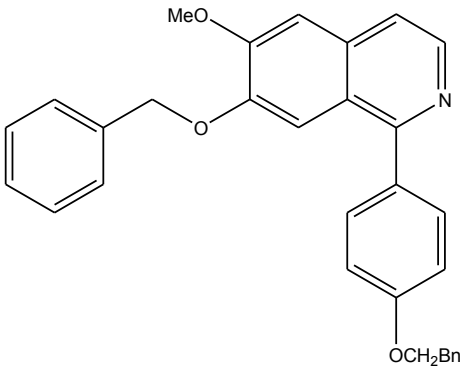

XVII

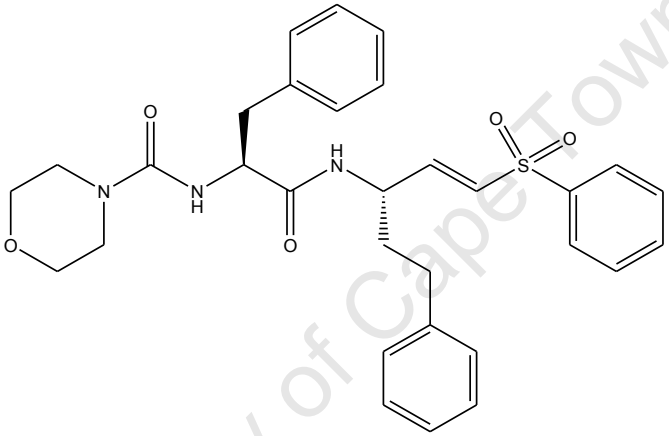

XVIII

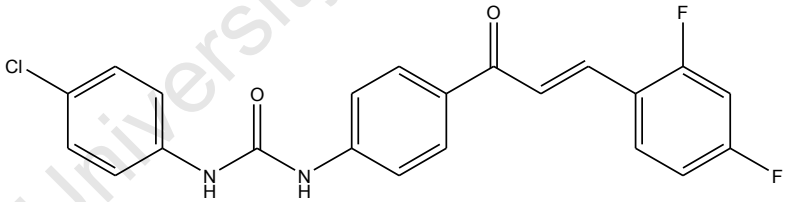

XVIX

Figure 1.8: Cysteine protease inhibitors fluoromethyl ketone (**XVI**, *Z*-Phe-Arg-CH_2F); isoquinolines (**XVII**); vinyl sulfones (**XVIII**, Mu-Phe-homoPhe-VSPh); calchones (**XVIX**).[32-35]

Biological agents containing particular moieties such as quinoline or trioxane still exhibit activity against the malaria parasite. Thus new derivatives are still being synthesized around these structures.[9,18,36-37]

1.3. Thiosemicarbazones

Thiosemicarbazones are used as biological agents and for the detection of various metal ions using spectrophotometric methods.[38-45]

Thiosemicarbazones are Schiff base compounds, which are formed by the condensation reaction occurring between a carbonyl and an amine group. Therefore, the thiosemicarbazone compounds in this project (Fig 1.9) were synthesized by reacting an aldehyde, or ketone, with thiosemicarbazide.

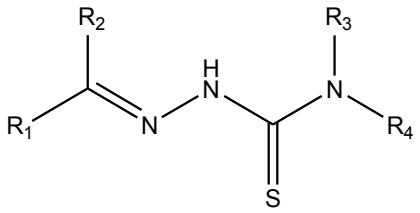

R_1, R_2, R_3, R_4 = H, alkyl, aryl or heteroaromatic group

Figure 1.9: The general structure of a thiosemicarbazone compound

Thiosemicarbazone systems contain donor atoms such as nitrogen, sulfur and oxygen which allow for chelation to various metals depending on the softness [Pd(II), Pt(II)] or hardness [Fe(III), Mg(II)] of the metal.[46]

Pharmacological properties such as antitumoral,[38-39,47-48] antibacterial,[49] antiviral[50-51] and antiparasitic[38,40,52-54] have been displayed by thiosemicarbazones. In most cases, it is believed that these compounds act through the entrapment of metal ions essential for cell function, or through the inhibition of enzymes.[55,56]

1.3.1. The application of thiosemicarbazones as biological agents

There has been significant interest in the use of thiosemicarbazones as antimalarial drug candidates, and thus various research projects have been pursued.[52-54] In a study by Greenbaum *et al.*, a series of thiosemicarbazone derivatives, which contained aromatic rings onto which various substituents were incorporated, were tested against the W2 (CQR) strain.[52] The compounds which were prepared by reacting 2-acetylpyridine or 2,6-diacetylpyridine with a thiosemicarbazide, with either a NH_2 or SMe group attached to the thione carbon, were most active. Compound **XX** (Fig. 1.10) is one of the compounds which yielded promising results. It is believed that these compounds act through chelation of endogenous iron.[52]

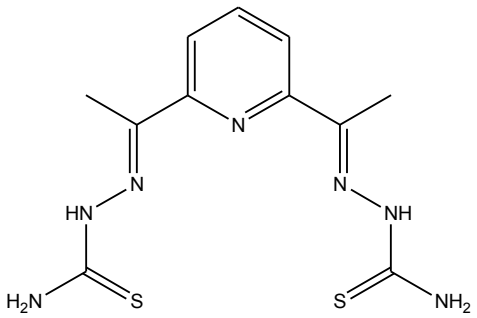

XX

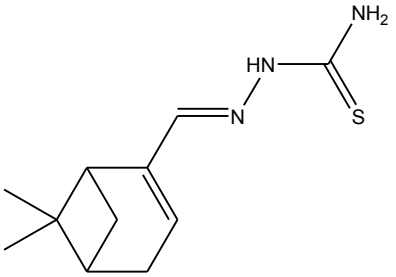

XXI

Figure 1.10: Thiosemicarbazone derivatives as potential antimalarial agents (**XX** and **XXI**).[52,53]

In a separate study by de Oliveira *et al.*, thiosemicarbazones were synthesized using naturally occurring aldehydes and ketones.[53] Compound **XXI** (Fig. 1.10), which was synthesized from 6,6-dimethylnorpin-2-ene-2-carboxaldehyde, exhibited the lowest IC_{50} value (7.2 μM) against the W2 (CQR) strain.[53]

Phenolic Mannich bases of benzaldehyde and thiosemicarbazone derivatives were synthesized by Chipeleme *et al.* as a potential inhibitors of the cysteine protease falcipain-2, and tested against a chloroquine-resistant strain of *P. falciparum*.[54] Of the thiosemicarbazone-containing Mannich base compounds, compound **XXII** (Fig. 1.11) showed the best overall inhibition of falcipain-2 (IC_{50} value = 2.25 μM) and antiplasmodial activity against W2 (IC_{50} value = 3.75 μM).[54] The presence of the quinoline suggests that the activity is related to haem-binding, and the ability of the compound to chelate to iron in the cell.[54]

Chiyanzu *et al*. have also investigated potential cysteine protease inhibitors in the form of thiosemicarbazone derivative of isatins.[56] The compounds were evaluated against three parasitic cysteine proteases cruzain, falcipain-2 and rhodesain. The thiosemicarbazone containing compound **XXIII** (Fig. 1.11) exhibited good activity (IC_{50} = 10.5, 9.4 and 3 μM respectively) against all three proteases.[56]

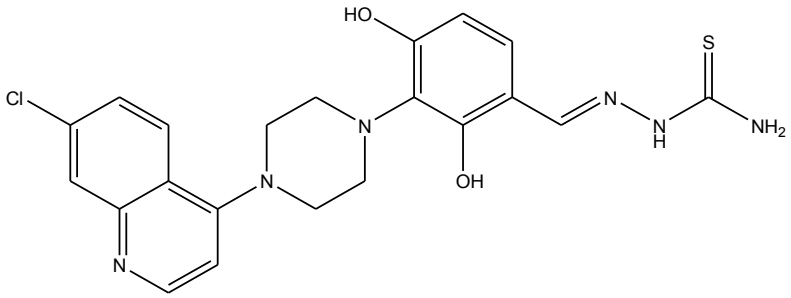

XXII

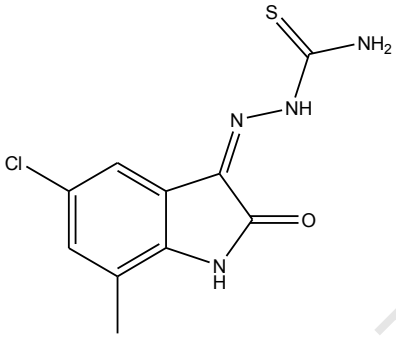

XXIII

Figure 1.11: Thiosemicarbazone-containing compounds which exhibits inhibitory activity against the cysteine protease falcipain-2 (**XXII, XXIII**).[54,56]

The first reported success of thiosemicarbazones having antitumour activity dates back to 1956 with the synthesis of pyridine-2-carboxaldehyde thiosemicarbazone, **XXIV** (Fig. 1.12), by Brockman *et al.*[47] This compound was tested *in vivo* on mice infected with L1210 leukaemia, where it exhibited anti-leukemic properties, by means of prolonging the lifespan of the mice.[47]

Due to the activity observed for pyridine-2-carboxaldehyde thiosemicarbazone, various α-*N*-heterocyclic thiosemicarbazone derivatives with a *N,N,S*-chelating nature (**XXV** and **XXVI**) were synthesized and studied (Fig. 1.12). These compounds were shown to be active antineoplastic agents.[48,55,58-59]

Triapine, **XXVII** (Fig. 1.12), is one of the α-*N*-heterocyclic thiosemicarbazone derivatives which exhibited the most potent activity, and is currently undergoing phase II clinical trials.[60-62] Triapine exhibited activity against hydroxyurea-resistant leukaemia cell, human KB nasopharyngeal carcinoma, murine M109 lung carcinoma and human A2780 ovarian carcinoma xenografts in mice.[63]

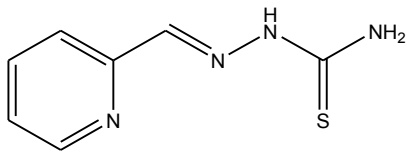

XXIV

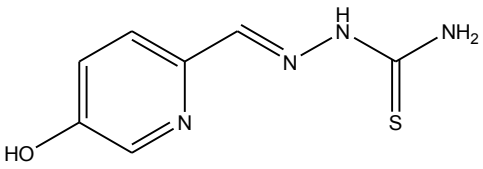

XXV

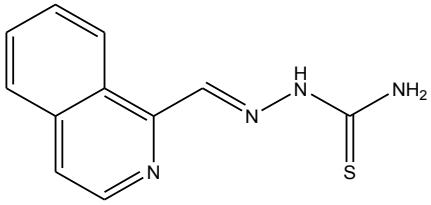

XXVI

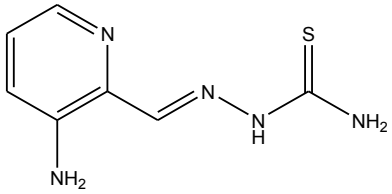

XXVII

Figure 1.12: The α-*N*-heterocyclic thiosemicarbazone derivatives pyridine-2-carboxaldehyde thiosemicarbazone (**XXIV**), 5-hydroxypyridine-2-carboxaldehyde thiosemicarbazone (**XXV**), isoquinoline-1-carboxaldehyde thiosemicarbazone (**XXVI**) and Triapine (**XXVII**).[47,58-60]

Various studies into the mode of action of these α-*N*-heterocyclic thiosemicarbazones revealed that ribonucleotide reductase (RNR) was the target of these compounds.[64-65] The iron required to maintain the tyrosyl radical of the RNR as well as intracellular iron is bonded, which leads to inhibition of DNA synthesis.[55,66-67]

1.4. The application of metals in the medical field

Throughout history, metals have been recognized for their medicinal properties. However, the role of metals as medicinal agents became more prominent as researchers began to understand how biological systems worked, and how metals fit into these systems. A variety of gold salts, such as [$KAu(CN)_2$] (tuberculosis)[68] and gold phosphine (rheumatoid arthritis),[69] antimony compounds (leishmaniasis)[21] and lanthanum carbonate (end stage renal disease)[21] have been used in the medical field.

Interest in transition metal complexes as biological agents began with the use of cisplatin [*cis*-diamminedichloridoplatinum(II)], **XXVIII** (Fig. 1.13). Cisplatin, is a drug whose anti-cancer activity was only discovered in 1969 by Rosenberg, despite initially being synthesized by Michele Peyrone in 1844.[70-71]

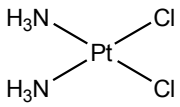

XXVIII

Figure 1.13: The structure of the platinum complex cisplatin (**XXVIII**).[71]

1.4.1. The use of transition metal complexes as antimalarial agents

The use of metal complexes as antimalarial agents has become prevalent in research. A trend is observed whereby upon complexation, an enhancement of activity is generally observed.[72-74] A large number of research projects attempt to use known antimalarial drugs, which are losing their effectiveness, and complex them with various metals to determine if there is an enhancement of activity.[75-78] Therefore, complexation of chloroquine has been of significant interest in various research projects, where the metal coordinates to either the quinoline nitrogen or the amine nitrogen.

One of the first organometallic complex evaluated as an antimalarial agent was RhCl(COD)CQ (**XXIX**) which was synthesized by Sánchez-Delgado *et al*. (Fig. 1.14).[79, 80] In addition to the rhodium complex, a binuclear ruthenium(II)-chloroquine complex (**XXXI**) was also synthesized by Sánchez-Delgado and co-workers (Fig 1.14).[79] In the case of the rhodium complex, the chloroquine binds to the metal via the quinoline nitrogen, whilst in **XXXI**, the ruthenium is coordinated to both chloroquines, through the quinoline N of one chloroquine molecule and the diethylamine N of the other, to form a dimer.[79]

Compounds **XXIX** and **XXXI** exhibited *in vitro* and *in vivo* activity against the rodent strain *P. berghei*. However, compound **XXXI** exhibited better activity than **XXIX**, as well as chloroquine diphosphate, with IC_{50} = 18 ± 7 nM (*in vitro*) and a 94 % reduction of parasitaemia (*in vivo*). Therefore, **XXXI** was also evaluated against two chloroquine-resistant strains FcB1 and FcB2 (IC_{50} = 10.5 ± 6.5 and 46.5 ± 9.0 nM respectively).[79] The structure and basicity of the complex, as well as the presence of the Ru(II), contributed to the enhanced activity of the complex.[79]

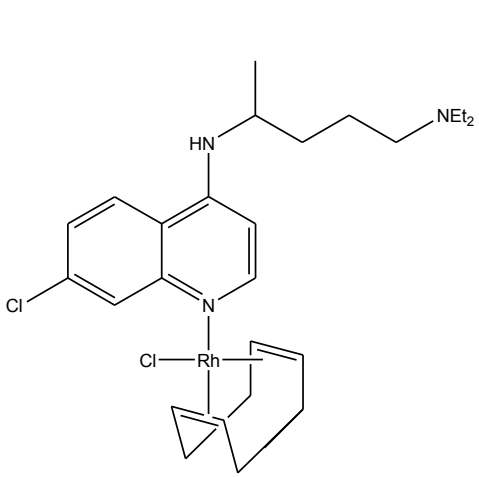

XXIX

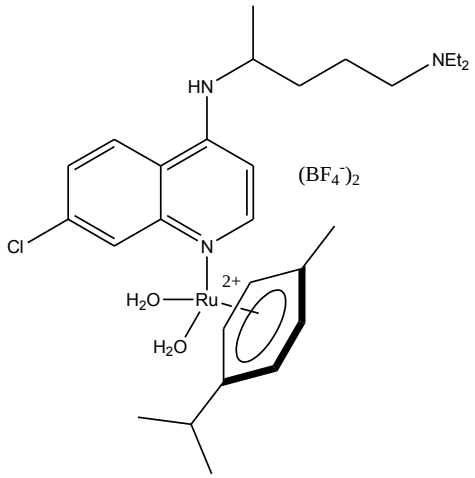

XXX

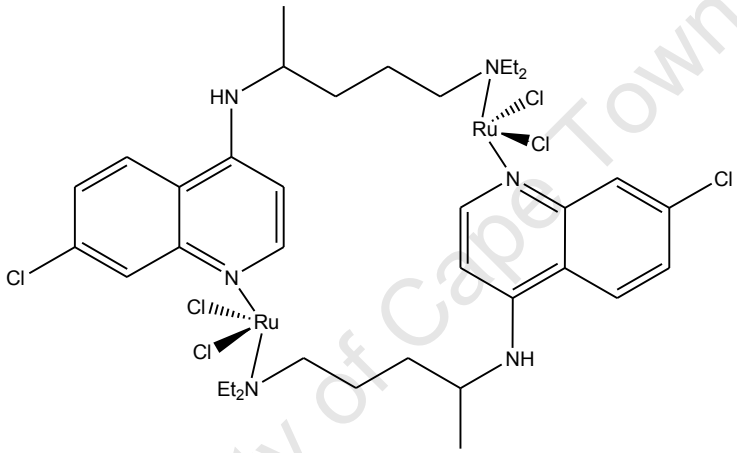

XXXI

Figure 1.14: The mononuclear rhodium complex RhCl(COD)CQ (**XXIX**), the mononuclear ruthenium complex $[Ru(\eta^6\text{-p-cymene})(CQ)(H_2O)_2][BF_4]_2$ (**XXX)** and the binuclear binuclear $[Ru(CQ)Cl_2]_2$ (**XXXI**).[79,81]

Due to the low toxicity exhibited by ruthenium complexes, further research has gone into the synthesis of ruthenium-chloroquine complexes.[81,82] The arene ring is present in order to stabilize the metal, as well as possibly altering the lipophilicity of chloroquine, thus retaining the complex within the active site. The ruthenium(II)-complexes were tested *in vitro*, and showed significant activity against the resistant strains, with compound **XXX** (Fig. 1.14) showing the highest activity.[81] Compound **XXX** exhibited IC_{50} values (234 nM for Dd2) which were significantly lower than CQDP (1184 nM for Dd2).[81]

In a study conducted by Ajibade *et al.*, the Mn(II), Co(II), Pt(II) and Cu(II) ions were coordinated to pyridyl derivatives, such as chloroquine, to yield various complexes.[75] Platinum was complexed to chloroquine, compound **XXXII** (Fig. 1.15), in an attempt to use chloroquine as an antimalarial agent against the K1 (CQR) strain.[75] Inhibition studies of the

complexes synthesized showed cytotoxic activity against the chloroquine-resistant strain, where the Mn(II) and Pt(II) complexes showed the most enhanced activity with IC_{50} values 1.13 and 0.16 μM respectively.[75]

Due to the medicinal purposes of gold, Au(III)-chloroquine complexes were synthesized by Navarro *et al.* and their antiplasmodial activity was evaluated (Fig. 1.15).[76] With the coordination of Au(III) to chloroquine, there is a change in the electronic properties of the 7-chloro-4-aminoquinoline base. The complex $[Au(PPh_3)(CQ)]PF_6$, **XXXIII**, showed good activity against *P. falciparum* chloroquine-resistant strains FcB1 and FcB2, with IC_{50} values of 5 nM and 23 nM respectively,[76] which was significantly lower than CQDP (47 ± 2.3 nM for FcB1[79] and 104.5 ± 9.2 nM for FcB2[79]).

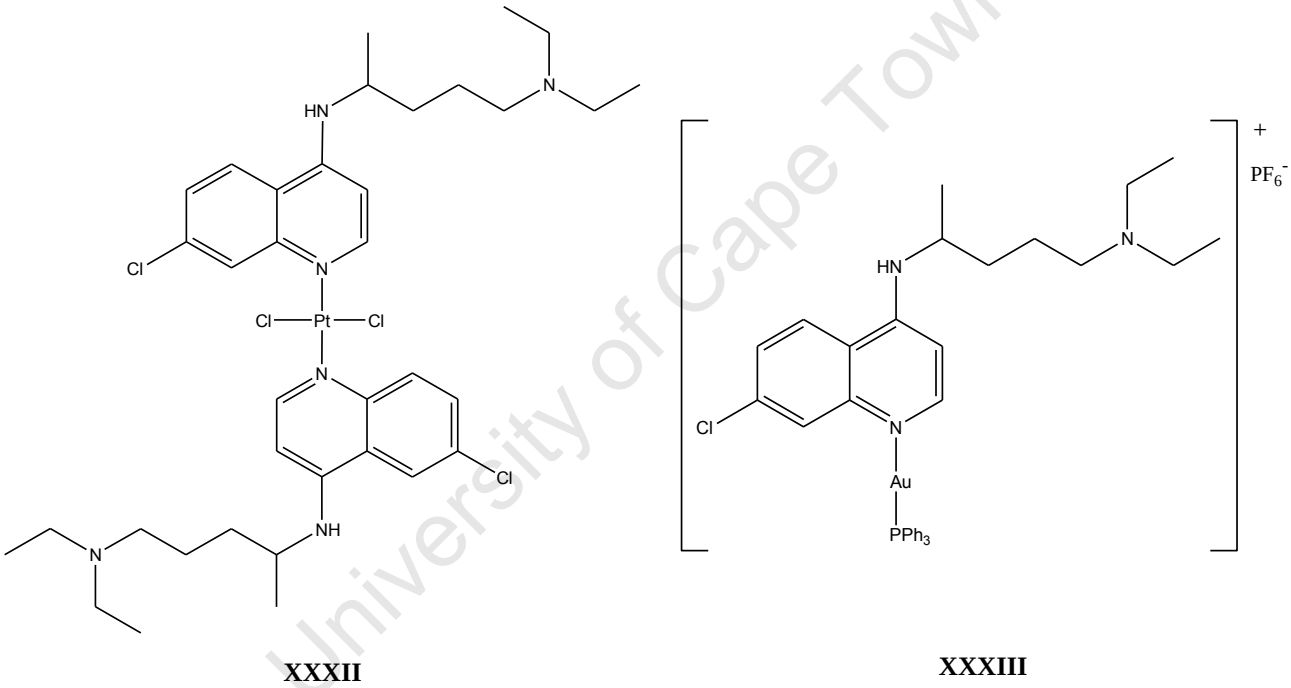

Figure 1.15: The proposed structure of $Pt(CQ)_2Cl_2$ (**XXXII**) and $[Au(PPh_3)(CQ)]PF_6$ (**XXXIII**).[75,76]

Due to the activity displayed by compound **XXXIII**, various derivatives of these Au(III)-chloroquine complexes were synthesized. $[Au(PEt_3)(CQ)]PF_6$ showed the highest activity against the chloroquine-resistant strain FcB1 with an IC_{50} value of 10 nM when compared to the activity of chloroquine diphosphate (IC_{50} = 50 nM).[83]

Ferroquine, **XXXIV** (Fig. 1.16), an aminoquinoline derivative with a ferrocenyl moiety incorporated into the side chain, has not only shown higher activity against *P. falciparum*

than chloroquine, but has also displayed activity against chloroquine-resistant strains.[84] Ferroquine and its derivatives are currently in clinical trials.[9]

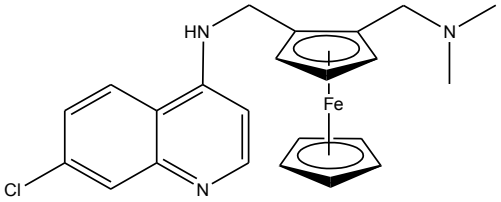

XXXIV

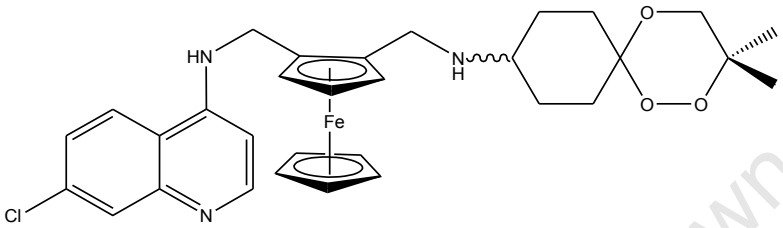

XXXV

Figure 1.16: The antimalarial compounds ferroquine (**XXXIV**) and trioxaferroquine (**XXXV**).[37,77]

Trioxaferroquine, which contain a 1,2,4-trioxane motif, a ferrocenyl moiety and 7-chloro-4-aminoquinoline, were synthesized by Bellot *et al*.[37] The trioxaferroquines and trioxaferrocenes, compounds which lack the 7-chloro-4-aminoquinoline, were tested against the chloroquine-resistant *P. falciparum* strains FcB1 and FcM29.[37] All the trioxaferroquines displayed activity similar to that of artemisinin and ferroquine, whilst they were more active than chloroquine. The activity of the trioxaferroquines was significantly higher than the trioxaferrocenes, which suggests that in this instance the quinoline is required for activity. Compound **XXXV** (Fig. 1.16), showed the highest activity with IC_{50} values 20 nM and 17 nM against the strains FcB1 and FcM29 respectively.[37]

Research into transition metal complexes as antimalarial agents is scarce. However, aside from quinoline-based complexes, the search for thiosemicarbazone complexes as antimalarial agents is still prevalent in research.[38,40-41]

1.5. Transition metal complexes prepared from thiosemicarbazones

1.5.1. Complexation of thiosemicarbazone ligands

The interest in thiosemicarbazone complexes originates from the enhanced activity exhibited by the complexes when compared to their free ligand.[44,85]

With the discovery of cisplatin and its activity, research into platinum(II)-based complexes became a regular occurrence. However, as toxicity problems became associated with platinum(II)-based complexes, research was directed at the use of other metals.[86] Platinum and palladium ions resemble each other in a given oxidation state, and thus palladium complexes were synthesized to determine if they were biologically active. Palladium can exist in the oxidation states Pd(0), Pd(II) and Pd(IV). However, the Pd(II) state is more stable and would provide a suitable comparison.[87]

Ruthenium is able to access the oxidation state Ru(II), Ru(III) and Ru(IV) under physiological conditions. Ruthenium(II) complexes are generally more biologically active and lower in toxicity due to their ability to mimic iron. Iron(II) is able to bind to biological molecules and be excreted. Thus, ruthenium is able to reduce its concentration in the body in a similar manner as Fe(II), and is less toxic.[88] Ruthenium(II) ions can also be oxidised in a similar manner to Fe(II), allowing for electron transfer, and generation of reactive oxygen species.

Coordination modes

Thiosemicarbazones act as ligands by chelating to an electron-deficient metal. They can act as either bidentate[85,89] or tridentate ligands (Fig. 1.17).[38-40] Bidentate ligands chelate to a metal in a [N,S] fashion,[85,89] whilst tridentate ligands may chelate in a [N,N,S],[90] [O,N,S][38-39] or [C,N,S][40] mode.

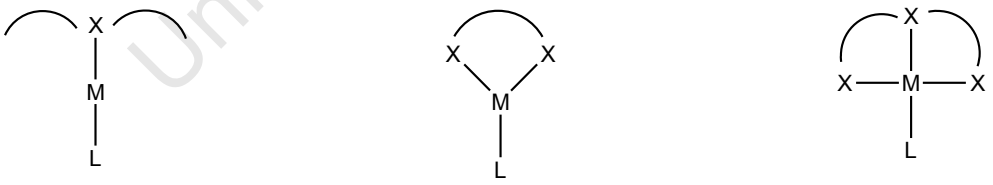

Figure 1.17: Illustration of a) monodentate, b) bidentate and c) tridentate chelation.

Thiosemicarbazone complexes containing metals such as mercury,[91] cobalt,[92] cadmium,[91] gold,[41,93] palladium[38-40] and platinum[38,91-92,94] to name a few, have been synthesized.

Cyclopalladation

Bidentate ligands can form a single palladacycle whilst the tridentate *C,N,S*-chelating ligand may result in the formation of two rings. The palladacycles formed using tridentate ligands

may involve two 5-membered rings[38-40] (Fig. 1.18) or it may involve a 5- and 6-membered ring.[95]

The palladacycle forms when the tridentate ligand chelates via the imine nitrogen, the thiolate sulfur and the carbon of the aryl or alkyl group, to the metal (Fig. 1.18). Palladium(II) ions are soft metals, and thus react easily with soft bases such as the imine nitrogen and the thione sulfur, in the ligand. Palladium(II) ions have a d^8 configuration, and thus a square planar geometry is expected.[96] The idea of a square planar geometry around the Pd(II) centre is supported by the rigid structure of the palladacycles. It is believed that for the *C,N,S*-chelating ligand, the complex is stabilized due to the aromatic nature of the palladacycles (C=N, C=C and the filled d-orbitals of Pd).[97]

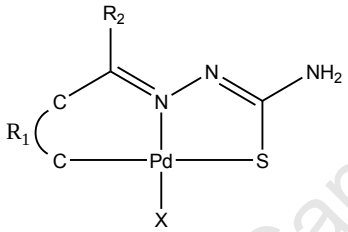

R_1 = aryl or alkyl group
R_2 = alkyl group

Figure 1.18: The general structure of palladacycles.

The chelation of the aryl group to the metal to form palladacycles occurs via various mechanisms including oxidative addition, transmetallation, alkoxy- and carbopalladation of alkenes, halopalladation of alkynes and C-H bond activation.[98] C-H bond activation occurs when a C-H bond is cleaved through electrophilic attack of Pd(II) ion to form a Pd-C bond between the palladium ion and the *ortho*-carbon on the aryl group. The palladium source is usually found in the form of salts such as palladium(II) chloride with a base, palladium(II) acetate in acetic acid or potassium tetrachloropalladate/sodium tetrachloropalladate.[99]

1.5.2. The use of thiosemicarbazone-based complexes as antimalarial agents

Some of the first thiosemicarbazone complexes evaluated as antimalarials were synthesized in the 1980's. Scovill and co-workers prepared Cu(II), Ni(II), Fe(II) and Mn(II) complexes with 2-acetylpyridine thio- and selenosemicarbazones.[100] The Cu(II), Ni(II) and Fe(II) complexes prepared using 2-acetylpyridine thiosemicarbazone ligands were evaluated *in vivo* against *P. berghei* in mice. The thiosemicarbazone ligands exhibited activity at dosage levels of 40 to 160 mg/kg, whereby 3/5 infected mice were cured. Upon complexation, the Cu(II) complexes which includes compound **XXXVI** were found to be the most active, curing 5/5

infected mice at a dose 160 mg/kg. The Ni(II) complexes were inactive and the Fe(II) complexes were less active than the Cu(II) complexes.[100]

In a study by Khanye *et al.*, a variety of Au(I)-thiosemicarbazone complexes were synthesized.[41] The Au(I) was coordinated to two ferrocenyl-derived thiosemicarbazones through the sulfur atoms to form linear complexes. The free ligands and their corresponding complexes were tested against *P. falciparum* D10 (CQS) and W2 (CQR) strains. Most of the complexes showed significant activity against the *P. falciparum* strains when compared to their free ligands. Compound **XXXVII** (Fig. 1.19) exhibited the highest activity against the W2 (IC_{50} value = 1.28 µM) strain. However, these compounds were less effective than chloroquine (IC_{50} value = 0.095 µM).[41]

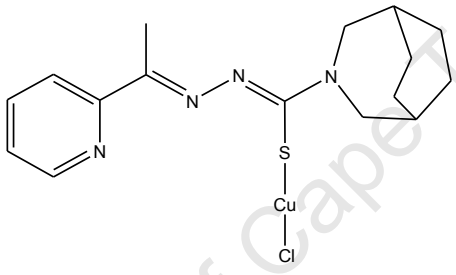

XXXVI

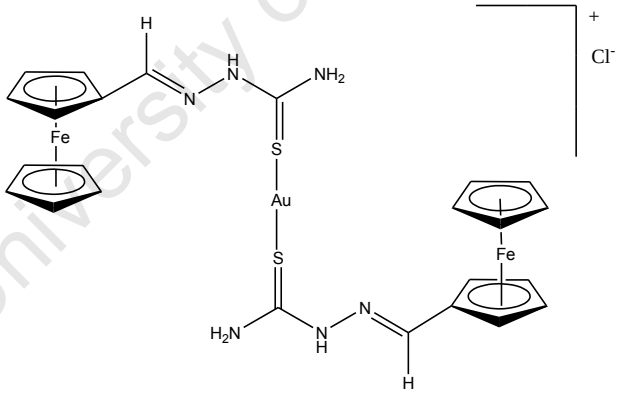

XXXVII

Figure 1.19: The thiosemicarbazone copper (**XXXVI**) and gold (**XXXVII**) complexes.[100,41]

It has been established that ferroquine- and thiosemicarbazone-derivatives are active against *P. falciparum*.[9,65] The ferrocenyl moiety in ferroquine has no cytotoxic activity. However, in the same way as the iron in haematin produces reactive oxygen species when oxidized, so does the iron in ferroquine.[9] A study carried out by Biot and co-workers aimed to utilizes the previously mentioned properties of ferroquine, and the chelating ability of thiosemicarbazones by synthesizing compounds which contained both components.[42] The

substituents on the aryl group of the thiosemicarbazone, as well as the group attached to the ferrocenyl moiety, were varied when the compounds were synthesize. Compound **XXXVIII** (Fig. 1.20) was one of the most active compounds synthesized by Biot *et al*.[42] The compound had IC_{50} values of 0.2 and 0.8 µM against the *P. falciparum* strains 3D7 (CQS) and W2 (CQR) respectively.

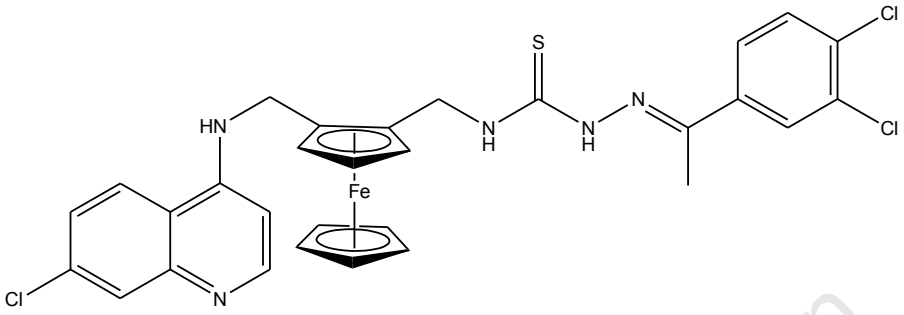

XXXVIII

Figure 1.20: A compound which incorporates thiosemicarbazone onto ferroquine (**XXXVIII**).[42]

The activity of various *C,N,S*-chelated thiosemicarbazone cyclopalladated complexes has been investigated in a study conducted by Chellan *et al*.[40] The complexes were synthesized using P-donor ligands, such as triphenylphosphine for mononuclear complexes (**XXXIX**) and the bridging ligands, 1,1'-bis(diphenylphosphino)ferrocene (Fig. 1.21) and trans-1,2-bis(diphenylphosphino)ethylene, for the binuclear complexes (**XXXX**).[40]

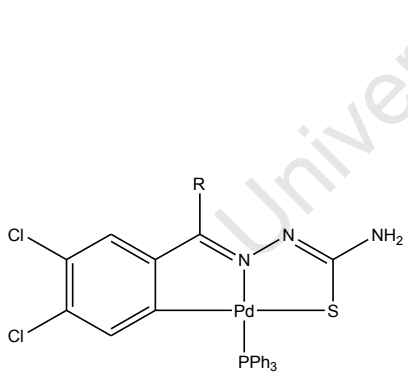

R = CH_3, CH_2CH_3

XXXIX

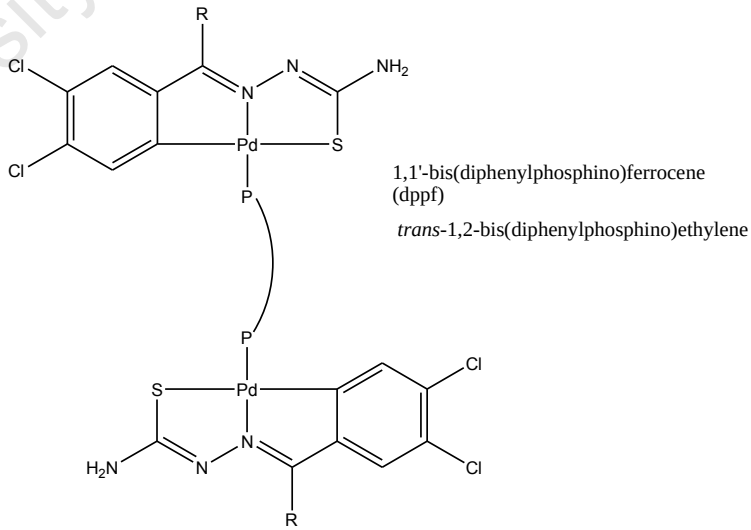

R = CH_3, CH_2CH_3

XXXX

Figure 1.21: Cyclopalladated complexes with P- donor ligands (**XXXIX** and **XXXX**).[40]

The complexes were tested against both 3D7 (CQS) and K1 (CQR) strains of *P. falciparum*. Moderate activity was exhibited by the mononuclear complexes, as well as the binuclear 1,1'-bis(diphenylphosphino)ferrocene complexes, which was higher than the activity of the free ligand. However, no conclusive evidence was gained to illustrate that a relationship exists between the activity and the increase in nuclearity of the complexes.[40]

1.6. Multinuclear complexes

It has been observed that in certain cases, with an increase in the number of metal centres, there is an enhancement of biological activity.[101-105] One of the most noted cases, involves the platinum-containing complexes BBR3005 [{*trans*-$PtCl(NH_3)_2$}$_2$μ-H_2N-$(CH_2)_6$-NH_2]$^{2+}$ (**XXXXI**) and BBR3464 [{*trans*-$PtCl(NH_3)_2$}$_2${*trans*-$Pt(NH_3)_2$(μ-H_2N-$(CH_2)_6$-NH_2)$_2$}]$^{4+}$ (**XXXXII**) which were evaluated as anticancer agents.[102] These complexes contain platinum centres linked by aliphatic diamine chains. BBR3464 shows enhanced anticancer activity compared to the other related binuclear compounds such as BBR3005 (**XXXXI**, Fig. 15) which has a lower nuclearity. BBR3464 has also shown activity significantly higher than cisplatin and against various cell lines which are resistant to cisplatin.[102]

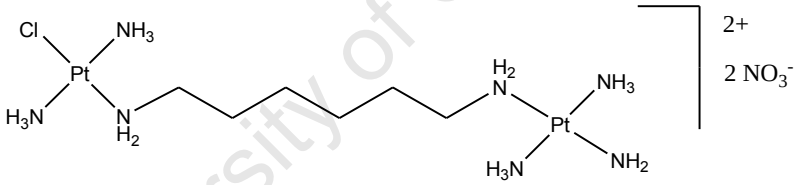

XXXXI

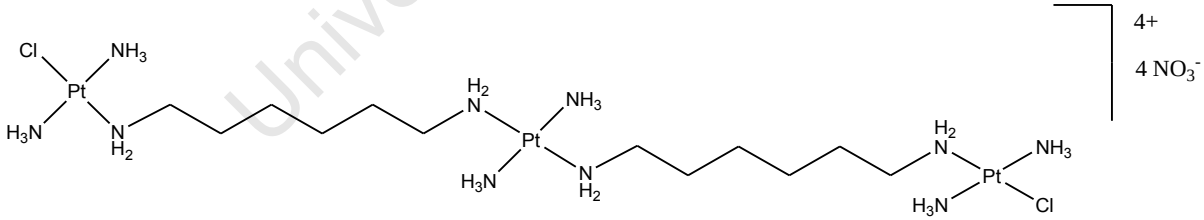

XXXXII

Figure 1.22: The platinum-containing complexes BBR3005 (**XXXXI**) and BBR3464 (**XXXXII**).[102]

1.6.1. Multinuclear transition metal complexes as antimalarial agents

Mono- and binuclear gold(III) complexes were synthesized by Gabbiani *et al.*, using dipyridyl derivatives, and their activity tested against the chloroquine-sensitive 3D7 strain.[101] All the binuclear complexes showed higher activity when compared to the mononuclear complex with **XXXXIV** being the most active. Compounds **XXXXIII** and **XXXXIV** (Fig.

1.23) had IC_{50} values of 12.2 and 2.3 µM respectively.[101] These gold(III) complexes have shown enhanced activity when the number of metal centres present increased.

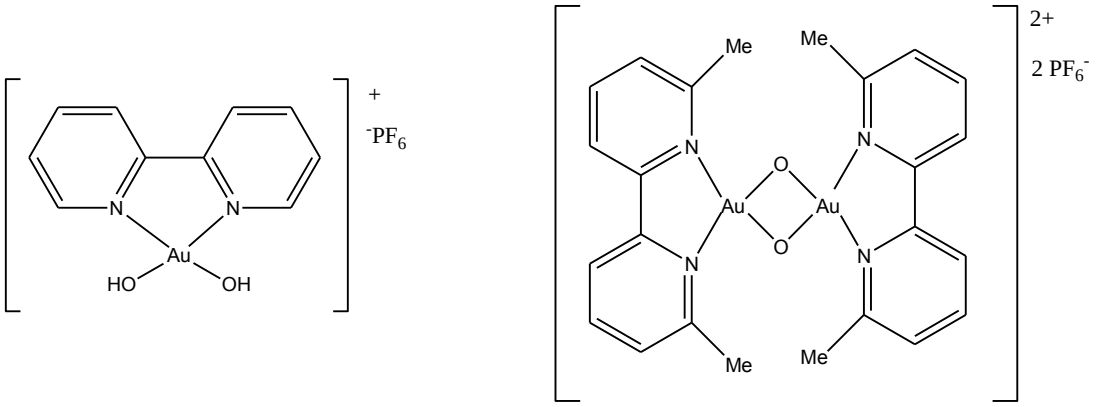

XXXXIII **XXXXIV**

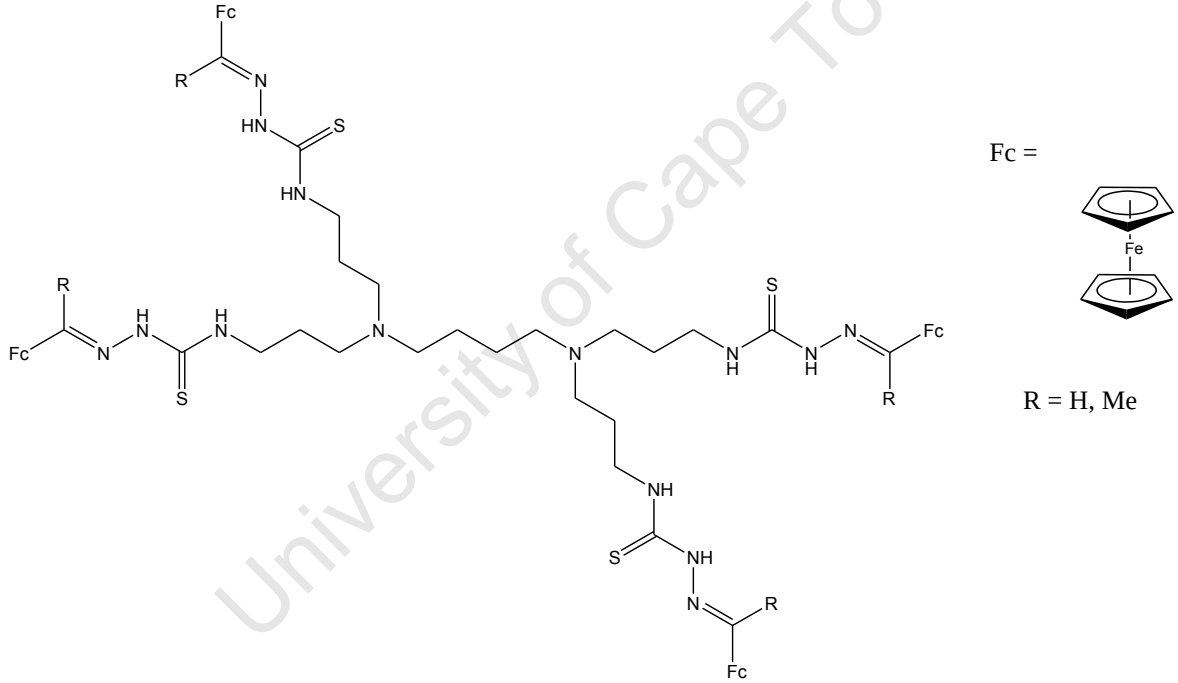

XXXXV

Figure 1.23: The structure of the mononuclear (**XXXXIII**) and binuclear (**XXXXIV**) gold(III)-complexes. The structure of the dendritic ferrocenylthiosemicarbazone (**XXXXV**).[101,104]

Ferrocenylthiosemicarbazones have been incorporated onto a poly(propyleneimine) dendrimer scaffold (Fig. 1.23) by Khanye *et al.*, and the antiplasmodial activity evaluated.[102] When comparing compounds **XXXXV** (R = H, Me), which contains four ferrocenyl moieties, to the scaffold without the ferrocenyl moiety, there is a significant increase in activity. These compounds were tested *in vitro* against the chloroquine-resistant W2 strain. Compounds **XXXXV** (R = H, Me) exhibited activity with IC_{50} values of 6.59 ± 0.078 and 1.79 ± 0.006

μM respectively, whilst the other compounds were inactive at the highest tested concentration (20 μM).[104]

Various other multinuclear complexes such as **XXXI** (Section 1.4.1., Fig. 1.14) and **XXXVI** (Section 1.5.1., Fig. 1.19) have exhibited good biological activity in comparison to their free ligands.[41,79] With results that suggest that multinuclear complexes are more active than their mononuclear complexes,[103] it can be inferred that the same concept may apply when dealing with the nuclearity of thiosemicarbazone complexes, though these results must be read with some caution. Therefore, multinuclear platinum group metal thiosemicarbazones complexes may prove promising as antimalarial agents.

1.7. Aims and objectives

General aims

The main aim of the project was to synthesize thiosemicarbazone ligands as well as their palladium(II) and ruthenium(II) complexes. The ligands and complexes were characterized, and the biological activity of selected compounds was evaluated.

Specific objectives

- To synthesize the monothiosemicarbazone ligands using 3,4-dichloroacetophenone, 3,4-dichloropropiophenone and ferrocenecarboxaldehyde.

- To synthesize the dithiosemicarbazone ligand by reacting dithiosemicarbazide with ferrocenecarboxaldehyde.

- To synthesize mono- and binuclear cyclopalladated complexes containing N- and P-donor ligands.

- To synthesize ruthenium(II)-arene complexes using the mono- and dimeric ferrocenylthiosemicarbazones.

- To synthesize the palladium(II)-ferrocenylthiosemicarbazone complexes with P-donor ligands.

- To characterize the ligands and complexes using ^{1}H, ^{13}C and ^{31}P, 2D (COSY and HSQC) NMR spectroscopy, IR spectroscopy and mass spectrometry.

- To evaluate the biological activity of the ligands and complexes against malaria parasite strains.

1.8. References

1 World Health Organisation.
< http://www.who.int/malaria/world_malaria_report_2011/WMR2011_factsheet.pdf>
(Accessed 29 April 2012)

2. C. Biot and D. Dive, *Top. Organomet. Chem.*, 2010, **32**, 155.

3. Malaria map
<http://www.cdc.gov/malaria/about/distribution.html >
(Accessed 8 April 2012)

4. I. Y. Gluzman, S. E. Francis, A. Oksman, C. E. Smith, K. L. Duffin and D. E. Goldberg, *J. Clin. Invest.*, 1994, **93**, 1602.

5. K. K. Eggleson, K. L. Duffin and D. E Goldberg, *J. Biol. Chem.*, 1999, **274**, 32411.

6. D. E. Goldberg, A. F. G. Slater, A. Cerami and G. B. Henderson, *Proc. Natl. Acad. Sci.*, 1990, **87**, 2931.

7. D. E. Goldberg, A. F. G. Slater, R. Beavis, B. Chait, A. Cerami and G. B. Henderson, *J. Exp. Med.*, 1991, **173**, 961.

8. I. W. Sherman, *Malaria: Parasite biology, pathogenesis and protection*, American Society for Microbiology, Washington, 1998, chap. 10.

9. N. Chavain, H. Vezin, D. Dive, N. Touati, J. F. Paul, E. Buisine and C. Biot, *Mol. Pharm.*, 2008, **5**, 710.

10. T. J. Egan, *Mol. Biochem. Parasitol*., 2008, **157**, 127.

11. S. Toovey, *The miraculous fever-tree. The cure that changed the world*, Fiametta Rocco, San Francisco, Harper Collins, 2004.

12. T. J. Egan, W. W. Mavuso, D. C. Ross and H. M. Marques, *J. Inorg. Biochem.*, 1997, **68**, 137.

13. U. Hellgren, I. Berggren-Palme, Y. Berggvist and M. Jerling, *Brit. J. Clin. Pharm*., 1997, **44**, 119.

14. K. Raynes, *Int. J. Parasitol*., 1999, **29**, 367.

15. K. Raynes, M. Foley, L. Tilley and L.W. Deady, *Biochem. Pharmacol*., 1996, **52**, 551.

16. P. M. O'Neill, P. G. Bray, S. R. Hawley, S. A. Ward and B. K. Park, *Pharmacol. Ther*., 1998, **77**, 29.
17. T. M. E. Davis, T. Hung, I. Sim, H. A. Karunajeewa and K. F. Ilett, *Drugs*, 2005, **65**, 75.
18. F. Coslédan, L. Fraisse, A. Pellet, F. Guillou, B. Mordmùller, P. G. Kremsner, A. Morena, D. Mazier, J-. P. Maffrand and B. Meunier, *Proc. Natl. Acad. Sci. USA*, 2008, **105**, 17579.
19. S. R. Meshnick, *Int. J. Parasitol.*, 2002, **32**, 1655.
20. M. del Pilar Crespo, T. D. Avery, E. Hanssen, E. Fox, T. V. Robinson, P. Valente, D. K. Taylor and L. Tilley, *Antimicrob. Agents Chemother.*, 2008, **52**, 98.
21. S. P. Fricker, *Dalton Trans.*, 2007, 4903.
22. A. Djimde and G. Lefevre, *Malaria J.*, 2009, **8**, 1.
23. P. E. Duffy and T. K. Mutabingwa, *Lancet.*, 2004, **363**, 3.
24. J. Swarbrick, P. Iliades, J. S. Simpson and I. Macreadie, *Open Enzyme Inhibition J.*, 2008, **1**, 12.
25. F. H. S. Curd, D. G. Davey and F. L. Rose, *Ann. Trop. Med. Parasitol.*, 1945, **39**, 208.
26. H. C. Carrington, A. F. Crowther, D. G. Davey, A. A. Levi and F. L. Rose, *Nature*, 1951, **168**, 1080.
27. A. Nzila, *J. Antimicrob. Chemother*., 2006, **57**, 1043.
28. G. H. Hitchings, G, B. Elion, E. A. Falco, P. B. Russell, M. B. Sherwood, *J. Biol. Chem.*, 1950, **183**, 1.
29. P. Wang, C.-S. Lee, R. Bayoumi, A. Djimde, O. Doumbo, G. Swedberg, L. D. Dao, H. Mshinda, M. Tanner, W. M. Watkins, P. F.G. Sims and J. E. Hyde, *Mol. Biochem. Parasitol.*, 1997, **89**, 161.
30. W. M. Watkins and M. Mosobo, *Trans. R. Soc. Trop. Med. Hyg.*, 1993, **87**, 75.
31. R. Ettari, F. Bova, M. Zappalà, S. Grasso and N. Micale, *Med. Res. Rev.*, 2010, **30**, 136.
32. P. J. Rosenthal, W.S. Wollish, J. T. Palmer and D. Rasnick, *J. Clin. Invest.*, 1991, **88**, 1467.
33. P. J. Rosenthal, J. E. Olson, G. K. Lee, J. T. Palmer, J. L. Klaus and D. Rasnick, *Antimicrob. Agents Chemother*., 1996, **40**, 1600.
34. J. N. Domìnguez, C. Leòn, J. Rodrigues, N. G. Domìnguez, J. Gut and P. J. Rosenthal, *J. Med. Chem.*, 2005, **48**, 3654.
35. S. Batra, Y. A. Sabnis, P. J. Rosenthal and M. A. Avery, *Bioorg. Med. Chem.*, 2003, **11**, 2293.

36. C. Biot, J. Dessolin, I. Ricard and D. Dive, *J. Organomet. Chem.*, 2004, **689**, 4678.
37. F. Bellot, F. Coslédan, L. Vendier, J. Brocard, B. Meunier and A. Robert, *J. Med. Chem.*, 2010, **53**, 4103.
38. P. Chellan, N. Shunmoogam-Gounden, D. T. Hendricks, J. Gut, P. J. Rosenthal, C. Lategan, P. J. Smith, K. Chibale and G. S. Smith, *Eur. J. Inorg. Chem.*, 2010, **22**, 3520.
39. T. Stringer, P. Chellan, B. Therrien, N. Shunmoogam- Gounden, D. T. Hendricks and G. S. Smith, *Polyhedron*, 2009, **28**, 2839.
40. P. Chellan, S. Nasser, L. Vivas, K. Chibale and G. S. Smith, *J. Organomet. Chem.*, 2010, **695**, 2225.
41. S. D. Khanye, G. S. Smith, C. Lategan, P. J. Smith, J. Gut, P. J. Rosenthal and K. Chibale, *J. Inorg. Biochem.*, 2010, **104**, 1079.
42. C. Biot, B. Pradines, M. H. Sergeant, J. Gut, P. J. Rosenthal and K. Chibale, *Bioorg. Med. Chem. Lett*., 2007, **17**, 6434.
43. J. M. Sayer, W. P. Jencks, *J. Am. Chem. Soc.*, 1973, **95**, 5637.
44. K. J. Reddy, J. R. Kumar, C. Ramachandraiah, T. Thriveni and A. V. Reddy, *Food Chem.*, 2007, **101**, 585.
45. V. Kaur, J. S. Aulakh and A. K. Malik, *Anal. Chim. Acta.*, 2007, **603**, 44.
46. R. G. Pearson, *J. Am. Chem. Soc.*, 1963, **85**, 3533.
47. R. W. Brockman, J. R. Thomson, M. J. Bell and H. E. Skipper, *Cancer Res.*, 1956, **16**, 167.
48. A. I. Matesanz and P. Souza, *Mini-Rev. Med. Chem.*, 2009, **9**, 1389.
49. S. A. Khan and M. Yusuf, *Eur. J. Med. Chem*., 2009, **44**, 2270.
50. P. Genova, T. Varadinova, A. I. Matesanz, D. Marinova and P. Souza, *Toxicol. App. Pharmacol.*, 2004, **197**, 107.
51. C. Shipman, Jr., S. H. Smith, J. C. Drach and D. L. Klayman, *Antimicrob. Agents Chemother.*, 1981, **19**, 682.
52. D. C. Greenbaum, Z. Mackey, E. Hansell, P. Doyle, J. Gut. C. R. Caffrey, J. Lehrman, P. J. Rosenthal, J. H. McKerrow and K. Chibale, *J. Med. Chem.*, 2004, **47**, 3212.
53. R. B. de Oliveira, E. M. de Souza-Fagundes, R. P. P. Soares, A. A. Andrade, A. U. Krettli and C. L. Zani, *Eur. J. Med. Chem*., 2008, **43**, 1983.
54. A. Chipeleme, J. Gut, P.J. Rosenthal and K. Chibale, *Bioorg. Med. Chem.*, 2007, **15**, 273.
55. R. A. Finch, M. C. Liu, A. H. Cory, J. G. Cory and A. C. Sartorelli, *Adv. Enzyme Regul.*, 1999, **39**, 3.

56. I. Chiyanzu, E. Hansell, J. Gut, P. J. Rosenthal, J. H. McKerrow and K. Chibale, *Bioorg. Med. Chem. Lett.*, 2003, **13**, 3527.
57. J. J. Walsh, D. Coughlan, N. Heneghan, C. Gaynor and A. Bell, *Bioorg. Med. Chem. Lett.*, 2007, **17**, 3599.
58. W. A. Creasey, K. C. Agrawal, R. L. Capizza, K. K. Stinson and A. C. Sartorelli, *Cancer Res.*, 1972, **32**, 565.
59. M. Liu and A. C. Sartorelli, *Prog. Med. Chem.*, 1995, **32**, 1.
60. M.-C. Liu, T.-S. Lin and A. C. Sartorelli, *J. Med. Chem.*, 1992, **35**, 3612.
61. C. M. Nutting, C. M. L. van Herpen, A. B. Miah, S. A. Bhide, J. P. Machiels, J. Buter, C. Kelly, D. De Raucourt and K. J. Harrington, *Ann. Oncol.*, 2009, **20**, 1275.
62. B. Ma, B. C. Goh, E. H. Tan, K. C. Lam, R. Soo, S. S. Leong, L. Z. Wang, F. Mo, A. T. Chan, B. Zee and T. Mok, *Invest. New Drugs*, 2008, **26**, 169.
63. R. A. Finch, M. C. Lui, S. P. Grill, W. C. Rose, R. Loomis, K. M. Vasquez, Y. C. Cheng and A. C. Sartorelli, *Biochem. Pharmacol.*, 2000, **59**, 983.
64. E. A. Enyedy, N. V. Nagy, E. Zsigó, C. R. Kowol, V. B. Arion, B. K. Keppler and T. Kiss, *Eur. J. Inorg. Chem.*, 2010, **11**, 1717.
65. C. R. Kowol, R. Trondl, P. Heffeter, V. B. Arion, M. A. Jakupec, A. Roller, M. Galanski, W. Berger and B. K. Keppler, *J. Med. Chem.*, 2009, **52**, 5032.
66. Z. Kovacevic, D. S. Kalinowski, D. B. Lovejoy, P. Quach, J. Wong and D. R. Richardson, *Curr. Drug Deliv.*, 2010, **7**, 194.
67. Y. Yu, D. S. Kalinowski, Z. Kovacevic, A. R. Siafakas, P. J. Jansson, C. Stefani, D. B. Lovejoy, P. C. Sharpe, P. V. Bernhardt and D. R. Richardson, *J. Med. Chem.*, 2009, **52**, 5271.
68. W. O. Foye, T. L. Lemke and D. A. Williams, in *Principles of medicinal chemistry*, Baltimore, Williams & Wilkins, 4th edn., 1995.
69. C. F. Shaw, III, *Chem. Rev.*, 1999, **99**, 2589.
70. B. Rosenberg, L. Van Camp, J. E. Trosko and V. H. Mansour, *Nature*, 1969, **222**, 385.
71. M. Peyrone, *Ann. Chem. Pharm.*, 1844, **51**, 1.
72. Z. Afrasiabi, E. Sinn, S. Padhye, S. Dutta, S. Padhye, C. Newton, C. E. Anson and A. K. Powell, *J. Inorg. Biochem.*, 2003, **95**, 306.
73. S.-G. Teoh, S.-H. Ang, H.-K. Fun and C.-W. Ong, *J. Organomet. Chem.*, 1999, **580**, 17.
74. D. Bahl, F. Athar, M. B. P. Soares, M. Santos de Sá, D. R. M. Moreira, R. M. Srivastava, A. C. L. Leite and A. Azam, *Bioorg. Med. Chem.*, 2010, **18**, 6857.

75. P. A. Ajibade and G. A. Kolawole, *Trans. Met. Chem*., 2008, **33**, 493.
76. M. Navarro, H. Pérez and R.A. Sanchez-Delgado, *J. Med. Chem.*, 1997, **40**, 1937.
77. C. Biot, W. Castro, C. Y. Botte and M. Navarro, *Dalton Trans.*, 2012, **41**, 6335.
78. M. Navarro, W. Castro and C. Biot, *Organometallics*, 2012, **31**, 5715.
79. R. A. Sánchez-Delgado, M. Navarro, H. Pérez and J. A. Urbina, *J. Med. Chem.*, 1996, **39**, 1095.
80. R. A. Sánchez-Delgado and A. Anzellotti, *Mini- Rev. Med. Chem.*, 2004, **4**, 23.
81. C. S. K. Rajapakse, A. Martínez, B. Naoulou, A. A. Jarzecki, L. Suárez, C. Deregnaucourt, V. Sinou, J. Schrével, E. Musi, G. Ambrosini, G K. Schwartz and R. A. Sánchez-Delgado, *Inorg. Chem.*, 2009, **48**, 1122.
82. L. Glans, A. Ehnbom, C. De Kock, A. Martínez, J. Estrada, P. J. Smith, M. Haukka, R. A. Sánchez-Delgado and E. Nordlander, *Dalton Trans.*, 2012, **41**, 2764.
83. M. Navarro, F. Vasquez, R.A. Sanchez-Delgado, H. Perez, V. Sinou and J. Schrevel, *J. Med. Chem.*, 2004, **47**, 5204.
84. C. Biot, G. Glorian, L. A. Maciejewski and J. S. Brocard, *J. Med. Chem*., 1997, **40**, 3715.
85. S. Gaur, N. Fahmi and R. V. Singh, *Phosphorus Sulfur*, 2007, **82**, 853.
86. E. Wong and C. M. Giandomenico, *Chem. Rev.*, 1999, **99**, 2451.
87. C. E. Housecroft and A. G. Sharpe, *Inorganic Chemistry*, third edition, England, Pearson Prentice Hall, Chap. 20, pg. 618.
88. C. S. Allardyce and P. J. Dyson, *Platinum Met. Rev.*, 2001, **45**, 62.
89. S. Chandra and U. Kumar, *Synth. React. Inorg. Met.-Org. Chem*., 2004, **34**, 1417.
90. J. M. Vila, M. Gayoso, M. T. Pereira, A. Suárez, J. J. Fernández, J. M. Ortigueira, A. Fernández, M. López-Torres, *Trends Organomet. Chem.*, 1997, **2**, 21.
91. A. A. El-Asmy, O. A. El-Gammal and H. S. Saleh, *Spec. Acta A–Mol. Biomol. Spec.*, 2008, **71**, 39.
92. R. M. El-Shazly, G. A. A. Al-Hazmi, S. E. Ghazy, M. S. El- Shahawi and A. A. El-Asmy, *J. Coord. Chem*., 2006, **59**, 845.
93. S. D. Khanye, B. Wan, S. G. Franzblau, J. Gut, P. J. Rosenthal, G. S. Smith and K. Chibale, *J. Organomet. Chem.*, 2011, **696**, 3392.
94. S. Halder, R. J. Butcher and S. Bhattacharya, *Polyhedron*, 2007, **26**, 2741.
95. A. Amoedo, L. A. Adrio, J.M. Antelo, J. Martínez, M. T. Pereira, A. Fernandez and J. M. Vila, *Eur. J. Inorg. Chem.*, 2006, 3016.

96. R. H. Crabtree, *The organometallic chemistry of the transition metals*, fifth ed., New Jersey, John Wiley & Sons, 2009, chap. 1.
97. J. Albert, J. M. Cadena, J. R. Granell, X. Solans and M. Font-Bardia, *Tetrahedron: Asymm*., 2000, **11**, 1943.
98. J. Dupont, C. S. Consorti and J. Spencer, *Chem. Rev*., 2005, **105**, 2527.
99. J. M. Vila, T. Pereira, J. M. Ortigueira, A. Amoedo, M. Graňa, G. Alberdi, M. López-Torres and A. Fernández, *J. Organomet. Chem*., 2002, **663**, 239.
100. J. P. Scovill, D. L. Klayman and C. F. Franchino, *J. Med. Chem.*, 1982, **25**, 1261.
101. C. Gabbiani, L. Messori, M. A. Cinellu, A. Casini, P .Mura, A. R. Sannella, C. Severini, G. Majori, A. R. Bilia and F. F. Vincieri, *J. Inorg. Biochem.*, 2009, **103**, 310.
102. N. J. Wheatea and J. G. Collins, *Curr. Med. Chem. - Anti-Cancer Agents.*, 2005, **5**, 267.
103. M. G. Mendoza-Ferri, C. G. Hartinger, M. A. Mendoza, M. Groessl, A. E. Egger, R. E. Eichinger, J. B. Mangrum, N. P. Farrell, M. Maruszak, P. J. Bednarski, F. Klein, M. A. Jakupec, A. A. Nazarov, K. Severin and B. K. Keppler, *J. Med. Chem.*, 2009, **52**, 916.
104. S. D. Khanye, J. Gut, P. J. Rosenthal, K. Chibale and G. S. Smith, *J. Organomet. Chem.*, 2011, **696**, 3296.
105. C. G. Hartinger, A. D. Phillips and A. A. Nazarov, *Curr. Top. Med. Chem.*, 2011, **11**, 2688.

CHAPTER 2

The synthesis and characterization of aryl-derived thiosemicarbazone cyclopalladated complexes containing N- and P-donor ligands

2.1. Introduction

As previously mentioned thiosemicarbazone ligands are well known for their ability to chelate to a range of metals through the use of donor atoms, such as oxygen, sulfur and nitrogen.[1-5] Cyclopalladated complexes characteristically contain a palladium-carbon sigma bond, where an aromatic sp^2 carbon is typically used. The additional donor atoms stabilize the metal when forming the cycle.[6-7] In this chapter, the aryl-monothiosemicarbazone ligands chelate in a tridentate *C,N,S*-mode (Fig. 2.1), whereby C-H activation of the aryl proton in the 6th position and further chelation through the imine nitrogen and sulfur atoms form two five-membered rings.[3,8-11]

The thiosemicarbazone systems chosen for the synthesis of *C,N,S*-chelated cyclopalladated complexes contain an alkyl group on the imine carbon. Ketones are preferred over aldehydes due to the steric interaction between the alkyl group and the aromatic ring, pushing the ring closer to the metal, and allowing for *ortho*-metallation to occur when forming the target complex.[8,12]

The complexes containing the P- and N-donor ligands (Section 2.2.4. and 2.2.5.) were derived from tetranuclear complexes, which were initially synthesized by Chellan *et al*.[3] The complex is tetranuclear due to a core around which four cyclopalladated units are situated. The palladium is coordinated to the sulfur atom in the unit with which it forms a palladacycle as well as with the sulfur atom in the adjacent unit. Therefore, as a result of the Pd-$S_{bridging}$ bonds, the Pd_4S_4 core of the tetranuclear structure forms (refer to Section 2.2.3).[13]

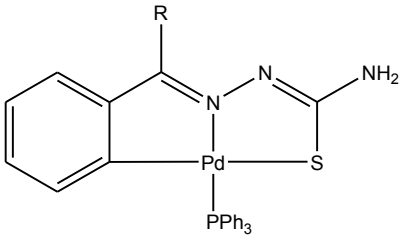

R = Me, Ph

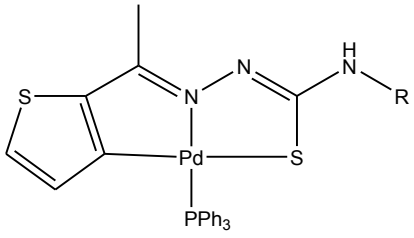

R= H, Me

Figure 2.1: Examples of *C,N,S*-chelated thiosemicarbazone cyclopalladated complexes.[12,14]

Various tridentate *C,N,S* cyclopalladated complexes containing P-donor ligands for example PR_3 or bis(diphenylphosphino) bridging compounds have been synthesized by Lobana *et al.* and Weis *et al.* to name a few.[12,14] Attempts to investigate complexes containing N-donor ligands are scarce due to limited reactivity when cleaving the Pd-$S_{bridging}$ bond of the tetranuclear complex.[15] Therefore, the preparation of complexes containing N- and P-donor ligands was attempted.

2.2. Results and discussion

2.2.1. The synthesis and characterization of the monothiosemicarbazone ligands (1, 2)

The aryl monothiosemicarbazone ligands were prepared via a Schiff base condensation reaction between the ketones, 3,4-dichloroacetophenone or 3,4-dichloropropiophenone, and thiosemicarbazide in ethanol (Scheme 2.1). This reaction results in the formation of the imine bond and the liberation of a water molecule.[16]

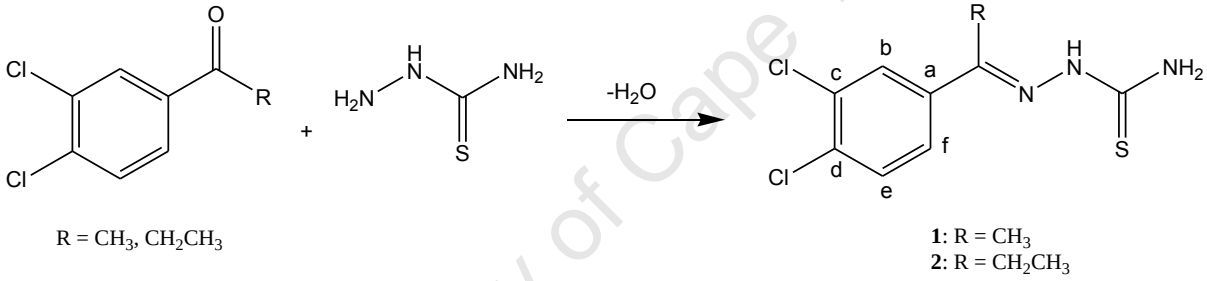

Scheme 2.1: The synthesis of the monothiosemicarbazone ligands (**1**, **2**).

Physical properties

Compounds **1** and **2** were isolated as white crystalline solids in moderate yields (Table 2.1). Compounds **1** and **2** have melting points comparable to literature values (Table 2.1), ranging between 196.0-197.9 °C and 185.6-186.4 °C respectively.[16] The ligands are soluble in dichloromethane, chloroform, acetone, ethyl acetate, tetrahydrofuran and dimethyl sulfoxide.

Table 2.1: The physical appearance, yield and melting point of the monothiosemicarbazone ligands (**1**, **2**)

Compound number	R	Yield (%)	Physical Appearance	Melting point (˚C)
1	CH_3	51	White crystalline solid	194.8-197.9
2	CH_2CH_3	54	White crystalline solid	186.6-188.1

Compounds **1** and **2** are known, and thus ^{1}H NMR spectroscopy and infrared spectroscopy were the only methods of characterization carried out.

^{1}H NMR spectroscopy

The NMR spectra for compounds **1** and **2** were recorded in DMSO-d_6. The ^{1}H NMR spectra of the ligands show characteristic peaks associated with thiosemicarbazones. The peak for the hydrazinic proton is observed at δ 10.24 and 10.36 for compounds **1** and **2** respectively. The aromatic proton H_b resonates as a doublet (J = 2.00 Hz) at δ 8.25 and 8.23 for **1** and **2** respectively.

The peaks associated with the aromatic protons H_e and H_f are observed as a doublet and a doublet of doublets respectively (see appendix, pg 132). The peak for H_e is observed at δ 7.61 and 7.60 ($^{3}J_{HH}$ ~ 8.60 Hz) for **1** and **2** respectively, whilst the peak for the aromatic proton H_f is observed at δ 7.88 and 7.86 respectively. The proton H_f couples to H_b ($^{4}J_{HH}$ = 2.00 Hz) and H_e ($^{3}J_{HH}$ ~ 8.60 Hz) which produces a doublet of doublets.[16]

The amine protons of compound **1** and **2** resonate at *ca.* δ 8.13 and 8.31. The nitrogen of the terminal amine group is able to delocalize its lone pair of electrons leading to restricted rotation of the amine group about the C-N axis, which results in different environments and thus two broad signals are observed.[1,8,17-18]

The alkyl substituent on the imine carbon is located upfield in the ^{1}H NMR spectrum. The peak for the methyl protons of compound **1** is observed as a singlet at δ 2.28, whilst the CH_3 and CH_2 protons of the ethyl chain of compound **2** are observed as a triplet ($^{3}J_{HH}$ = 7.60 Hz) and quartet ($^{3}J_{HH}$ = 7.60 Hz) at δ 0.99 and 2.86 respectively. The data correspond to that reported in literature by Du *et al.*[16]

Infrared (IR) spectroscopy

Upon synthesis of compounds **1** and **2**, an absorption band is observed in the IR spectrum at 1594 and 1596 cm^{-1} respectively, for the imine bond. Imine absorption bands are typically observed in the region 1690–1590 cm^{-1}.[19]

2.2.2. The synthesis and characterization of the mono- and dimeric iminophosphine and aminophosphine ligands (3-6)

The aminophosphine ligands (**4** and **6**) were prepared via reductive amination. The iminophosphine ligands were synthesized via a Schiff base condensation reaction between (2-diphenylphosphino)benzaldehyde and *n*-propylamine (**3**) or *p*-phenylenediamine (**5**) in toluene or methanol (Scheme 2.2).[20-22] Compounds **3** and **5** were reduced using sodium borohydride to produce the aminophosphine ligands (**4** and **6**).[21] The monomeric ligand (**4**) was synthesized as a model to determine if complexation would occur (Section 2.2.4.a.), and if this would be a feasible system for the complexation of multimeric ligands. The dimeric aminophosphine ligand (**6**) was synthesized as a bridging ligand between two cyclopalladated units (Section 2.2.4.b.).

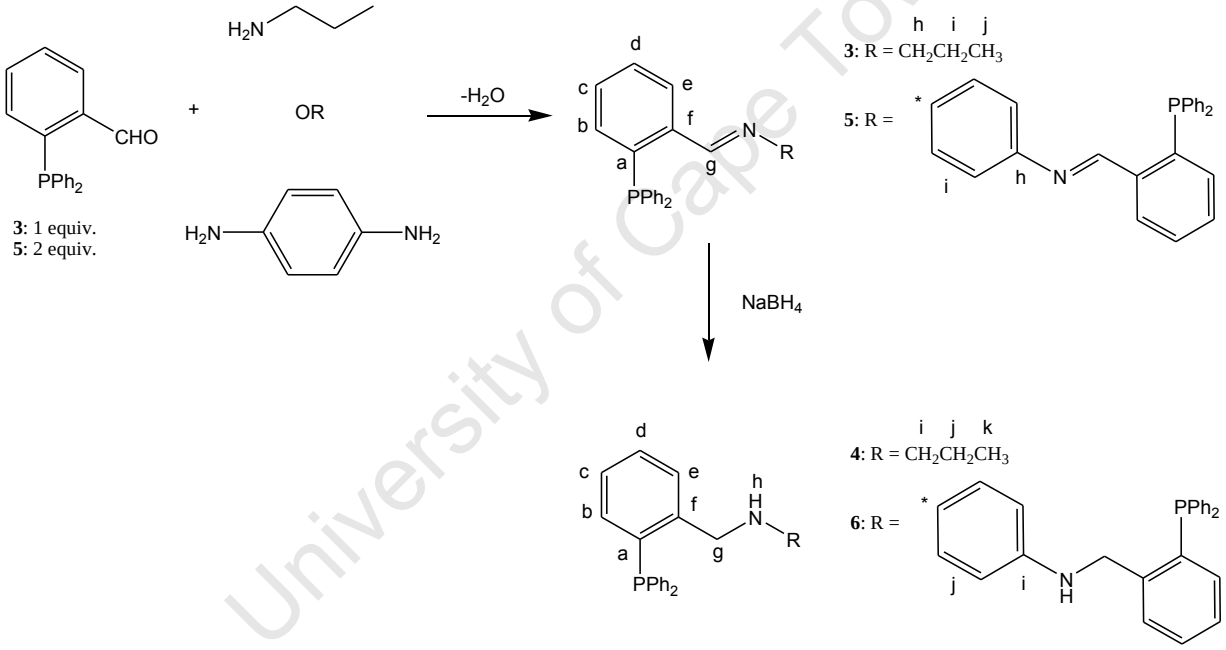

Scheme 2.2: The synthesis of the imino (**3** and **5**) - and aminophosphine (**4** and **6**) ligands.

Physical properties

Compounds **3** and **4** were isolated as yellow oils and compounds **5** and **6** were isolated as yellow powders in relatively high yields (Table 2.2). Compounds **5** and **6** have high melting points. Compounds **3** and **6** are soluble in chlorinated solvents, dimethyl sulfoxide and acetone while **3** and **4** are also soluble in methanol.

Table 2.2: Physical appearance and yield of the ligands (**3-6**)

Compound number	Yield (%)	Physical Appearance	Melting point (˚C)
3	90	Yellow oil	-
4	91	Yellow oil	-
5	88	Light-yellow powder	206.4-210.4
6	94	Yellow powder	194.8-198.5

Spectroscopic and analytical techniques such as NMR spectroscopy, infrared spectroscopy and mass spectrometry were used to characterize compounds **3-6**.

^{1}H NMR spectroscopy

The NMR spectra of compounds **3-5** were recorded in $CDCl_3$, whilst the spectrum of compound **6** was recorded in DMSO-d_6. Upon formation of the iminophosphine ligands **3** and **5**, a doublet corresponding to the imine proton is observed at *ca.* δ 9.00. The peak corresponding to the aldehyde proton of the starting material is not observed at δ 10.51 which confirms condensation. Coupling constants of *ca.* 5.00 Hz for **3** and **5** suggests a four bond coupling of the imine proton with phosphorus, which is comparable with that seen in literature ($^4J_{HP}$ = 3 - 6 Hz).[20-23]

Reduction of the imine bond is confirmed by the absence of the imine peak in the ^{1}H NMR spectra of compounds **4** and **6**, and the appearance of a signal for the H_g proton which resonates at δ 3.90 and 4.19 for **4** and **6** respectively (see appendix, pg. 132 and 133). The amine proton H_h is observed as a broad signal at δ 1.72 and 5.30 respectively for **4** and **6**.

The signals for the aromatic protons are observed in the range δ 6.76-8.19. The signal for H_e is observed as a multiplet due to coupling with H_d and phosphorus. For compounds **3**, **4** and **6**, the signal for H_b is observed as a doublet of doublets, whereas for compound **5** a multiplet is observed. A coupling constant of *ca.* 7.50 Hz corresponds to coupling with the adjacent aromatic proton H_c, whilst a coupling constant of *ca.* 4.50 Hz corresponds to a three bond coupling with phosphorus.[21-23] The aromatic protons H_c (**4** and **6**) and H_d (**5** and **6**) are observed as a triplet (J ~ 7.60 Hz) due to coupling with adjacent aromatic protons (Table 2.3). A coupling constant in the range 7.00-8.00 Hz is typical for three bond coupling between aromatic protons.[23]

Table 2.3: ^{1}H NMR chemical shifts for selected protons of compounds **3-6**

Compound number	HC=N (ppm, *J* = Hz)	N-H (ppm)	Aromatic protons (ppm, *J* = Hz)
3	8.87 (d, $^{4}J_{HP}$ = 4.77)	-	7.98 (m, H_e); 7.31 (m, H_c & H_d & H_{Ar}); 6.88 (dd, J_{HH} = 7.51, J_{HP} = 4.48, H_b).
4	-	3.90 (s)	7.58 (m, H_e); 7.40 (m, H_d); 7.23 (m, H_{Ar}); 7.09 (t, $^{3}J_{HH}$ = 7.64, H_c); 6.83 (dd, J_{HH} = 7.32, J_{HP} = 4.39, H_b).
5	9.06 (d, $^{4}J_{HP}$ = 5.10)	-	8.19 (m, H_e); 7.45 (t, $^{3}J_{HH}$ = 7.44, H_d) 7.33 (m, H_c & H_{Ar}); 6.94 (m, H_b).
6	-	4.19 (br s)	7.60 (m, H_e); 7.41 (m, H_{Ar}); 7.31 (t, $^{3}J_{HH}$ = 7.80, H_d); 7.24 (m, H_{Ar}); 7.17 (t, $^{3}J_{HH}$ = 7.60, H_c); 6.76 (dd, J_{HH} = 7.51, J_{HP} = 4.76, H_b).

The aromatic protons of the phenyl groups are observed as multiplets. In the ^{1}H NMR spectrum for **3**, the signal overlaps with those of H_c and H_d whereas for compound **5** the signal overlaps with that of H_c. The protons of the rigid aromatic spacer are observed as a singlet at δ 6.88 and 6.14 for compounds **5** and **6** respectively. This observation is due to the symmetry of the compounds about a two-fold rotation axis.

For compounds **3** and **4**, the protons of the propyl chain are observed upfield in the aliphatic region. For **3** and **4**, the CH_3 protons are observed as a triplet (J ~ 7.40 Hz) at δ 0.75 and 0.73 respectively due to coupling with the adjacent CH_2 protons. The -CH_2- protons are observed as a multiplet at δ 1.51 and 1.26 for **3** and **4** respectively, whilst the remaining N-CH_2- protons of **3** and **4** are observed as a triplet (J ~ 7.00 Hz) at δ 3.44 and 2.39 respectively (Table 2.3).

$^{13}C\{^{1}H\}$ NMR spectroscopy

Compounds **4** and **6** are similar in structure and thus comparable trends are expected in the $^{13}C\{^{1}H\}$ NMR spectra. Several signals in the $^{13}C\{^{1}H\}$ NMR spectra of **4** and **6**, are observed as doublets due to coupling with phosphorus (Table 2.4), including the quaternary carbons (C_f, C_a and *ipso*-C). The signals for the carbons C_f and C_a are observed at *ca.* δ 144 and 135 respectively.

The PPh_2 carbons are observed as doublets in the range δ 128-136. However, for compound **4** one of the carbons is observed as a singlet at δ 128.7 (Table 2.4). The aromatic carbon C_b resonates as a doublet at δ 129.3 ($^2J_{CP}$ = 5.20 Hz) and 131.3 ($^2J_{CP}$ = 9.46 Hz) for compounds **4** and **6** respectively. The signals for the aromatic carbons $C_{c\text{-}e}$ are observed as singlets in the range δ 126-134.

Table 2.4: $^{13}C\{^1H\}$ NMR chemical shifts for selected carbons of compounds **4** and **6**

Compound number	Phenyl group (ppm, *J* = Hz)	Quaternary carbons (ppm, *J* = Hz)
4	136.6 (d, $^1J_{CP}$ = 10.1); 133.9 (d, $^2J_{CP}$ = 20.1); 128.5 (d, $^3J_{CP}$ = 6.87); 128.7 (s).	135.6 (d, $^1J_{CP}$ = 13.5, C_a); 144.6 (d, $^2J_{CP}$ = 24.1, C_f).
6	135.7 (d, $^1J_{CP}$ = 10.3); 133.5 (d, $^2J_{CP}$ = 19.8); 128.8 (d, $^3J_{CP}$ = 6.97); 127.0 (d, $^4J_{CP}$ = 4.40).	134.4 (d, $^1J_{CP}$ = 14.7, C_a); 144.1 (d, $^2J_{CP}$ = 22.0, C_f); 139.7 (s, C_i).

The aromatic carbons of the rigid spacer in compound **6** are observed as singlets at δ 139.7 (C_i) and 113.5 (C_j), which corroborates the statement that these compounds are symmetrical. For compounds **4** and **6**, the carbon C_g is observed as a doublet at δ 52.7 ($^3J_{CP}$ = 20.7 Hz) and 46.1 ($^3J_{CP}$ = 25.7 Hz) respectively due to the three bond coupling experienced with phosphorus. The signals for the carbons C_i, C_j and C_k of the propyl chain are observed in the aliphatic region at δ 51.4, 23.2 and 11.9 respectively for compound **4**. These chemical shifts and coupling constants correspond to those seen in literature for the compound *N*-(2-(diphenylphosphinobenzyl)butylamine, which is similar in structure to compound **4**.[21]

^{31}P NMR spectroscopy

In the ^{31}P NMR spectra of compounds **3** and **5** a peak is observed at δ -13.9 and -12.2 respectively, which is upfield from δ -11.96 (2-diphenylphosphinobenzaldehyde). Upon reduction of **3** and **5**, the peaks shifted upfield to δ -16.1 and -16.9 for compounds **4** and **6** respectively. Similar trends are observed for other ligands as the iminophosphine is reduced to aminophosphine.[21]

Infrared (IR) spectroscopy

The IR spectra of compounds **3** and **4** were recorded using NaCl solution cell (dichloromethane), whilst **5** and **6** were recorded using KBr pellets. For iminophosphine ligands **3** and **5**, the absorption band for the imine bond is observed at 1637 and 1610 cm^{-1} respectively. No absorption band is observed in the imine region for the aminophosphine ligands **4** and **6**, whilst a weak absorption band is observed at 3405 and 3427 cm^{-1} respectively; in the region for N-H stretching frequency of secondary amines.[19] This confirms reduction of the imine bond present in compounds **3** and **5**.

Mass spectrometry

EI^+-mass spectra were recorded for compounds **5** and **6**. The molecular ion peak for **5** and **6** is observed at *m/z* 653 (40 %) and 656 (40 %) respectively. The peaks corresponding to the $[M-H]^+$ ion are observed at *m/z* 652 (94 %) and 655 (100 %) respectively for **5** and **6**.

2.2.3. The synthesis and characterization of *C,N,S*-chelated thiosemicarbazone cyclopalladated tetranuclear complexes (7, 8)

The synthesis of the tetranuclear palladium(II) complexes (**7** and **8**) involves the reaction between the aryl-monothiosemicarbazone ligands (**1** and **2**) and potassium tetrachloropalladate/sodium tetrachloropalladate in an ethanol-water mixture (Scheme 2.3).

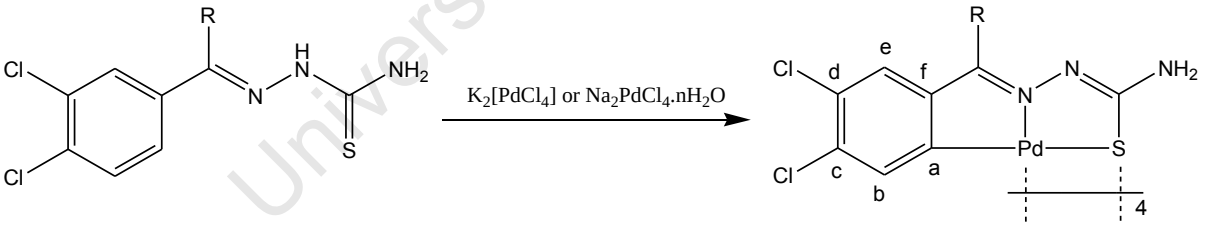

1: R = CH_3
2: R = CH_2CH_3

7: R = CH_3
8: R = CH_2CH_3

Scheme 2.3: The synthesis of the tetranuclear complexes (**7**, **8**).

Physical properties

Compounds **7** and **8** were isolated as yellow powders in low yields of 44 and 25 % respectively (Table 2.5). The onset of decomposition without melting is observed at 322 and 327 ˚C for **7** and **8** respectively. The compounds show solubility in ethyl acetate, tetrahydrofuran and dimethyl sulfoxide, whilst **7** also shows good solubility in diethyl ether and **8** in dichloromethane and toluene.

Table 2.5: Physical appearance, melting point and yield of the tetranuclear complexes (**7**, **8**)

Compound number	R	Yield (%)	Physical Appearance	Melting point (˚C)
7	CH_3	44	Yellow powder	Decomp. without melt: 327-331
8	CH_2CH_3	25	Yellow powder	Decomp. w/o melt 322-327

^{1}H NMR spectroscopy

The NMR spectra of compounds **7** and **8** were recorded in DMSO-d_6. It is observed that upon complexation, the peak associated with the hydrazinic proton is absent in the ^{1}H NMR spectra due to formation of a second C=N bond as a result of chelation of the ligand in the thiolate form. The aromatic proton H_e resonates as a singlet at δ 6.72 and 6.65 for **7** and **8**, whilst the peak for H_b is observed as a singlet at δ 7.37 and 7.34 for **7** and **8** respectively (see appendix, pg. 133). Observing a singlet for H_b, and the absence of a peak for H_a, suggests that the Pd-C bond has formed.

The amine protons for compounds **7** and **8** resonate as a singlet at δ 7.07 and 7.16 respectively. With the formation of the Pd-S bond in the complex, there is free rotation about the amine bond, which results in one signal for the amine protons.[3,8] The peak for the methyl protons in compound **7** is observed as a singlet at δ 2.00, while vicinal coupling with two protons results in the observation of a triplet ($^3J_{HH}$ = 7.00 Hz) at δ 1.06 for the CH_3 protons of compound **8**. The CH_2 protons for compound **8** are observed as two quartets at δ 1.79 ($^3J_{HH}$ = 7.32 Hz) and 2.86 ($^3J_{HH}$ = 7.71 Hz), where one quartet corresponds to one proton. The data corresponds to that reported in literature.[3]

Infrared (IR) spectroscopy

When the ligand chelates to the palladium in a *C,N,S* tridentate fashion, electron density is donated onto the metal. In order to stabilize the metal, electron density is donated from the metal to empty π*-orbitals of the nitrogen, which results in a change in the length of the imine bond.[11,19] However, due to the distribution of electron density across the compound, the two imine bonds have similar lengths, and thus only one absorption band is observed in the IR spectrum.

Table 2.6: The imine absorption bands observed in the IR spectra of complexes (**7**, **8**)

Compound number	C=N *v* (cm^{-1})
7	1600
8	1595

For compounds **7** and **8**, the imine absorption band shifted from 1594 and 1596 cm^{-1} in the ligand (**1** and **2**), to 1600 and 1595 cm^{-1} respectively (Table 2.6).[19] These absorption bands correspond to literature data.[3]

Molecular structure of complex 7

Single crystals, crystallized with three molecules of tetrahydrofuran, were obtained from the slow evaporation of a solution of compound **7** dissolved in tetrahydrofuran/hexane. The molecular structure of **7** was determined by single-crystal X-ray diffraction, and is shown in Fig. 2.2. Table 2.7 list the crystallographic data, while selected bond lengths and angles are given in Table 2.8.

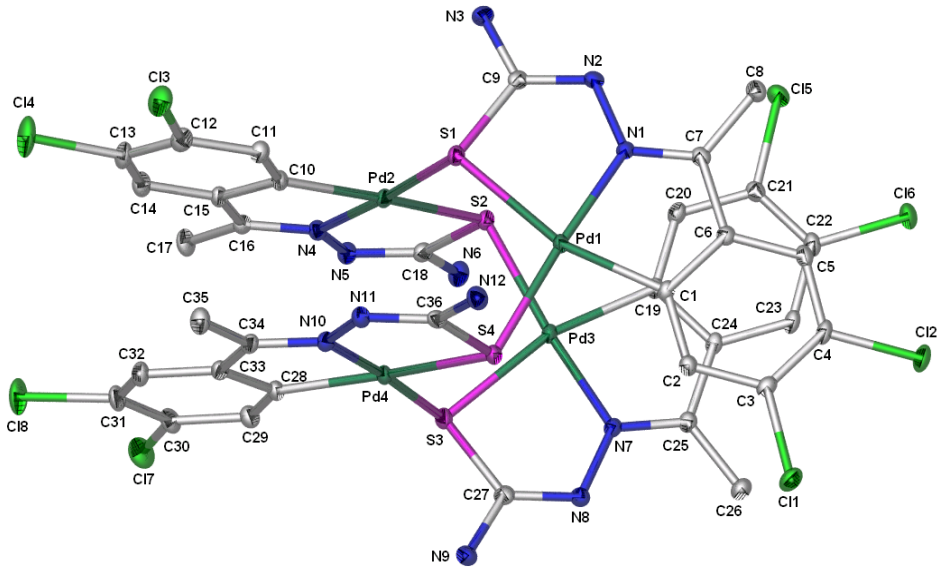

Figure 2.2: The molecular structure of compound **7**.

Compound **7** crystallizes in a monoclinic system with space group *P*21/*n* (Table 2.7). The formation of the expected two 5-membered rings are seen as the thiosemicarbazone ligand chelates to the palladium(II) ion in a tridentate *C*,*N*,*S*-mode.[3,14] The Pd_4S_4 core reported in literature is observed in Figure 2.2, whereby the four cyclopalladated units are situated around the core.[13,24-25]

Table 2.8: Crystal data and structure refinement data for compound **7**

Empirical formula	$C_{36}H_{28}Cl_8N_{12}Pd_4S_4.3C_4H_8O$
Formula weight	1682.46
Temperature (K)	173(2)
Wavelength (Å)	0.71073
Crystal system	Monoclinic
Space group	*P*21/*n*
a (Å)	16.4634(9)
b (Å)	9.1883(5)
c (Å)	38.962(2)
α (˚)	90
β (˚)	93.4590(10)
γ (˚)	90
V (Å^3)	5883.1(6)
Z	4
D_{calc} (Mg.m^{-3})	1.900
Absorption coefficient (mm^{-1})	1.762
F(000)	3328
Crystal size (mm^3)	0.18 x 0.17 x 0.16
θ Range for data collection (˚)	2.06 to 28.40
Index range	$-22 \leq h \leq 19$; $-10 \leq k \leq 12$; $-52 \leq l \leq 52$
Reflections collected	67481
Independent reflections [*R*(int)]	14734 [0.0604]
Data / restraints / parameters	14734 / 0 / 723
Goodness-of-fit on F^2	1.011
Transmission	0.7658, 0.7422
Final *R* indices [$I>2\sigma(I)$]	R_1 = 0.0365, wR_2 = 0.0681
R indices (all data)	R_1 = 0.0598, wR_2 = 0.0758
Largest difference in peak and hole (e. Å $^{-3}$)	0.722 and -0.520

Upon formation of compound **7**, the bonds N(1)-C(7) and N(2)-C(9) have equal bond lengths of 1.303(4) Å, which confirms the formation of the second imine bond (Table 2.8). The S(1)-C(9) bond has a length of 1.787(4) Å, which is longer than that of the imine bond suggesting a loss of double bond character. This confirms that upon formation of the cyclopalladated

complex, the thiosemicarbazone chelates to the palladium in the thiolate form. For a perfect four-coordinate planar geometry, the sum of the acute and obtuse angles around the palladium(II) centre would be equal to 720˚. Compound **7** has a slightly distorted square-planar geometry around the metal centre, where the sum of the aforementioned angles deviates from 720˚ by approximately 20˚ (Table 2.8).

Table 2.8: Selected bond lengths (Å) and angles (˚) for compound **7**.

Pd(1)-N(1)	2.002(3)	N(1)-Pd(1)-C(1)	81.24(13)
Pd(1)-C(1)	1.998(3)	N(1)-Pd(1)-S(1)	83.15(8)
Pd(1)-S(1)	2.3637(9)	N(1)-Pd(1)-S(4)	175.63(8)
Pd(1)-S(4)	2.3194(9)	S(4)-Pd(1)-S(1)	100.56(3)
S(1)-C(9)	1.787(4)	C(1)-Pd(1)-S(4)	94.91(10)
N(1)-C(7)	1.303(4)	C(1)-Pd(1)-S(1)	164.06(11)
N(2)-C(9)	1.303(4)	Pd(1)-S(4)-Pd(4)	110.11(4)

2.2.4. The synthesis and characterization of *C,N,S*-chelated thiosemicarbazone cyclopalladated complexes containing P-donor ligands

a. Mononuclear *C,N,S*–chelated thiosemicarbazone cyclopalladated complexes (9-11)

The mononuclear cyclopalladated complexes (**9-11**) were synthesized by reacting the tetranuclear complexes (**7** or **8**) with the P-donor ligands, PTA or aminophosphine (**4**) (Scheme 2.4). According to the HSAB (Hard Soft Acid Base) principle, the Pd(II) ion is a soft acid, whilst sulfur and phosphorus donor ligands are soft bases.[26] In addition to it being more likely that a stronger bond would form via the softer phosphorus atom than the borderline amine nitrogen, there is a greater chance of coordination occurring via phosphorus as it is a stronger base. Due to the basicity of the phosphorus donor ligands, there is competition between the phosphorus and the sulfur, which leads to the cleavage of the Pd-$S_{bridging}$ bond in the tetranuclear complex and the insertion of the phosphorus ligand into the fourth coordination site on the metal.

The essential structural feature of cell membranes is the phospholipid bilayer, and thus if a compound enters the cell via membrane crossing, factors such as lipophilicity becomes important. A compound should ideally be lipophilic enough to interact and cross the membrane into the cell, but not too lipophilic that it is retained at the membrane. Therefore, various ligands such as 1,3,5-triaza-7-phosphaadamantane (PTA) may be incorporated into a

compound. As seen in Section 2.2.2., aminophosphine ligands have also been synthesized. However, when the complex [Pd(3,4-dichloroacetophenone thiosemicarbazone)(N-(2-(diphenylphosphino)benzylidene)propan-1-amine)] was synthesized, and attempts were made to purify by column chromatography (silica gel), the imine bond in the complex was hydrolysed and the aldehyde starting material remained coordinated to palladium. Therefore, the aminophosphine ligand (**4**) was synthesized and used to synthesize compound **11**.

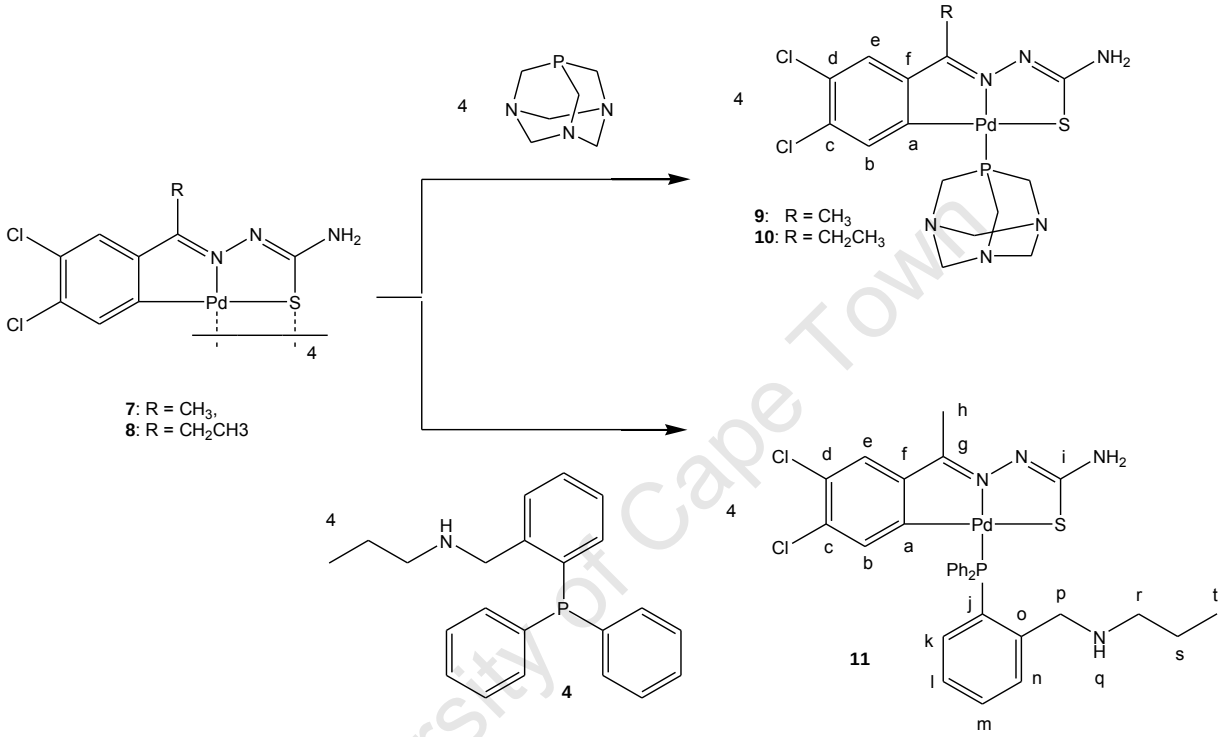

Scheme 2.4: The reaction between the tetranuclear complex (**7** or **8**) and the P-donor ligands, PTA or the aminophosphine (**4**).

Physical properties

Compounds **9-11** were isolated as yellow powders in varying yields between 40-94 % (Table 2.9). Compounds **9-11** melt in ranges noted in Table 2.9. The compounds are soluble in chloroform, tetrahydrofuran and dimethyl sulfoxide. Compounds **10** and **11** are also soluble in dichloromethane, acetone and ethyl acetate.

Table 2.9: Melting points and yields of the mononuclear complexes (**9-11**)

Compound number	R	Yield (%)	Melting point (˚C)
9	CH_3	94	243.0-248.4
10	CH_2CH_3	74	235.9-239.4
11	CH_3	40	179.7-184.1

The NMR spectra were recorded using DMSO-d_6.

^{1}H NMR spectroscopy

As the Pd-$S_{bridging}$ bond is cleaved, the mononuclear complex is formed. The peak associated with the aromatic proton H_b of compounds **9** and **11** is observed as a doublet (J ~ 3.50 Hz) at δ 7.10 and 6.13 which is due to a four bond coupling with the phosphorus of the P-donor ligand (see appendix, pg 134). The peak associated with H_b of compound **10** is observed as a broad signal at δ 7.11. A doublet is expected for compound **10**, and perhaps further resolving of the broad signal would reveal a doublet, with a coupling constant comparable to that seen for compounds **9** and **11.**

The peak corresponding to the aromatic proton H_e is shifted downfield when compared to that seen for **7** and **8**, to *ca.* δ 7.25. With the formation of the mononuclear complex, H_b became more shielded whilst H_e became more deshielded. The electron density donated by the ligand may have shielded H_b when compared to the tetranuclear complex whilst when the imine bond donates electron density onto the metal, H_e is more deshielded.

Table 2.10: ^{1}H NMR chemical shifts for selected protons of compounds **9-11**

Compound number	PTA protons (ppm, J = Hz)		Aromatic protons (ppm, J = Hz)
	PCH_2N	**N-$CH_{2(eq)}$-N N-$CH_{2(ax)}$-N**	
9	4.27 (s)	4.59 (d, J_{HP} = 12.4) 4.44 (d, J_{HP} = 13.2)	7.27 (s, H_e); 7.10 (d, $^4J_{HP}$ = 3.42, H_b).
10	4.26 (s)	4.58 (d, J_{HP} = 12.8) 4.44 (d, J_{HP} = 12.8)	7.27 (br s, H_e); 7.11 (br s, H_b).
11	-	-	7.74 (m, H_n); 7.49 (m, H_k & H_{Ar}); 7.32 (t, $^3J_{HH}$ = 7.70, H_l); 7.23 (s, H_e); 7.00 (m, H_m); 6.13 (d, $^4J_{HP}$ = 3.85, H_b).

The signal for the amine protons of the thiosemicarbazone unit shifted slightly upfield to *ca.* δ 7.00 for compounds **9**-**11**. For compounds **9** and **10**, a singlet associated with the PCH_2N protons of PTA is observed at *ca.* δ 4.27. The NCH_2N protons are in an AB spin system resulting in two doublets corresponding to the different environments experienced by the axial and equatorial NCH_2N. The doublet associated with the protons in the axial and equatorial protons are observed at δ 4.44 and *ca.* δ 4.58 respectively for **9** and **10** (Table 2.10).[2]

For compound **11**, a multiplet observed at δ 7.49 is associated with the overlapping signals of the phenyl protons as well as the aromatic H_k proton. The multiplets observed at δ 7.74 and 7.00 correspond to the protons H_n and H_m, due to coupling with adjacent protons, as well as phosphorus. A triplet observed at δ 7.32 ($^3J_{HH}$ = 7.70 Hz) corresponds to H_l, which is due to coupling with H_k and H_m (Table 2.10).

For compound **11**, the signal for the proton H_p is observed as a singlet at δ 4.12. The CH_3 (H_t) protons of the propyl chain are observed as a triplet ($J \sim 7.28$ Hz) at δ 0.71, due to coupling with the adjacent CH_2 protons. The signal for the -CH_2- protons is observed as a multiplet at δ 2.26 due to coupling with adjacent H_t and H_r protons of the propyl chain. The peak corresponding to the H_r protons overlaps with the DMSO-d_6 peak, which was confirmed using 2D (HSQC) NMR spectroscopy.

For compound **9**, the singlet corresponding to the methyl protons shifted downfield to δ 2.21 from δ 2.00 for compound **7**. For compound **10**, a triplet ($^3J_{HH}$ = 7.60 Hz) is observed at δ 1.02 which corresponds to the methyl protons. One quartet ($^3J_{HH}$ = 7.60 Hz) is observed at δ 2.70 for the -CH_2- protons as opposed to the two quartets observed for compound **8**. For compound **11**, the H_h protons are observed as a singlet at δ 2.22.

$^{13}C\{^1H\}$ NMR spectroscopy

For compounds **9**-**11**, the signal for the thiolate carbon shifted downfield to *ca.* δ 177.0 when compared to that observed for the tetranuclear complexes (Table 2.11).[3] For compound **11**, a doublet (J = 9.43 Hz) is observed due to three bond coupling with phosphorus. The imine carbons are observed at δ 163.6, 168.3 and 172.4 for compounds **9**-**11** respectively.

For compounds **9** and **10**, the aromatic carbons C_{a-f} are observed as singlets at *ca.* δ 164.0, 127.2, 136.0, 130.6, 127.0 and 152.5 respectively. For **11**, the aromatic carbons C_a, C_f, C_{c-e} are observed as singlets at δ 163.7, 153.2, 131.3, 130.8 and 126.7. The aromatic carbons C_b as well as the remaining aromatic carbons are observed as doublets in the range δ 127.2-163.6 due to coupling with phosphorus (Table 2.11).

The carbons of PTA, NCH_2N and PCH_2N, are observed as doublets at δ 72.4 ($^3J_{CP}$ = 7.40 Hz) and 51.5 ($^1J_{CP}$ = 15.5 Hz) for **9** and **10**. The carbons of the alkyl chains are observed in the aliphatic region of the spectra. The methyl carbon of the thiosemicarbazone unit is observed at δ 13.6, 11.5 and 13.7 for compounds **9**, **10** and **11** respectively. The CH_2 group of compound **10** is observed at δ 20.0. In the ^{13}C NMR spectrum of **11**, the C_t, C_s and C_r carbons resonate as singlets at δ 12.0, 51.5 and 56.2 whilst C_p is observed as a doublet at δ 52.8 ($^3J_{CP}$ = 12.8 Hz).

Table 2.11: $^{13}C\{^1H\}$ NMR shifts for selected carbons of compounds **9-11**

Compound number	**PCH_2N NCH_2N (ppm, *J* = Hz)**	**C-S (ppm, *J* = Hz)**	**C=N (ppm)**	**Aromatic carbons (ppm, *J* = Hz)**
9	51.5 (d, J_{CP} = 15.5); 72.4 (d, J_{CP} = 7.40)	177.2 (s)	163.7 (s)	163.6 (s, C_a); 153.2 (s, C_f); 136.4 (s, C_c); 130.6 (s, C_d); 127.2 (s, C_b); 127.1(s, C_e).
10	51.5 (d, J_{CP} = 15.5); 72.4 (d, J_{CP} = 7.40)	177.4 (s)	168.3 (s)	164.2 (s, C_a); 151.9 (s, C_f); 136.6 (s, C_c); 130.6 (s, C_d); 127.2 (s, C_b); 127.0 (s, C_e).
11	-	177.2 (d, $^3J_{CP}$ = 9.43)	172.4 (s)	163.6 (d, $^2J_{CP}$ = 4.70, C_o); 145.2 (d, $^3J_{CP}$ = 11.4, C_n); 135.9 (d, $^1J_{CP}$ = 8.10, C_j); 135.0 (d, $^1J_{CP}$ = 12.8, C_{Ph}); 130.7 (d, $^2J_{CP}$ = 8.10, C_{Ph}); 130.1 (d, $^4J_{CP}$ = 3.40, C_{Ph}); 129.3 (d, $^2J_{CP}$ = 10.1, C_b); 127.2 (d, $^3J_{CP}$ = 8.10, C_{Ph}).

^{31}P NMR spectroscopy

A singlet is observed at δ -49.5, -49.6 and 29.5 in the ^{31}P NMR spectra for compounds **9**-**11** respectively. This testifies to the presence of only one phosphorus species and no unreacted ligand. These values correspond to chemical shifts for similar compounds.[2-3]

Infrared (IR) spectroscopy

Upon displacement of the Pd-$S_{bridging}$ bond by the PTA or aminophosphine ligand, the absorption band for the imine bond chelated to the metal is found at a lower wavenumber for **9**-**11** when compared to the tetranuclear complexes **7** and **8** (Table 2.6).

For compounds **9**-**11**, the second C=N absorption band is observed at a higher wavenumber when compared to compounds **7** and **8** (Table 2.12). The P-donor ligand donates electron density onto the metal. When back-donation occurs, more electron density is donated to the P-donor ligand when compared to the atoms of the thiosemicarbazone. Therefore, less electron density is located on the C=N bonds when compared to the tetranuclear complex.[3]

Table 2.12: The absorption bands of the imine bond in the IR spectra (**9**-**11**)

Compound number	C=N ν (cm^{-1})
9	1624, 1574
10	1641, 1559
11	1618, 1582

Mass spectrometry

For compounds **9** and **10**, the EI^+-mass spectra were recorded, whilst the ESI^+-mass spectrum was recorded for **11**. The molecular ion peak for compounds **9**-**11** is observed at *m/z* 524 (4 %), 538 (2.4 %) and 700 (45 %) respectively. The base peak for compound **11** is observed at *m/z* 701 (100 %) which corresponds to the $[M+H]^+$ ion.

Molecular structure of complex 10 and 11

Single crystals of compound **10** were obtained by the slow diffusion of hexane into a minimal amount of tetrahydrofuran, which the compound had been dissolved in. The slow evaporation of a solution of compound **11** dissolved in chloroform/hexane allowed for the formation of crystals with two molecules of chloroform. The molecular structures of **10** and **11** were

determined by single-crystal X-ray diffraction, and are shown in Fig. 2.3. Table 2.13 lists selected bond lengths and angles, and the crystallographic data is given in Table 2.14.

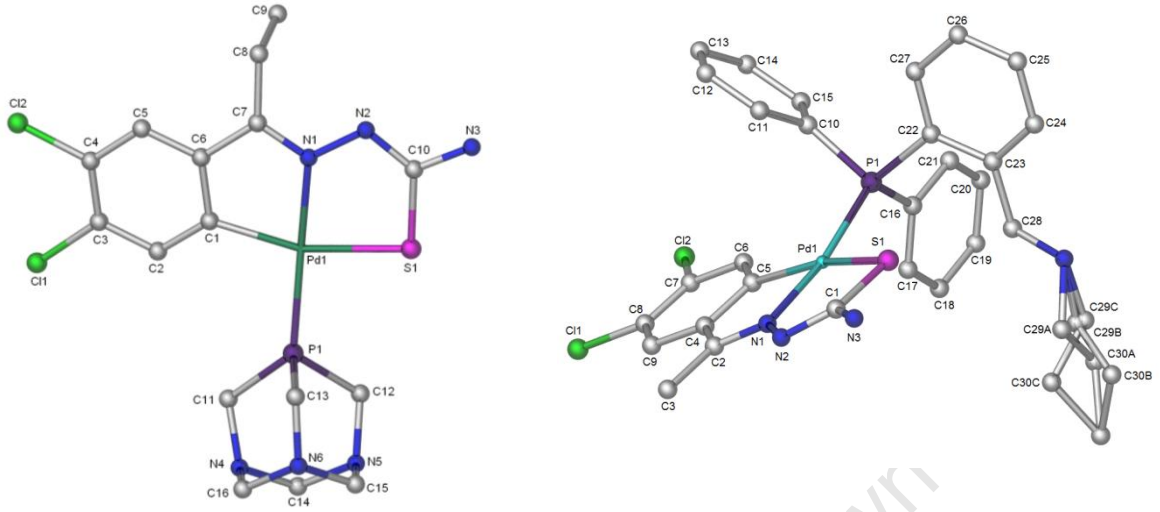

a) **b)**

Figure 2.3: The molecular structure of compound **10** (a) and **11** (b).

Table 2.13: Selected bond lengths (Å) and angles (°) for compounds **10** and **11**.

10		**11**	
Bond lengths			
Pd(1)-N(1)	2.022(2)	Pd(1)-N(1)	2.033(5)
Pd(1)-C(1)	2.024(3)	Pd(1)-C(5)	2.029(4)
Pd(1)-P(1)	2.2412(7)	Pd(1)-P(1)	2.2571(14)
Pd(1)-S(1)	2.3397(7)	Pd(1)-S(1)	2.3181(15)
S(1)-C(10)	1.768(3)	S(1)-C(1)	1.755(6)
N(2)-C(10)	1.310(3)	N(2)-C(1)	1.331(8)
N(1)-C(7)	1.302(3)	N(1)-C(2)	1.298(7)
Bond angles			
N(1)-Pd(1)-C(1)	80.71(10)	N(1)-Pd(1)-C(5)	81.34(18)
N(1)-Pd(1)-S(1)	83.19(6)	N(1)-Pd(1)-S(1)	83.24(13)
C(1)-Pd(1)-P(1)	101.45(8)	C(5)-Pd(1)-P(1)	96.42(14)
P(1)-Pd(1)-S(1)	95.16(2)	P(1)-Pd(1)-S(1)	99.11(5)
C(1)-Pd(1)-S(1)	163.28(8)	C(5)-Pd(1)-S(1)	164.47(14)
N(1)-Pd(1)-P(1)	170.63(6)	N(1)-Pd(1)-P(1)	171.14(15)

Table 2.14: Crystal data and structure refinement data for compound **10** and **11**

	10	**11**
Empirical formula	$C_{16}H_{21}Cl_2N_6PPdS$	$C_{31}H_{31}Cl_2N_4PPdS.2CHCl_3$
Formula weight	537.72	938.66
Temperature (K)	173(2)	173(2)
Wavelength (Å)	0.71073	0.71073
Crystal system	Monoclinic	Triclinic
Space group	*C*2/*c*	*P*-1
a (Å)	35.7802(19)	11.7431(9)
b (Å)	6.9559(4)	12.8847(11)
c (Å)	16.2229(9)	14.7987(11)
α (˚)	90	69.656(2)
β (˚)	92.3610(10)	84.069(2)
γ (˚)	90	72.202(2)
V (Å^3)	4034.2(4)	1999.0(3)
Z	8	2
D_{calc} (Mg.m^{-3})	1.771	1.542
Absorption coefficient (mm^{-1})	1.383	1.120
F(000)	2160	924
Crystal size (mm^3)	0.09 x 0.08 x 0.07	0.07 x 0.08 x 0.12
θ Range for data collection (˚)	2.28 - 28.44	1.8 - 28.3
Index range	$-47 \leq h \leq 47$; $-9 \leq k \leq 9$; $-21 \leq l \leq 21$	$-15 \leq h \leq 14$; $-17 \leq k \leq 17$; $-11 \leq l \leq 19$
Reflections collected	35350	21501
Independent reflections [*R*(int)]	5077 [0.0666]	9946 [0.041]
Data / restraints / parameters	5077 / 0 / 244	9946 / 21 / 414
Goodness-of-fit on F^2	1.009	1.042
Transmission	0.9094, 0.8857	0.9256, 0.8772
Final *R* indices [$I>2\sigma(I)$]	R_1 = 0.0291, wR_2 = 0.0586	R_1 = 0.0664, wR_2 = 0.1719
R indices (all data)	R_1 = 0.0443, wR_2 = 0.0644	R_1 = 0.0928, wR_2 = 0.1909
Largest difference in peak and hole (e. Å $^{-3}$)	0.469 and -0.457	1.98 and 1.51

Compound **10** crystallizes in a monoclinic system and space group *C*2/*c*. The formation of the expected two 5-membered rings are observed as the thiosemicarbazone ligand bonds to the palladium(II) ion in a tridentate *C,N,S*-mode.[3,14] The fourth coordination site on the metal is occupied by the PTA ligand. Compound **11** crystallizes in a triclinic system with a *P*-1 space group. For compound **11**, the propyl chain was disordered and carbons 29 and 30 were refined with equal site occupancy factors of one-third each. As seen with **10**, the thiosemicarbazone chelates to the palladium(II) ion in a tridentate mode with the aminophosphine occupying the fourth coordination site.

Upon formation of compounds **10** and **11**, the imine bond containing the nitrogen coordinated to palladium is slightly shorter than that observed for compound **7**, while the second C=N bond is slightly longer (Tables 2.8 and 2.13). The S(1)-C(10) (**10**) and S(1)-C(1) (**11**) bonds have lengths of *ca.* 1.76 Å, which is slightly shorter than that observed for **7** (Table 2.8).

Compounds **10** and **11** have slightly distorted square-planar geometries around the palladium centre. For compounds **10** and **11**, the bond angles formed between the ligands and the palladium centre deviates from that expected for square-planar complexes, where as seen with compound **7**, the sum of the acute and obtuse angles deviate from 720˚ (Table 2.13). This observed geometry corresponds to that seen with other similar cyclopalladated complexes containing phosphorus ligands.[3,8,14-15]

b. Binuclear *C,N,S*-chelated thiosemicarbazone cyclopalladated complexes (12)

The binuclear complex (**12**) was synthesized by reacting the tetranuclear complex (**7**) with the aminophosphine ligand (**6**) in acetone. The aminophosphine ligand occupies the fourth coordination site on palladium via phosphorus (Scheme 2.5) where it is used as a bridging ligand between two cyclopalladated thiosemicarbazone units.

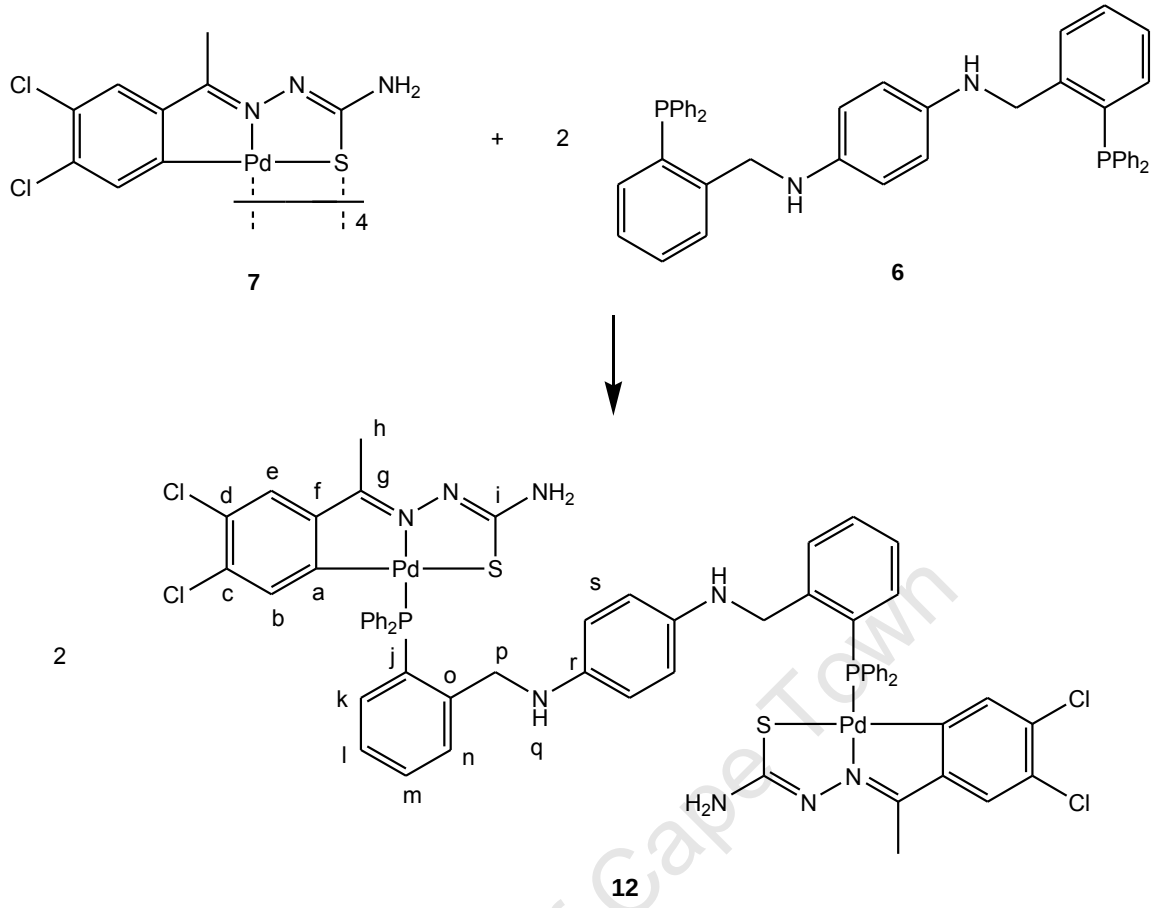

Scheme 2.5: The reaction between the tetranuclear complex (**7**) and the aminophosphine ligand (**6**)

Physical properties

Compound **12** was isolated as a bright yellow powder in moderate yield of 58 %, and melted in the range 246.5-249.3 ˚C. Compound **12** is soluble in dichloromethane, chloroform and dimethyl sulfoxide.

The NMR spectra were recorded using DMSO-d_6.

^{1}H NMR spectroscopy

Upon formation of compound **12**, a doublet is observed at δ 6.18 ($^4J_{HP}$ = 3.70 Hz), which corresponds to the aromatic proton H_b, due to coupling with the phosphorus of the aminophosphine ligand. A multiplet observed at δ 7.50 corresponds to the overlapping signals for the aromatic protons H_k, H_n and the phenyl groups. The multiplet observed at δ 7.08, due to coupling with protons on adjacent carbons is associated with the aromatic proton H_m.

The proton H_l is observed as a triplet (J = 7.50 Hz) at δ 7.35 due to coupling with adjacent aromatic protons H_k and H_n. A singlet is observed for both the aromatic protons H_e and H_s at δ 7.21 and 5.87 respectively. As seen with compound **6**, the protons of the aromatic spacer resonate as a singlet due to the symmetrical nature of the compound. The amine protons of the thiosemicarbazone unit and aminophosphine ligand are observed as broad signals at δ 6.91 and 5.32 respectively. The -CH_2-N protons are observed as a broad signal at δ 4.65 whereas the CH_3 protons resonate as a singlet at δ 2.24.

$^{13}C\{^1H\}$ NMR spectroscopy

In the ^{13}C NMR spectrum for compound **12**, the signal for the thiolate carbon is observed at δ 177.1 (J = 10.1 Hz) due to three bond coupling with phosphorus. The imine carbon resonates as a singlet at δ 164.0. The carbons of the phenyl groups are observed as doublets in the aromatic region δ 127.0-135.0 (Table 2.15).

Table 2.15: $^{13}C\{^1H\}$ NMR chemical shifts for selected carbons of compound **12**

Phenyl carbons (ppm, J = Hz)	**Aromatic carbons (ppm, J = Hz)**
135.0 (d, $^1J_{CP}$ = 12.1, C_{Ph}); 130.1 (d, $^4J_{CP}$ = 3.89, C_{Ph}); 129.3 (d, $^2J_{CP}$ = 10.4, C_{Ph}); 127.0 (d, $^3J_{CP}$ = 10.8, C_{Ph}).	163.5 (d, $^2J_{CP}$ = 4.71, C_o); 144.6 (d, $^3J_{CP}$ = 10.1, C_n); 135.7 (d, $^3J_{CP}$ = 7.40, C_j); 133.0 (d, $^2J_{CP}$ = 3.40, C_k); 128.6 (d, $^3J_{CP}$ = 8.17, C_b).

The signals for the aromatic carbons C_a, $C_{c\text{-}f}$ and $C_{l\text{-}m}$ are observed as singlets at δ 163.3, 130.3, 130.8, 153.3, 126.8 and 131.8 respectively. The quaternary carbon C_r as well as the remaining aromatic carbons (C_s) of the rigid spacer resonates as singlets at δ 140.0 and 114.0 respectively. The aromatic carbons C_b, $C_{j\text{-}k}$ and $C_{n\text{-}o}$ are observed as doublets in the region δ 128.6-163.5 due to coupling with phosphorus (Table 2.15). A doublet observed at δ 47.9 ($^3J_{CP}$ = 14.8 Hz) corresponds to C_p whilst the methyl carbon is observed as a singlet at δ 13.8.

^{31}P NMR spectroscopy

A single peak is observed at δ 29.0, which is upfield from δ -16.9. This is comparable with the chemical shift observed for **11**, the mononuclear complex.

Infrared (IR) spectroscopy

Compound **12** contains two imine bonds, and thus two absorption bands are observed in the IR spectrum at 1597 and 1574 cm^{-1}. Upon moving from the tetranuclear complex to the binuclear complex, the absorption band for both imine bonds shifts to a lower wavenumber. The absorption band associated with the imine bond not directly coordinated to the metal is expected to shift to a higher wavenumber as seen with **11** (Section 2.2.4.a.).

Mass spectrometry

In the ESI^+ mass spectrum of compound **12**, the molecular ion peak and the $[M+H]^+$ ion are observed at *m/z* 1390 (10 %) and 1391 (12 %) respectively.

2.2.5. The synthesis and characterization of *C,N,S*-chelated thiosemicarbazone cyclopalladated complexes containing N-donor ligands (13-15)

Mono- (**13**) and binuclear (**14** and **15**) complexes containing pyridyl ligands were synthesized by reacting the tetranuclear complex **7** with N-donor ligands 4-picoline, 4,4'-dipyridyl and 1,2-bis(4-pyridyl)ethylene (Scheme 2.6). According to the HSAB (Hard Soft Acid Base) principle, Pd(II) and sulfur are soft acids and bases respectively, while pyridyl ligands are borderline bases and not as basic as sulfur.[26] Therefore, the cleavage of $Pd\text{-}S_{bridging}$ bonds by a borderline base will not occur as readily as when a softer base is used. These reactions occurred sluggishly in comparison to those in Section 2.2.4, and harsh conditions (e.g. high temperatures) were required for cleavage to occur.

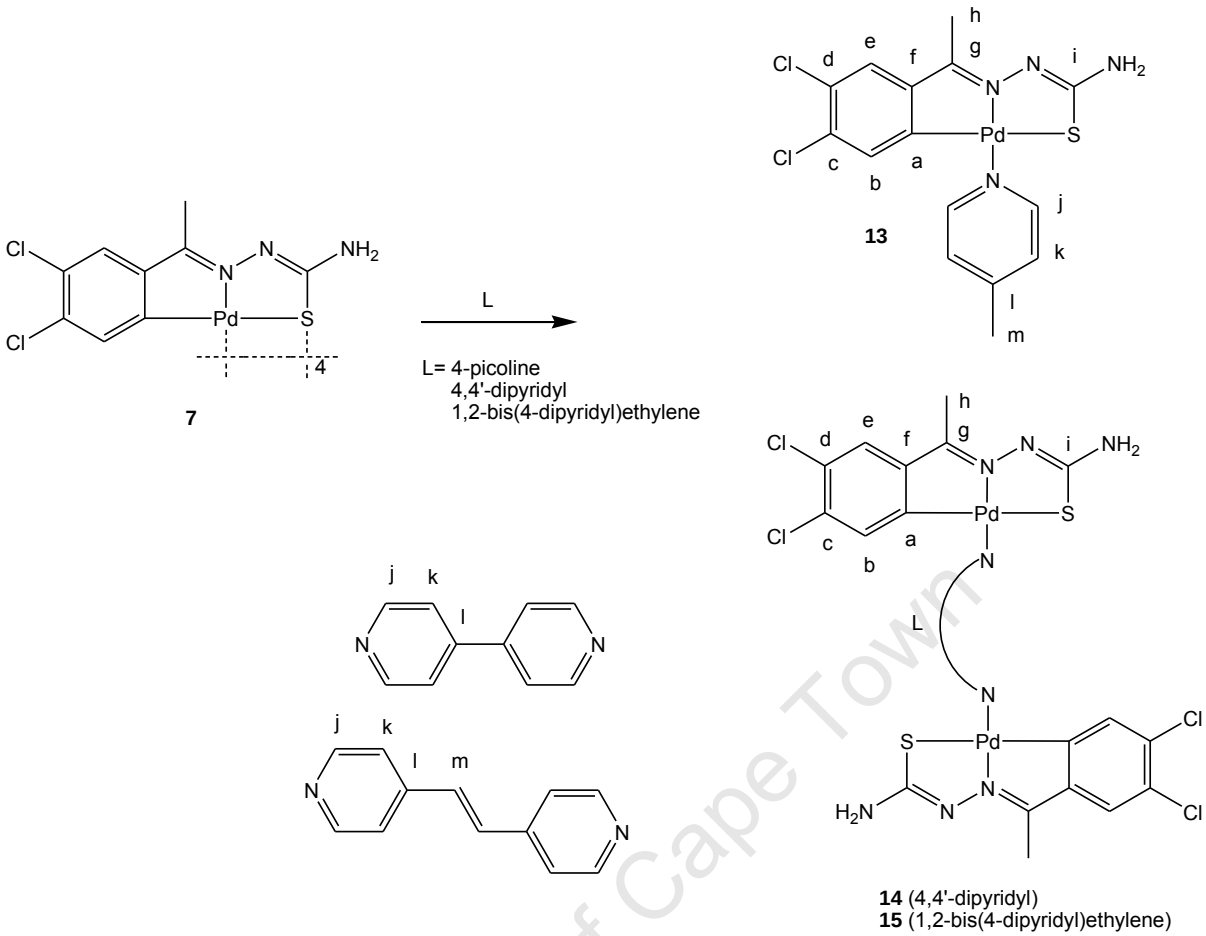

Scheme 2.6: The reaction of the tetranuclear complex (**7**) with the N-donor ligands, 4-picoline (**13**), 4,4'-dipyridyl (**14**) and 1,2-bis(4-pyridyl)ethylene (**15**) .

Physical properties

The compounds were isolated as yellow (**13** and **15**) and brown (**14**) powder in low to moderate yields (Table 2.16). The compounds exhibit high thermal stability and decompose without melting (Table 2.16). The compounds are soluble in dimethyl sulfoxide and tetrahydrofuran. Compound **13** is also soluble in ethyl acetate, dichloromethane and acetone, while compound **15** is also soluble in diethyl ether and ethyl acetate.

Table 2.16: Physical appearance, melting point and yield of the complexes **13-15**

Compound number	Yield (%)	Physical Appearance	Melting point (˚C)
13	69	Yellow powder	Decomp. w/o melting 311.0
14	34	Brown powder	Decomp. w/o melting 287.8
15	15	Yellow powder	Decomp. w/o melting 274.6

The NMR spectra were recorded using DMSO-d_6.

^{1}H NMR spectroscopy

The NMR spectra of compounds **13-15** were recorded using DMSO-d_6. The H_b and H_e protons are observed as singlets at *ca.* δ 7.38 and 6.73 respectively. The amine protons are observed as broad signals at δ 7.08 for compounds **13** and **15**, while a peak is observed at δ 7.19 for compound **14**.

The pyridyl protons H_j resonate as a doublet ($^3J_{HH}$ = 5.86 Hz) at δ 8.41 and 8.59 for compounds **13** and **15** respectively, and a broad signal is observed for compound **14** at δ 8.73. A doublet is observed at δ 7.20 ($^3J_{HH}$ = 4.90 Hz) and 7.59 ($^3J_{HH}$ = 5.86 Hz) for the H_k protons of compounds **13** and **15** respectively. The H_k protons of compound **14** resonate as a broad signal at δ 7.83.

A singlet observed at δ 7.50 corresponds to the H_m protons of the ethylene bridge in compound **15**. The methyl protons of the thiosemicarbazone unit are observed as a singlet at δ 2.00 for the compounds whilst the methyl group on the 4-picoline ligand is observed at δ 2.31 for compound **13**.

No change in the chemical shift is observed for the complexes when compared to the starting material. This suggests that either the complex dissociates in solution, or that the bond between the palladium and the nitrogen is so weak that the effect on the shifts is minimal. However, when stoichiometric amounts of the tetranuclear complex and the ligand are used to synthesize the binuclear complexes, it has been observed that in certain cases the integration of peaks associated with the thiosemicarbazone protons account for only one unit. This suggests that only one of the pyridyl nitrogens has a cyclopalladated unit coordinated to it.

^{13}C{^{1}H} NMR spectroscopy

The thiolate carbon resonates as a singlet at *ca.* δ 167.0, with the imine carbon being observed as a singlet at *ca.* δ 165.5. The aromatic carbons of the thiosemicarbazone unit are observed as singlets in the range δ 121.8-164.8 (Table 2.17). The pyridyl carbons resonate as

singlets at *ca.* δ 150.0 for the carbons C_j and C_k. For compound **13** the C_l carbon is observed at δ 146.5, while C_l is observed at δ 133.6 for compounds **14** and **15**.

The carbon of the ethylene bridge, C_m, of compound **15** is observed as a singlet at δ 131.1. The methyl group of the thiosemicarbazone unit is observed at *ca.* δ 14.0 for compounds **13-15** and the H_m of compound **13** is observed at δ 20.2.

Table 2.17: $^{13}C\{^1H\}$ NMR shifts for selected carbons of compounds **13-15**

Compound number	Pyridyl carbons (ppm)	Aromatic carbons (ppm)
13	149.6 (s, C_j & C_k); 146.5 (s, C_l).	164.0 (s, C_a); 149.1 (s, C_f); 132.8 (s, C_c); 125.8 (s, C_d); 126.6 (s, C_e); 124.4 (s, C_b).
14	151.1 (s, C_j & C_k); 133.6 (s, C_l).	164.8 (s, C_a); 150.4 (s, C_f); 129.7 (s, C_c); 126.5 (s, C_d); 126.4 (s, C_e); 121.8 (s, C_b).
15	150.7 (s, C_j & C_k); 133.6 (s, C_l); 131.1 (s, C_m).	164.8 (s, C_a); 150.4 (s, C_f); 129.7 (s, C_c); 126.5 (s, C_d); 126.4 (s, C_e); 121.8 (s, C_b).

Infrared (IR) spectroscopy

The absorption band for the imine bonds in the tetranuclear complex is observed at 1600 cm^{-1} (Table 2.6). As the nitrogen of the 4-picoline binds to palladium, the absorption band associated with the pyridyl imine bond shifts to higher wavenumbers. For compound **13**, the absorption bands shifted to 1568 and 1617 cm^{-1} while the C=N bond in 4-picoline is observed at 1559 cm^{-1}. The absorption band associated with the imine bond, whose nitrogen chelated to the palladium, is observed at the lower wavenumber (1568 cm^{-1}).

Table 2.18: The imine absorption bands in the IR spectra for the compounds **13-15**

Compound number	C=N *v* (cm^{-1})
13	1617, 1568, 1559
14	1643, 1624, 1594
15	1628, 1611, 1596

When the pyridyl nitrogen binds to the metal, there is delocalisation of electron density throughout the complex. Therefore less electron density is situated on the imine bonds in the cyclopalladated unit. For compounds **14** and **15**, the absorption band for the imine bond directly attached to the metal shift to lower wavenumber (1594 and 1596 cm^{-1} respectively). On the other hand the absorption band for the second C=N bond as well as the pyridyl imine bond shifts to higher wavenumbers (Table 2.18).

Mass Spectrometry

The EI^+-mass spectrum was generated for compound **13**, whist the ESI^+-mass spectra were recorded for **14** and **15**.

A peak in the mass spectrum of compound **13** is observed at *m/z* 459 (2.2 %), which corresponds to the $[M]^+$ ion. In the mass spectrum of compound **14**, a peak is observed at *m/z* 409 (100 %) which corresponds to the $[M\text{-}2Cl]^{2+}$ ion. For compound **15**, the peak which corresponds to the molecular ion and the $[M+H]^+$ ion is observed at *m/z* 915 (4 %) and 916 (5 %) respectively.

2.3. Summary

Monothiosemicarbazone (**1** and **2**), iminophosphine (**3** and **5**) and aminophosphine (**4** and **6**) ligands have been synthesized and characterized. The monothiosemicarbazone ligands were reacted with palladium salts ($K_2[PdCl_4]$ or $Na_2[PdCl_4]$) to form the cyclopalladated tetranuclear complexes (**7** and **8**), where the thiosemicarbazones (**1**-**2**) chelate in a *C*,*N*,*S*-mode. In turn, these tetranuclear complexes were reacted with P-donor ligands, which includes the aminophosphine ligands (**4** and **6**), and N-donor ligands to yield homometallic mono- (**9**-**11**, **13**) and binuclear (**12**, **14** and **15**) cyclopalladated complexes. The complexes containing the P-donor ligands were synthesized more readily than those containing the N-donor ligands, where reactions occurred more sluggishly and required harsher conditions. Molecular structures of compounds **7** and **10** and **11** were determined, and found to have a slightly distorted square planar geometry. The molecular structures confirmed that the P-donor ligands PTA and the aminophosphine ligand **4** are positioned in the fourth site of the metal, and coordinates via the phosphorus atom. Therefore, cyclopalladated complexes with varying nuclearity, such as mono-, bi- and tetranuclear, have been synthesized.

2.4. References

1. T. S. Lobana, A. Sánchez, J. S. Casas, A. Castiñeiras, J. Sordo, M. S. García-Tasend and E. M. Vázquez-López, *J. Chem. Soc*., *Dalton Trans*., 1997, 4289.
2. T. Stringer, D. T. Hendricks, H. Guzgay and G. S. Smith, *Polyhedron*, 2012, **31**, 486.
3. P. Chellan, S. Nasser, L. Vivas, K. Chibale and G. S. Smith, *J. Organomet. Chem.*, 2010, **695**, 2225.
4. S. D. Khanye, B. Wan, S G. Franzblau, J. Gut, P. J. Rosenthal, G. S. Smith and K. Chibale, *J. Organomet. Chem.*, 2011, **696**, 3392.
5. L. Adrio, G. Alberdi, A. Amoedo, D. Lata, A Fernández, J. Martínez, M. T. Pereira and J. M. Vila, *Z. Anorg. Allg. Chem.*, 2005, **631**, 2197.
6. M. Benito, C. López and X. Morvan, *Polyhedron*, 1999, **18**, 2583.
7. J. Dupont, C. S. Consorti and J. Spencer, *Chem. Rev.*, 2005, **105**, 2527.
8. T. S. Lobana, G. Bawa, G. Hundal and M. Zeller, *Z. Anorg. Allg. Chem*., 2008, **634**, 931.
9. J. M. Antelo, L. Adrio, M. T. Pereira, J. M. Ortigueira, A. Fernández and J. M. Vila, *Eur. J. Inorg. Chem.*, 2011, 368.
10. J. J. Fernández, A. Fernández, D. Vázquez-García, M. López-Torres, A. Suárez, J. M. Vila, *Polyhedron*, 2007, **26**, 4567.
11. J. M. Vila, T. Pereira, A. Amoedo, M. Graña, J. Martínez, M. López-Torres and A. Fernández, *J. Organomet. Chem.*, 2001, **623**, 176.
12. T. S. Lobana, P. Kumari, R. J. Butcher, T. Akitsu, Y. Aritake, J. Perles, F. J. Fernández and M. C. Vega, *J. Organomet. Chem.*, 2012, **701**, 17.
13. J. Martínez, L. A. Adrio, J. M. Antelo, J. M. Ortigueira, M. T. Pereira, J. J. Fernández, A. Fernández and J. M. Vila, *J. Organomet. Chem.*, 2006, **691**, 2721.
14. H. Weiss and F. Mohr, *J. Organomet. Chem.*, 2011, **696**, 3150.
15. L. A. Adrio, A. Amoedo, J. M. Antelo, J. J. Fernández, J. Martínez, J. M. Ortigueira, M. T. Pereira and J. M. Vila, *Z. Anorg. Allg. Chem*,. 2005, **631**, 2204.
16. X. Du, C. Guo, E. Hansell, P. S. Doyle, C. R. Caffrey, T. P. Holler, J. H. McKerrow and F. E. Cohen, *J. Med. Chem.*, 2002**, 45**, 2695.
17. T. S. Lobana, G. Bawa, G. Hundal and M. Zeller, *Organometallics.* 2008, **27**, 175.
18. T. S. Lobana, G. Bawa, G. Hundal, R. J. Butcher, A. Castineiras, *Z. Anorg. Allg. Chem.*, 2009, **635**, 1447.
19. G. Socrates, *Infrared and Raman characteristic group frequencies: tables and charts*, John Wiley and Sons, West Sussex, 2001, third edition, pg. 8.

20. S. Doherty, J. G. Knight, T. H. Scanlan, M. R. J. Elsegood and W. Clegg, *J. Organomet. Chem.*, 2002, **650**, 231.
21. D. B. G. Williams and M. Pretorius, *J. Mol. Catal. A: Chem.*, 2008, **284**, 77.
22. C. A. Ghilardi, S. Midollini, S. Moneti, A. Orlandini and G. Scapacci, *J. Chem. Soc*., *Dalton Trans*., 1992, **1**, 3371.
23. P. Crochet, J. Gimeno, J. Borge and S. García-Granda, *New J. Chem.*, 2003, **27**, 414.
24. J. M. Vila, M. T. Pereira, J. M. Ortigueira, M. Graña, D. Lata, A. Suárez, J. J. Fernández, A. Fernández, M. López-Torres and H. Adams, *J. Chem. Soc*., *Dalton Trans*., 1999, 4193.
25. J. Martínez, M. T. Pereira, J. M. Ortigueira, B. Bermúdez, J. M. Antelo, A. Fernández, J. M. Vila, *Polyhedron*, 2012, **31**, 217.
26. R. G. Pearson, *J. Am. Chem. Soc.*, 1963, **85**, 3533.

CHAPTER 3

The synthesis and characterization of ferrocenyl-derived *N,S*-chelated thiosemicarbazone ruthenium(II) and palladium(II) complexes

3.1. Introduction

Ferroquine, an analogue of chloroquine which has a ferrocenyl moiety incorporated into the side chain, has exhibited better activity than chloroquine and against chloroquine-resistant strains of malaria.[1] Therefore, with the medicinal success of ferroquine, a variety of compounds containing the ferrocenyl moiety have been synthesized.[1-6] Organic antimalarial drugs such as mefloquine have also been modified with the incorporation of a ferrocenyl moiety to determine if this will also result in an enhancement of activity.[6-9] However, despite activity displayed by these compounds, none have shown better activity than ferroquine.

Structure-activity relationship studies have been carried out on ferroquine to determine the significance of the various components.[10] The hydrophobic nature of the ferrocenyl moiety is believed to assist with the lipophilicity of the compound while iron is able to undergo oxidation from Fe(II) to Fe(III), providing electrons for the formation of reactive oxygen species.[11]

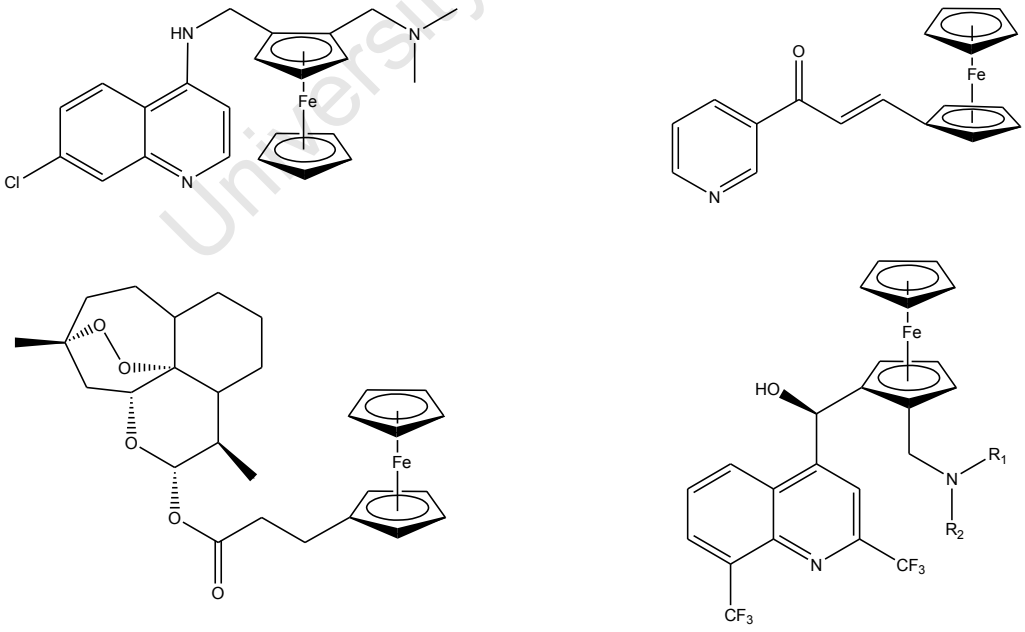

Figure 3.1: Examples of compounds containing a ferrocenyl moiety.[1-5]

As stated above and seen in Chapter 1, a variety of compounds containing a ferrocenyl moiety have been synthesized. The ferrocenyl moiety was coupled with other active moieties such as trioxanes, chalcones and thiosemicarbazones.[1,12-16] In this chapter, ferrocenyl-derived complexes were synthesized and chelated in a *N,S* bidentate mode in an effort to utilize the properties of the ferrocenyl moiety.

3.2. Results and discussion

3.2.1. The synthesis and characterization of ferrocenyl-derived thiosemicarbazones (16, 18)

The monomeric ferrocenylthiosemicarbazone **16** was synthesized via a Schiff base condensation reaction between ferrocenecarboxaldehyde and thiosemicarbazide in either water or ethanol (Scheme 3.1).[17-18] The dithiosemicarbazide (**17**) was synthesized from the reaction of hydrazine hydrate with 1,4-phenyldiisothiocyanate.[12] The dithiosemicarbazide was reacted with two equivalents of ferrocenecarboxaldehyde in a Schiff base condensation reaction to synthesize the dimeric ferrocenyldithiosemicarbazone **18**.

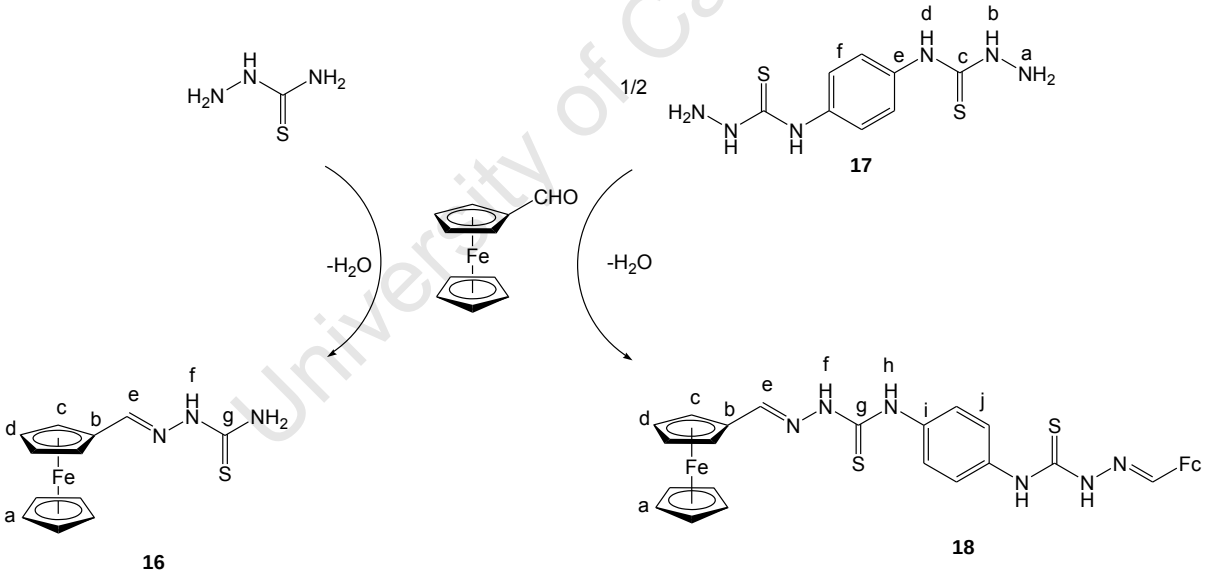

Scheme 3.1: The synthesis of the monomeric ferrocenylthiosemicarbazone (**16**) and the dimeric ferrocenyldithiosemicarbazone (**18**).

Physical properties

Compounds **16-18** were isolated as powders in relatively high yields (Table 3.1). Compound **17** melts between 197.2-198.6 ˚C and compounds **16** and **18** decompose without melting (Table 3.1). Compound **16** is soluble in organic solvents such as dichloromethane, ethanol, acetone, diethyl ether and dimethyl sulfoxide, whilst compound **17** is insoluble in most

organic solvents, with the exception of dimethyl sulfoxide. Compound **18** is soluble in dimethyl sulfoxide, and is partially soluble in organic solvents such as tetrahydrofuran, chloroform, acetone and ethyl acetate.

Table 3.1: Physical appearance, melting point and yield of compounds **16**-**18**

Compound number	Yield (%)	Physical Appearance	Melting point (˚C)
16	85	Orange powder	Decomp. w/o melting 150.4
17	84	White powder	197.2-198.6
18	86	Reddish-brown powder	Decomp. w/o melting 208.1

The NMR spectra were recorded using DMSO-d_6.

^{1}H NMR spectroscopy

Formation of the ferrocenyl-derived compounds **16** and **18** is confirmed by the presence of a singlet at *ca.* δ 7.95, which corresponds to the imine proton H_e. The protons of the ferrocenyl moiety resonate in the range δ 4.18-4.84 (Table 3.2). For compound **16**, the adjacent H_c and H_d protons resonate as triplets (J = 1.60 Hz, see appendix, pg. 134) due to three bond coupling whereas the remaining ferrocenyl protons of **16** and **18** resonate as singlets.[17]

In the ^{1}H NMR spectrum of **18**, the singlet at δ 7.59 corresponds to the aromatic spacer which is observed slightly downfield from δ 7.54 for compound **17**.

For compounds **16** and **18**, the hydrazinic proton is observed as a singlet at *ca.* δ 11.3 whilst two singlets are observed at δ 7.55 and 7.96 for the primary amine protons of compound **16**. The observation of two singlets, accounting for one proton each, has been reported for similar compounds.[13,19-21] The restricted rotation of the amino group about the C-N axis results in the protons being in different environments, and thus resonating at different chemical shifts.[13,17,19-21]

The peak for the secondary amine protons of **18**, which are located adjacent to the aromatic spacer, is observed as a singlet at δ 9.76. This is downfield from δ 8.94 for compound **17**,

whereby the ferrocenyl moiety has a deshielding effect on the rest of the compound. The remaining amine protons of **17** are observed as a broad signal at δ 4.79.

Table 3.2: ^{1}H NMR chemical shifts for selected protons of compounds **16-18**

Compound number	H-C=N (ppm)	Aromatic protons (ppm, *J* = Hz)
16	7.88 (s)	4.18 (s, H_a); 4.39 (t, *J* = 1.60, H_d); 4.71 (t, *J* = 1.60, H_c).
17	-	7.54 (s, H_f).
18	8.02 (s)	4.25 (s, H_a); 4.46 (s, H_d); 4.84 (s, H_c); 7.59 (s, H_i).

$^{13}C\{^{1}H\}$ NMR spectroscopy

In the $^{13}C\{^{1}H\}$ NMR spectra of compounds **16** and **18**, the imine carbon resonates at *ca.* δ 143.6 (Table 3.3). The thiolate carbon of compound **16** resonates at δ 176.9 whereas the peak in the spectrum of **18** shifted upfield from δ 179.4 (**17**) to 174.4 upon formation of the dithiosemicarbazone. The carbons of the ferrocenyl moiety resonate in the range δ 67.5-69.9 with the quaternary carbon (C_b) of the ferrocenyl moiety observed at *ca.* δ 78.6 (Table 3.3).

The carbons of the aromatic spacer in compounds **17** and **18** are observed as a singlet due to a two-fold symmetry axis. The quaternary carbon is observed at *ca.* δ 135.5 for **17** and **18**, whilst the peak for the remaining aromatic carbons (C_j) shifts slightly downfield in the ^{13}C NMR spectrum of compound **18**.

Table 3.3: $^{13}C\{^{1}H\}$ NMR chemical shifts for selected carbons of compounds **16-18**

Compound number	C=S (ppm)	C=N (ppm)	Aromatic protons (ppm)
16	176.9 (s)	143.3 (s)	67.5 (s, C_c); 68.8 (s, C_a); 69.9 (s, C_d); 78.8 (s, C_b).
17	179.4 (s)	-	123.2 (s, C_f); 135.4 (s, C_e).
18	174.4 (s)	143.9 (s)	67.6 (s, C_c); 68.7 (s, C_a); 69.9 (s, C_d); 78.4 (s, C_b); 124.2 (s, C_j); 135.5 (s, C_i).

Infrared (IR) spectroscopy

In the IR spectra of compounds **16**-**18**, absorption bands observed in the range 3154 - 3440 cm^{-1} correspond to the stretching vibrations of both the primary (**16** and **17**) and secondary amine (**16**-**18**) functionalities.

Table 3.4: The absorption bands observed in the IR spectra of compounds **16**-**18**

Compound number	C=N *v* (cm^{-1})	C=S *v* (cm^{-1})
16	1599	818
17	-	821
18	1600	831

Compounds **16** and **18** contain imine bonds whose absorption bands are observed at 1599 and 1600 cm^{-1} respectively. The C=N stretchings are typically observed in this region.[22] Compounds **16**-**18** contain C=S bonds whose absorption bands are observed between 818-831 cm^{-1} (Table 3.4). As compound **18** is formed from **17**, the C=S absorption band shifts to a higher wavenumber. Due to the deshielding effect of the ferrocenyl moiety, electron density is drawn from the C=S bond resulting in a longer bond.

Mass spectrometry

The molecular ion peaks for compounds **16** and **17** were observed at *m/z* 287 (100 %) and 256 (23 %) respectively. A peak corresponding to the $[M+H]^+$ ion is observed at *m/z* 649 (100 %) for **18**.

3.2.2. The synthesis and characterization of *N,S*-chelating thiosemicarbazone ruthenium(II)-arene complexes

a. Heterobimetallic binuclear *N,S*-chelated thiosemicarbazone ruthenium(II)-arene complexes (22-24)

The ruthenium(II)-arene dimers (**19**-**21**), in which the arenes were *p*-cymene, benzene or phenoxyethanol rings, were synthesized following literature methods.[23-25] The ruthenium(II)-arene dimers (**19**-**21**) were subsequently reacted with two equivalents of the ferrocenylthiosemicarbazone (**16**) in either dichloromethane or methanol (Scheme 3.2). The $Ru\text{-}Cl_{bridging}$ bond is displaced upon chelation of compound **16** to form the desired cationic Ru(II)-arene complexes (**22**-**24**). Compounds **22** and **23** were stable as the chloride salts. However, decomposition was observed for compound **24**. It is generally observed that if the

stability of a compound becomes problematic, increasing the size of the counter-ion enhances stability of the compound.[26] Therefore, in the case of compound **24** an anion metathesis using sodium hexafluorophosphate, resulting in the chloride counter-ion being exchanged to hexafluorophosphate.

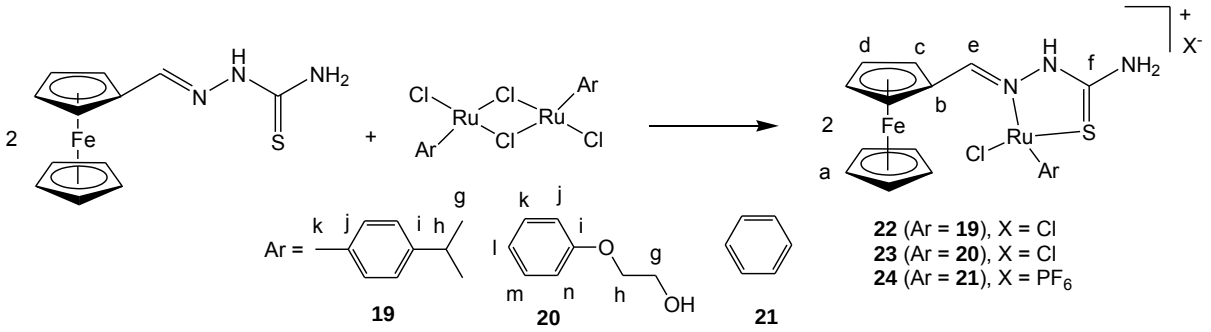

Scheme 3.2: The synthesis of binuclear ruthenium(II)-arene complexes (**22-24**)

Physical properties

Compounds **22-24** were isolated as powders in moderate to high yields. The compounds decompose without melting (Table 3.5). Compounds **22-24** are soluble in methanol and dimethyl sulfoxide. Compound **22** is also soluble in most organic solvents. The compounds are partially soluble in water.

Table 3.5: Physical appearance, melting point and yield of complexes **22-24**

Compound number	Yield (%)	Physical Appearance	Melting point (˚C)
22	92	Reddish-brown powder	Decomp. w/o melting 162.1
23	67	Orange powder	Decomp. w/o melting 155.1
24	69	Orange powder	Decomp. w/o melting 173.8

Compounds **22-24** were characterized using ^{1}H NMR, ^{13}C NMR, ^{31}P NMR, 2D (COSY, HSQC) NMR, IR spectroscopy and mass spectrometry.

^{1}H NMR spectroscopy

The ^{1}H NMR spectrum of **22** was recorded in acetone-d_6 and the spectra of **23** and **24** were recorded in methanol-d_4. Upon coordination of ruthenium to compound **16**, the expected downfield shift of the peak associated with the imine proton is observed at *ca.* δ 8.60 in the ^{1}H NMR spectra of compounds **22-24**.

A singlet corresponding to the H_a protons is observed at *ca.* δ 4.25 for **22-24**. In the ^{1}H NMR spectra, one proton in the *c*-position of the ferrocenyl moiety is observed at *ca.* δ 6.04, which is significantly downfield from the other ferrocenyl protons, particularly the remaining H_c proton (see appendix, pg. 135). Due to the orientation of the ferrocenyl moiety with respect to the rest of the complex, one proton in the *c*-position experiences through space coupling with the imine proton resulting in the proton being more deshielded. For compound **22**, the H_d protons and the remaining H_c proton, resonates at δ 4.64 and 4.84 respectively. However, for **23** and **24** the H_c and H_d protons overlapped with the water peak, which was confirmed using 2D (COSY) NMR.

The amine protons of compounds **23** and **24** and the hydrazinic protons of compound **22** are not observed due to exchange with the deuterated solvent. However, the primary amine protons of compound **22** are observed as a singlet at δ 7.92.

Table 3.6: ^{1}H NMR chemical shifts for selected protons of compounds **22-24**

Compound number	**H-C=N (ppm)**	**Ferrocenyl protons (ppm, *J* = Hz)**	**Arene protons (ppm, *J* = Hz)**
22	8.74 (br s)	4.21 (s, H_a); 4.64 (m, H_d); 4.84, 6.02 (br s, H_c).	1.01 (d, J = 6.80, H_g); 1.06 (d, J = 6.96, H_k); 1.99 (s, H_h); 2.57 (m, H_{Ar}); 5.14 (d, J = 5.84, H_{Ar}); 5.25 (d, J = 5.60, H_{Ar}); 5.31 (d, J = 5.60, H_{Ar}); 5.60 (d, J = 5.84, H_{Ar}).
23	8.48 (s)	4.30 (s, H_a); 6.06 (br s, H_c).	3.87 (m, H_g); 4.15 (m, H_h); 5.11 (t, J = 5.31, H_l); 5.26 (d, J = 6.41, H_j); 5.30 (d, J = 6.04, H_n); 5.72 (t, J = 5.95, H_k); 5.82 (t, J = 5.68, H_m).
24	8.50 (s)	4.34 (s, H_a); 6.08 (s, H_c).	5.69 (s, $H_{benzene}$).

Another approach to confirming chelation of compound **16** to yield **22** and **23** lies in the splitting of the aromatic protons of the arene ring. Due to the stereogenic nature of the ruthenium centre, which has four different substituents coordinated to itself, these complexes are chiral. For compound **19**, two doublets are observed which account for two protons each

(if one $^{i}PrC_6H_4CH_3$ ring is considered). However, upon formation of **22**, the characteristic four doublets are observed between δ 5.14-5.60, which accounts for each proton.[27] As seen with **22**, upon formation of compound **23** the three triplets observed in the ^{1}H NMR spectrum of **20** split further into triplets for H_{k-m}, and doublets for H_j and H_n (Table 3.6). This splitting is due to three bond coupling with adjacent aromatic protons. However, for compound **24**, the aromatic protons of the benzene arene are equivalent, and thus a singlet is observed at δ 5.69.

For **22**, the isopropyl methyl groups (H_g) are observed as two doublets at δ 1.01 and 1.06 with a coupling constant of δ 6.80 and 6.96 Hz respectively. The singlet observed at δ 1.99 corresponds to the other methyl group (H_k).[27] This is indicative of the diastereotopic character of the arene ring.

$^{13}C\{^1H\}$ NMR spectroscopy

The $^{13}C\{^1H\}$ NMR spectra of compounds **22-24** were recorded using MeOD-d_4.

In the ^{13}C NMR spectra of **22-24**, the thione carbon is observed at *ca.* δ 178.7, whilst the imine carbon resonates at *ca.* δ 163.6. The arene quaternary carbons C_i and C_j are observed at δ 104.2 and 103.8 respectively for **22**, whilst the C_i carbon of **23** resonates at δ 139.2.

Table 3.7: $^{13}C\{^1H\}$ NMR chemical shifts for selected carbons of compounds **22-24**

Compound number	C=S (ppm)	C=N (ppm)	Aromatic carbons (ppm)
22	178.7 (s)	163.1 (s)	18.7 (s, C_k); 21.8, 22.9 (s, C_g); 32.1 (s, C_h); 83.9 (s, C_{Ar}); 85.5 (s, C_{Ar}); 89.2 (s, C_{Ar}); 90.1 (s, C_{Ar}).
23	178.8 (s)	163.6 (s)	61.0 (s, C_g); 66.1 (s, C_j); 70.0 (s, C_n); 72.8 (s, C_h); 76.7 (s, C_l); 93.2 (s, C_k); 93.4 (s, C_m).
24	178.7 (s)	164.0 (s)	88.6 (s, C_{Ar}).

The carbons corresponding to the ferrocenyl moiety are observed in the range δ 71.0-77.8. In the ^{1}H NMR spectroscopy section above, it was mentioned that one of the H_c protons is shifted significantly downfield when compared to the other. This is also observed in the ^{13}C NMR spectrum where the carbon attached to the more deshielded proton is more shielded.

The quaternary C_b carbon is the most deshielded and is observed as a singlet at *ca.* δ 77.4. The C_a carbons resonate at δ 71.6 for **22-24**.

In the ^{13}C NMR spectra of **22-24**, the aromatic carbons of the arene ring resonate as singlets in the range δ 66.1-93.4 (Table 3.7). Only one signal is observed at δ 88.6 for the benzene arene of compound **24**. For **22**, the carbons of the methyl and isopropyl group resonate as singlets in the aliphatic region δ 18.7-32.1. The observation that the two methyl groups of the isopropyl group are different is once again confirmed as two peaks are seen in the ^{13}C NMR spectrum.

^{31}P NMR spectroscopy

A septet is observed at δ -144.6 in the ^{31}P NMR spectrum of **24** which corresponds to the hexafluorophosphate counter-ion. This confirms that an exchange of the counter-ion occurred.

Infrared (IR) spectroscopy

In the IR spectra, the absorption bands corresponding to the amine (N-H) stretchings (**22-24**) and the hydroxyl (O-H) stretching (**23**) are observed between 3435-3064 cm^{-1}. As seen in the IR spectra of similar cationic complexes upon chelation of **16**, there is a shift of both the C=N and the C=S absorption bands to higher wavenumbers (Table 3.8).[27] This is as a result of less electron-density being localized on the C=N and C=S bonds due to a more electron-deficient metal centre.

Table 3.8: The absorption bands observed in the IR spectra for compounds **22-24**

Compound number	C=N *v* (cm^{-1})	C=S *v* (cm^{-1})
22	1615	824
23	1615	833
24	1617	843

Mass spectrometry

In the case of these complexes, M refers to the cationic portion (excluding the counter-ion). The ESI$^+$-mass spectra for compounds **22-24** displayed a base peak at *m/z* 522, 526 and 466 respectively, which corresponds to the $[M\text{-}Cl]^+$ ion (see appendix, pg 135).

b. Heterobimetallic tetranuclear *N,S*-chelated thiosemicarbazone ruthenium(II)-arene complexes (25, 26)

The tetranuclear ruthenium(II)-arene complexes (**25** and **26**) were synthesized by reacting the ferrocenyldithiosemicarbazone (**18**) with the ruthenium(II)-dimers (**19** and **20**) in a methanol: dichloromethane mixture (Scheme 3.3). Attempts were made to synthesize the complex containing the benzene ring, but efforts to fully characterize this complex were unsuccessful, as the complex was not air-stable. These complexes were synthesized as higher nuclearity versions of complexes **22**-**24**. However, over a short period of time these complexes decompose in DMSO, and thus were not considered for antiplasmodial testing.

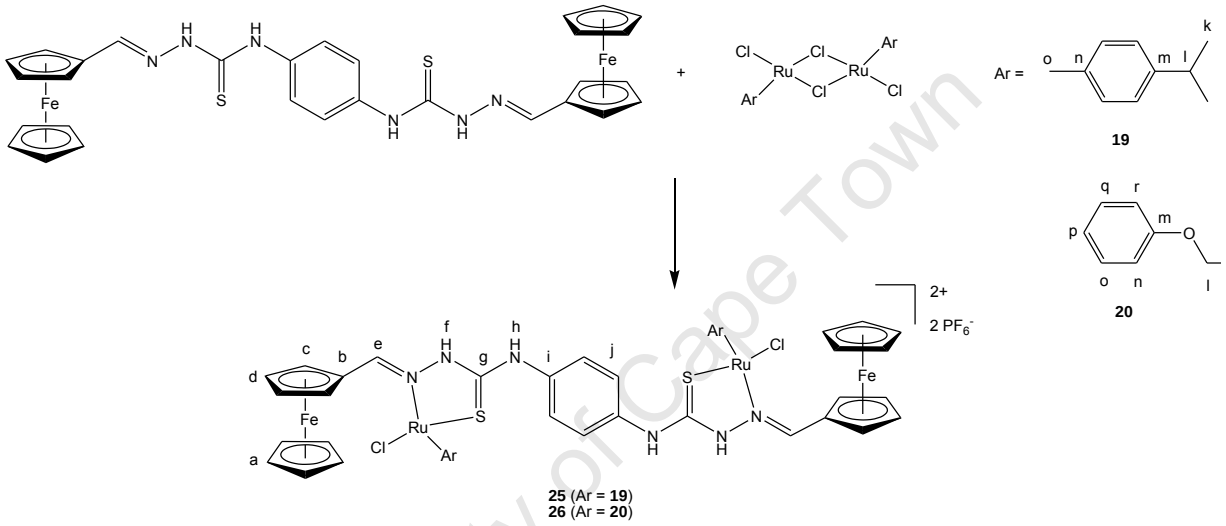

Scheme 3.3: The synthesis of tetranuclear Ru(II)-arene thiosemicarbazone complexes (**25**, **26**).

Compounds **25** and **26** were characterized using ^{1}H NMR, ^{13}C NMR, ^{31}P NMR, 2D (COSY, HSQC) NMR, IR spectroscopy and mass spectrometry (ESI^{+}).

Physical properties

Compounds **25** and **26** were isolated as powders in moderate to high yields (Table 3.9). Compound **25** is soluble in acetone whereas **25** and **26** is partially soluble in organic solvents such as chloroform, tetrahydrofuran and ethanol.

Table 3.9: Physical appearance and yields for complexes **25** and **26**

Compound number	Yield (%)	Physical Appearance	Melting point (˚C)
25	64	Dark red powder	Decomp. w/o melt 167.1
26	90	Red-brown powder	Decomp. w/o melt 120.6

The NMR spectra of compounds **25** and **26** were recorded using acetone-d_6 and methanol-d_4 respectively.

^{1}H NMR spectroscopy

For compounds **25** and **26** the imine proton resonates at *ca.* δ 8.76, which is downfield relative to the free compound (*ca.* δ 8.60). In the ^{1}H NMR spectrum of **25**, the hydrazinic and secondary amine protons are observed as broad signals at δ 10.4 and 9.14 respectively. These protons are not observed for **26** due to solvent exchange in deuterated methanol. The aromatic protons of the rigid aromatic spacer are observed as a broad signal at *ca.* δ 7.54 for **25** and **26**.

Table 3.10: ^{1}H NMR chemical shifts for selected protons of compounds **25** and **26**

Compound number	H-C=N (ppm)	Ferrocenyl protons (ppm, *J* = Hz)	Arene protons (ppm, *J* = Hz)
25	8.81 (br s)	4.33 (m, H_a); 4.77 (d, *J* = 7.69, H_d); 4.86 (br s, H_c); 6.16 (d, *J* = 8.06, H_c).	1.14 (m, H_k); 1.20 (m, H_k); 1.99 (s, H_o); 2.70 (m, H_l); 5.31 (br s, H_{Ar}); 5.44 (m, H_{Ar}); 5.78 (d, *J* = 6.23, H_{Ar}).
26	8.71 (s)	4.36 (m, H_a); 6.12 (br s, H_c).	3.87 (m, H_k); 4.15 (m, H_l); 5.18 (t, *J* = 5.70, H_p); 5.31 (d, *J* = 6.00, H_n); 5.35 (d, *J* = 6.22, H_r); 5.78 (t, *J* = 6.00, H_o); 5.88 (t, *J* = 6.00, H_q).

As mentioned in Section 3.2.2.a., these complexes are chiral with ruthenium being a stereogenic centre**.** Due to the presence of two stereogenic centres, the product could result in a compound with four (2^2) different orientations. As a result of this, there is a loss of the two-fold symmetry observed for **18**.

In the ^{1}H NMR spectra of **25** and **26**, a multiplet is observed around δ 4.34 for the H_a protons. As observed for **22-24**, one proton in the *c*-position of the ferrocenyl moiety is observed at *ca.* δ 6.14 whilst the remaining H_c and H_d protons of compound **25** are observed at δ 4.86 and 4.77 respectively. The H_c and H_d protons of **26** overlap with the water peak, and their positions are confirmed using 2D (COSY) NMR. The isopropyl methyl groups (H_k) of **25** are observed as multiplets at δ 1.14 and 1.20, whilst the other methyl group (H_o) is observed as a singlet at δ 1.99.[27]

For compound **26**, the aromatic protons of the arene ring are observed as triplets for H_{o-q}, and doublets for H_n and H_r (Table 3.10). The coupling constant of *ca.* 5.96 Hz suggests that the triplets and doublets observed are due to three bond coupling with the adjacent aromatic protons.

$^{13}C\{^1H\}$ NMR spectroscopy

Due to the poor solubility of compound **26**, even in dimethyl sulfoxide, the compound could not be characterized using ^{13}C NMR. In the ^{13}C NMR spectrum of **25**, the imine and thione carbons resonate at δ 164.2 and 176.6 respectively. As observed for compound **22**, the aliphatic carbons of the *p*-cymene ring resonate in the aliphatic region of the ^{13}C NMR spectrum in the range δ 18.8-31.7 (Table 3.11).

The quaternary carbons C_i, C_m and C_n resonate as singlets at δ 136.9, 104.3 and 103.7, and the aromatic carbons of the *p*-cymene ring are observed in the range δ 84.1-89.9. However, upon formation of **25**, the carbons of the aromatic spacer are observed in the range δ 126.4-126.6, suggesting a loss of the two-fold symmetry seen for **18**. The ferrocenyl carbons resonate as singlets in the range δ 71.2-78.0 where the quaternary C_b carbon is observed as the most deshielded carbon.

Table 3.11: $^{13}C\{^1H\}$ NMR chemical shifts for selected carbons of compounds **25**

Compound number	C=S (ppm)	C=N (ppm)	Aromatic carbons (ppm)
25	176.6 (s)	164.2 (s)	18.8 (s, C_o); 22.1, 23.1 (s, C_k); 31.7 (s, C_l); 84.1 (s, C_{Ar}); 85.4 (s, C_{Ar}); 89.2 (s, C_{Ar}); 89.9 (s, C_{Ar}), 126.4-126.6 (C_j), 136.9 (C_i).

^{31}P NMR spectroscopy

The observation of a septet at δ -144.2 and -144.6 in the ^{31}P NMR spectra of compounds **25** and **26** which correspond to the hexafluorophosphate counter-ion, confirms counter-ion exchange.

Infrared (IR) spectroscopy

Upon complexation, the C=N stretching bands of **25** and **26** are observed at 1611 cm^{-1}, whilst the C=S stretching bands are observed at 841 cm^{-1} (Table 3.12). These absorption bands are

found at higher wavenumbers when compared to **18** (Table 3.4). This is an expected observation when considering cationic complexes. A more electron-deficient metal centre leads to less electron-density localized on the C=N and C=S bonds resulting in the absorptions bands shifting to a higher wavenumber. The absorption bands corresponding to the secondary amines are observed between 3086 and 3436 cm^{-1}.

Table 3.12: The absorption bands observed in the IR spectra of compounds **25** and **26**

Compound number	C=N *v* (cm^{-1})	C=S *v* (cm^{-1})
25	1611	841
26	1611	841

Mass spectrometry

In the ESI^+-mass spectra of compounds **25** and **26**, the $[M\text{-}Cl]^{2+}$ peaks are observed at *m/z* 559 (100 %) and 563 (70 %) respectively.

There is evidence for the complex containing the benzene arene in the ESI^+-mass spectrum of the solid obtained. The $[M\text{-}Cl]^+$ and $[M\text{-}2Cl]^{2+}$ ions are observed at *m/z* 1041 (3 %) and 503 (100 %) respectively.

3.2.3. The synthesis and characterization of *N,S*-chelated thiosemicarbazone palladium(II) complexes containing P-donor ligands

a. Heterobimetallic binuclear *N,S*-chelated thiosemicarbazone palladium(II) complexes (28, 29)

Attempts were made to synthesize the $[Pd(ferrocenylthiosemicarbazone)]_4$ complex described by Mariño *et al*., in which compound **16** was reacted with potassium tetrachloropalladate in a water-ethanol mixture.[17] However, analysis of the solid suggests the synthesis of a chloro-bridged complex, $[Pd(ferrocenylthiosemicarbazone)(\mu\text{-}Cl)]_2$ (**27**). As explained in Chapter 2 section 2.1., C-H activation is more likely to occur if an alkyl substituent is present on the imine carbon, forcing the compound into a geometry which allows cyclometalation to take place.[8] Attempts to prepare compound **27** using $Na_2[PdCl_4]$ under the same conditions were unsuccessful as only a decomposed solid was collected. Binuclear palladium(II) complexes (**28** and **29**) were prepared by reacting **27** with P-donor ligands PTA and triphenylphosphine (PPh_3) in acetone (Scheme 3.4).

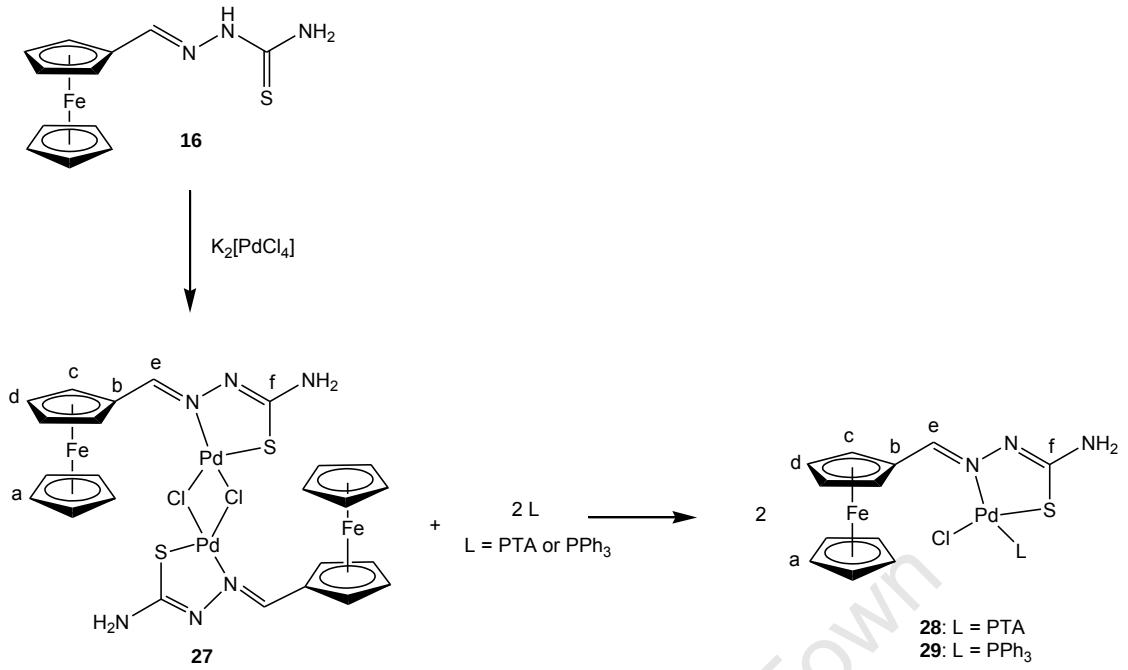

Scheme 3.4: The synthesis of binuclear ferrocenylthiosemicarbazone palladium(II) complexes containing P-donor ligands (**28**, **29**).

Physical properties

Compound **27** was isolated as a reddish-brown powder with a yield of 47 %. Compounds **28** and **29** were isolated in moderate yields as reddish-orange and red powders respectively (Table 3.13). Compound **27** is only soluble in dimethyl sulfoxide. Compounds **28** and **29** are soluble in dimethyl sulfoxide, chloroform and tetrahydrofuran. The onset of decomposition for compounds **28** and **29** occurs at 241.3 and 164.7 ˚C respectively.

Table 3.13: Physical appearance, melting point and yield of the compounds (**27**-**29**)

Compound number	Yield (%)	Physical Appearance	Melting point (˚C)
27	47	Reddish-brown powder	-
28	54	Reddish-orange powder	Decomp. w/o melting 241.3
29	75	Red powder	Decomp. with melting 164.7

The NMR spectra of compounds **27**-**29** were recorded using DMSO-d_6.

^{1}H NMR spectroscopy

In the ^{1}H NMR spectra for compound **27**, the peak observed at δ 7.44 corresponds to the imine proton, which is shifted upfield from the free compound (**16**). For **28**, the peak

corresponding to the imine proton is observed as a doublet at δ 7.87 (see appendix, pg. 136), and for **29** the peak is observed at δ 8.14. The proton experiences a four bond coupling (J = *ca.* 4.00 Hz) with the phosphorus of the P-donor ligand. The terminal amine protons are observed as a broad signal at δ 6.91 in the ^{1}H NMR spectrum of **27** whilst a broad signal is observed at *ca.* δ 6.80 for **28** and **29**.

The ferrocenyl protons H_a are observed at *ca.* δ 4.20 whereas the H_d protons (**27** and **29**) are observed as a triplet ($^{3}J_{HH}$ = 1.60 Hz) at *ca.* δ 4.54. For **27**-**29**, the H_c protons are observed as a triplet ($^{3}J_{HH}$ = 1.60 Hz) at *ca.* δ 5.06. These triplets are due to coupling with adjacent H_d protons.

Table 3.14: ^{1}H NMR chemical shifts for selected protons of compounds **27**-**29**

Compound number	**H-C=N (ppm, *J* = Hz)**	**PCH_2N (ppm, *J* = Hz)**	**$N\text{-}CH_{2(ax)}\text{-}N$ $N\text{-}CH_{2(eq)}\text{-}N$ (ppm, *J* = Hz)**	**Aromatic protons (ppm, *J* = Hz)**
27	7.44 (s)	-	-	4.22 (s, H_a); 4.56 (t, $^{3}J_{HH}$ = 1.60 Hz, H_d); 5.04 (t, $^{3}J_{HH}$ = 1.60 Hz, H_c).
28	7.87 (d, *J* = 3.66)	4.32 (s)	4.38 (d, *J* = 13.0); 4.54 (m), overlap with H_d.	4.17 (s, H_a); 5.07 (t, *J* = 1.60, H_c).
29	8.14 (d, *J* = 4.00)	-	-	4.22 (s, H_a); 4.53 (t, *J* = 1.60, H_d); 5.08 (t, *J* = 1.60, H_c); 7.49-7.68 (m, H_{Ph}).

In the ^{1}H NMR spectrum of compound **28**, a similar splitting is observed as seen with other palladium complexes containing PTA.[28] The PCH_2N protons are observed as a singlet at δ 4.32 whilst the NCH_2N protons split into an AB spin system. Two doublets are observed due to the different environments experienced by the axial and equatorial NCH_2N protons (Table 3.14). The doublet observed at δ 4.38 corresponds to the $NCH_{2(ax)}N$ protons, whilst the peak observed at δ 4.54 corresponds to the $NCH_{2(eq)}N$ as well as the H_d protons. For compound **29**, the phenyl protons of the triphenylphosphine ligand are observed as a multiplet between δ 7.49-7.68.

$^{13}C\{^1H\}$ NMR spectroscopy

In the ^{13}C NMR spectrum of **27**, the thiolate carbon resonates at δ 169.9. For compounds **28** and **29**, a doublet is observed in the ^{13}C NMR spectra at *ca.* δ 171.9, which corresponds to the thiolate carbon as a result of three bond coupling with phosphorus. The imine carbon of **27** resonates at δ 155.2 and shifts slightly upfield to δ 151.6 and 152.7 for **28** and **29** respectively.

The quaternary carbon C_b resonates as a singlet at δ 73.2 for **27**. For the ferrocenyl carbons of **28** and **29**, the quaternary C_b carbon resonates as a doublet (J ~ 4.72 Hz) at *ca.* δ 73.7, and experiences four bond coupling with phosphorus. The remaining ferrocenyl carbons of **27**-**29** resonate as singlets in the range δ 69.1-72.7.

Table 3.15: $^{13}C\{^1H\}$ NMR chemical shifts for selected carbons of compounds **27**-**29**

Compound number	C-S (ppm, *J* = Hz)	C=N (ppm, *J* = Hz)	NCH_2N (ppm, *J* = Hz)	PCH_2N (ppm, *J* = Hz)	Aromatic carbons (ppm, *J* = Hz)
27	169.9 (s)	155.2 (s)	-	-	73.2 (s, C_b)
28	172.1 (d, *J* = 11.4)	151.6 (s)	71.8 (d, *J* = 8.08)	51.6 (d, *J* = 17.5)	73.8 (d, *J* = 4.71, C_b)
29	171.6 (d, *J* = 11.5)	152.7 (s)	-	-	73.7 (d, *J* = 4.73, C_b)

As observed with other PTA containing complexes, the PTA carbons of **28** resonate as doublets due to coupling with phosphorus. The NCH_2N carbons are observed at δ 71.8, while the PCH_2N carbons are observed at δ 51.6 (Table 3.15). For compound **29**, the phenyl carbons are observed in the range δ 128.2-133.9.

^{31}P NMR spectroscopy

A peak for free PTA and triphenylphosphine is observed at δ -104.0 and -6.60 respectively. However, upon formation of the complex a peak is observed downfield at δ -33.5 and 27.6 for **28** and **29** respectively.

Infrared (IR) spectroscopy

In the IR spectrum of compound **27**, the strong and broad absorption band observed at 1602 cm^{-1} corresponds to the two imine bonds. For compounds **28** and **29**, two absorption bands

are observed in the range 1592-1614 cm^{-1}, which corresponds to the two imine bonds. As observed with other palladium complexes (Chapter 2, Section 2.2.4.a.), upon coordination of the P-donor ligand, the absorption band corresponding to the imine bond directly coordinated to the metal shifts to a lower wavenumber, while the second absorption band is observed at a higher wavenumber.

Table 3.16: The absorption bands observed in the IR spectra of compounds **27-29**

Compound number	C=N *v* (cm^{-1})
27	1602
28	1614, 1598
29	1607, 1592

Mass spectrometry

The mass spectra of **27** and **29** were recorded using electrospray ionisation, whilst the EI^+-mass spectrum of **28** was recorded.

For compound **27**, the peak observed at *m/z* 854 (5 %) refers to the molecular ion peak $[M]^+$ (see appendix, pg. 136). For compounds **28** and **29** the fragments $[M+H]^+$ and $[M-HCl]^+$ were observed at *m/z* 585 (6.7 %) and 654 (100 %) respectively.

Molecular structure of complex 28

Single crystals of compound **28** were obtained by the slow evaporation of a solution of **28** dissolved in ethyl acetate/hexane and the molecular structure was determined by single-crystal X-ray diffraction. The molecular structure of **28** is shown in Fig. 3.2 and Table 3.17 lists selected bond lengths and angles. The crystallographic data is given in Table 3.18. Compound **28** crystallizes in a monoclinic system with space group *P*21/*n*. The ferrocenylthiosemicarbazone compound chelates to the palladium(II) ion in a bidentate *N*,*S*-mode to form the observed 5-membered ring (Fig. 3.2).[29-30] The fourth coordination site on the metal is occupied by the PTA ligand via the phosphorus atom.

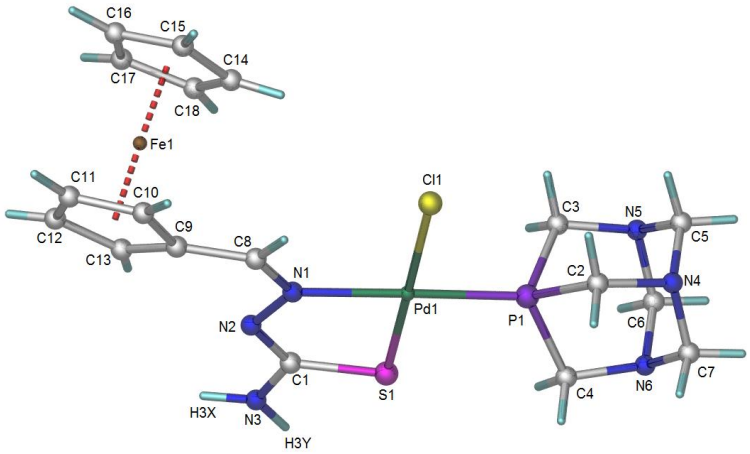

Figure 3.2: The molecular structure of compound **28**.

Palladium(II) complexes are generally square planar complexes, and therefore due to the environment around the palladium centre where the sum of the acute and obtuse bond angles deviates from 720˚ by approximately 12˚, compound **28** has a slightly distorted square planar geometry. This geometry is observed for other similar complexes containing phosphorus ligands.[20,29-31]

Table 3.17: Selected bond lengths (Å) and angles (˚) for compound **28**.

Bond lengths		*Bond angles*	
Pd(1)-N(1)	2.090(2)	N(1)-Pd(1)-Cl(1)	96.69(8)
Pd(1)-Cl(1)	2.3489(9)	N(1)-Pd(1)-S(1)	83.68(8)
Pd(1)-P(1)	2.2213(8)	Cl(1)-Pd(1)-P(1)	89.41(3)
Pd(1)-S(1)	2.2466(8)	P(1)-Pd(1)-S(1)	89.93(3)
S(1)-C(1)	1.752(3)	Cl(1)-Pd(1)-S(1)	176.41(3)
N(2)-C(1)	1.306(4)	N(1)-Pd(1)-P(1)	172.20(8)
N(1)-C(8)	1.296(4)		

As observed with compounds **10** and **11** (Chapter 2, Section 2.2.4.a.), the lengths of the two imine bonds are different, with the imine coordinated to the metal being slightly shorter than the other. The S(1)-C(1) bond has a length of 1.752(3) Å, which is equivalent to a single bond, and thus confirms coordination of the thiosemicarbazone in the thiolate form.

Table 3.18: Crystal data and structure refinement data for compound **28**

Empirical formula	$C_{18}H_{24}ClFeN_6PPdS$
Formula weight	585.16
Temperature (K)	173(2)
Wavelength (Å)	0.71073
Crystal system	Monoclinic
Space group	*P*21/n
a (Å)	7.0423(3)
b (Å)	25.1284(6)
c (Å)	12.5604(5)
α (˚)	90
β (˚)	90.041(2)
γ (˚)	90
V ($Å^3$)	2222.71(14)
Z	4
D_{calc} ($Mg.m^{-3}$)	1.749
Absorption coefficient (mm^{-1})	1.765
F(000)	1176
Crystal size (mm^3)	0.04 x 0.10 x 0.11
θ Range for data collection (˚)	3.2- 26.4
Index range	$-8 \leq h \leq 8$; $-31 \leq k \leq 31$; $-15 \leq l \leq 15$
Reflections collected	48765
Independent reflections [*R*(int)]	4527 [0.055]
Data / restraints / parameters	4527 / 2 / 270
Goodness-of-fit on F^2	1.051
Transmission	0.9094, 0.8857
Final *R* indices [$I>2\sigma(I)$]	$R_1 = 0.0306$, $wR_2 = 0.0808$
R indices (all data)	$R_1 = 0.0432$, $wR_2 = 0.0850$
Largest difference in peak and hole (e. $Å^{-3}$)	-0.91 and 1.60

b. Heterobimetallic tetra- and pentanuclear *N,S*-chelated thiosemicarbazone palladium(II) complexes containing P-donor ligands (30-32)

Polynuclear palladium(II) complexes were synthesized by either reacting **27** with a dimeric P-donor ligand, or reacting the dimeric ferrocenyl-derived thiosemicarbazone with P-donor

ligands. The pentanuclear complex (**30**) was synthesized by reacting [Pd(ferrocenylthiosemicarbazone)(μ-Cl)]$_2$ (**27**) with 1,1'-bis(diphenylphosphino)ferrocene (dppf) in acetone (Scheme 3.5).[17] With the incorporation of dppf, an additional ferrocenyl moiety may contribute to the antiplasmodial activity.

The tetranuclear palladium(II) complexes **31** and **32** were synthesized by reacting ferrocenyldithiosemicarbazone (**18**) with two equivalents of the palladium-precursor, $PdCl_2(PTA)_2$ and $PdCl_2(PPh_3)_2$ respectively, in an ethanol:acetone mixture. Compounds **31** and **32** were synthesized to allow comparison with compounds **28** and **29**, which contains only one ferrocenyl moiety and P-donor ligand. The Pd-precursors, $PdCl_2(PTA)_2$ and $PdCl_2(PPh_3)_2$, were synthesized following literature methods.[32]

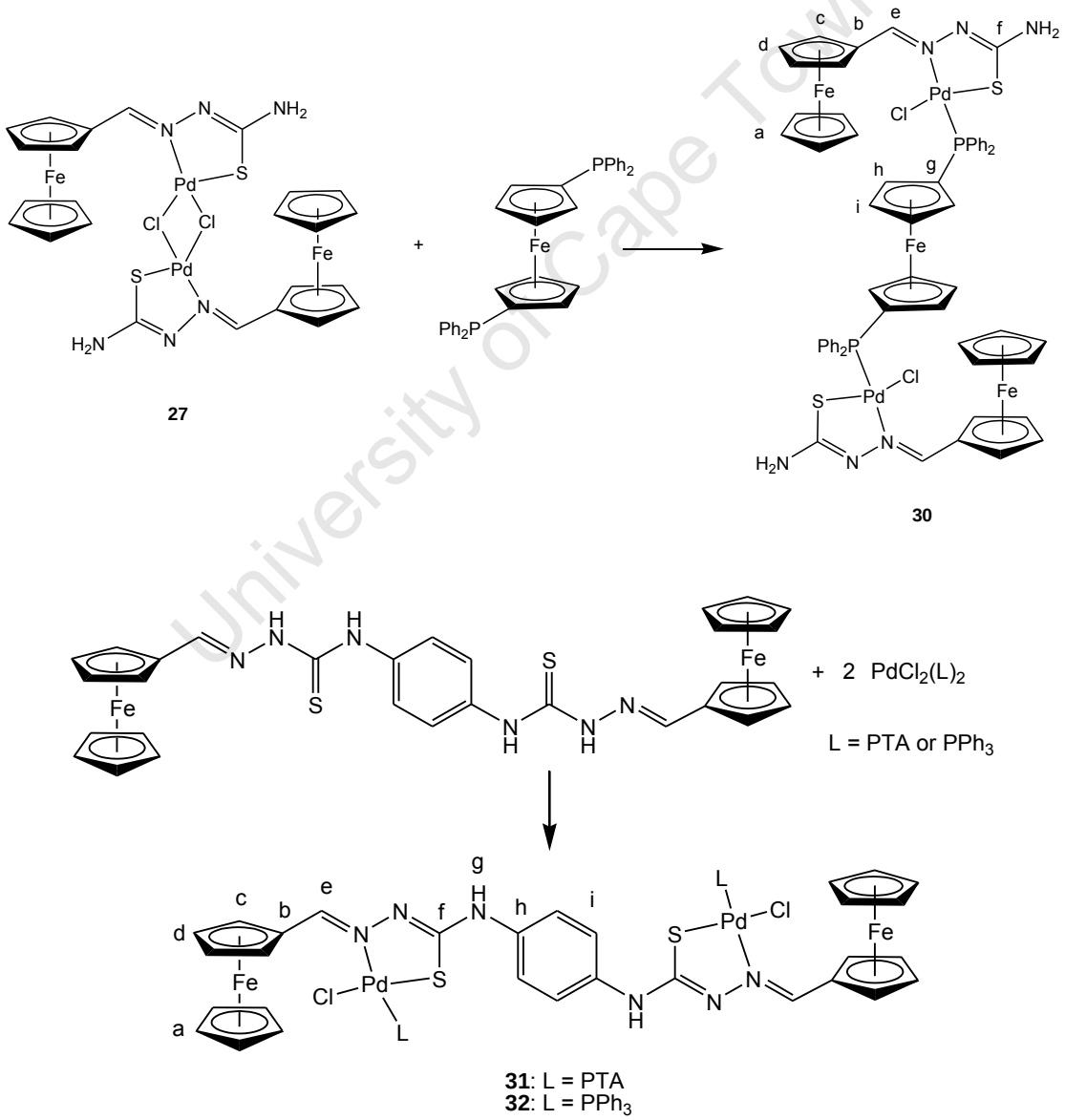

Scheme 3.5: The synthesis of multinuclear thiosemicarbazone palladium(II) complexes (**30**-**32**)

Physical properties

Compound **30** was isolated as an orange powder whilst **31** and **32** were isolated as reddish-orange powders in moderate to high yield (Table 3.19). Compounds **30**-**32** decompose without melting with the onset of decomposition occurring at 200.0, 218.3 and 237.2 ˚C respectively. Compounds **30**-**32** are soluble in dimethyl sulfoxide, while **30** and **32** are also soluble in chloroform, dichloromethane and tetrahydrofuran.

Table 3.19: Physical appearance, melting point and yield of the compounds **30**-**32**

Compound number	Yield (%)	Physical Appearance	Melting point (˚C)
30	78	Orange powder	Decomp. w/o melting 200.0
31	99	Reddish-orange powder	Decomp. w/o melting 218.3
32	70	Reddish-orange powder	Decomp. w/o melting 237.2

The NMR spectra of compounds **30**-**32** were recorded using DMSO-d_6.

^{1}H NMR spectroscopy

In the ^{1}H NMR spectra of compounds **30**-**32**, the peak corresponding to the imine proton is observed as a doublet at *ca.* δ 8.24. The proton experiences a four bond coupling, with a coupling constant of *ca.* 4.02 Hz, with the phosphorus of the P-donor ligand.

Table 3.20: ^{1}H NMR chemical shifts for selected protons of compounds **30**-**32**

Compound number	H-C=N (ppm, *J* = Hz)	PCH_2N (ppm, *J* = Hz)	$N\text{-}CH_{2(ax)}\text{-}N$ $N\text{-}CH_{2(eq)}\text{-}N$ (ppm, *J* = Hz)	Aromatic protons (ppm, *J* = Hz)
30	8.19 (d, *J* = 4.03)	-	-	4.14 (s, H_a); 4.51 (br s, H_i); 4.87 (br s, H_d); 5.07 (br s, H_h); 5.18 (br s, H_c); 7.47-7.87 (m, H_{Ph}).
31	8.14 (d, *J* = 4.00)	4.38 (s)	4.41 (d, *J* = 13.4) 4.58 (d, *J* = 12.8)	4.19 (s, H_a); 4.52 (br s, H_d); 5.01 (br s, H_c); 7.59 (s, H_i).
32	8.39 (d, *J* = 4.00)	-	-	4.22 (s, H_a); 4.52 (br s, H_d); 4.99 (br s, H_c); 7.47 (m, H_{Ph} & H_i).

In the ^{1}H NMR spectrum of compound **31**, similar splitting is observed as seen with other palladium complexes containing PTA.[28] The PCH_2N protons are observed as a singlet at δ 4.38 whilst the NCH_2N protons are split into two doublets due to an AB spin system (Table 3.20). The doublets corresponding to the $NCH_{2(ax)}N$ and $NCH_{2(eq)}N$ protons are observed at δ 4.41 and 4.58 respectively. The phenyl protons of **30** are observed between δ 7.47-7.87. A multiplet at δ 7.47 corresponds to the phenyl protons of **32**.

The ferrocenyl protons H_a are observed as a singlet at *ca.* δ 4.18 whilst the H_c and H_d protons are observed as broad signals at *ca.* δ 5.06 and 4.64 respectively for **30**-**32**. The remaining ferrocenyl protons H_h and H_i, contributed by the dppf ligand, are observed as broad signals at δ 5.07 and 4.51 respectively. The primary amine protons of **30** are observed as a broad signal at δ 6.74. Upon formation of compounds **31** and **32**, the peak corresponding to the hydrazinic proton (**18**) is absent as the second imine bond forms. The secondary protons (H_g) are observed as a singlet at *ca.* δ 9.38, which is upfield from the free dithiosemicarbazone (**18**).

$^{13}C\{^{1}H\}$ NMR spectroscopy

For compound **30**, a doublet is observed in the ^{13}C NMR spectrum at δ 171.5, whereas for **31** and **32** a doublet is observed at *ca.* δ 167.5 which corresponds to the thiolate carbon. The imine carbon resonates as a singlet at δ 152.5, 154.8 and 156.0 for **30**-**32** respectively. For the ferrocenyl carbons of **30** and **31**, the quaternary C_b carbon resonates as a doublet (J = 4.68 Hz) at *ca.* δ 73.4, whilst a singlet is observed at δ 72.3 for **32**. The remaining ferrocenyl carbons resonate as singlets in the range δ 66.9-73.7. The $C_{h\text{-}i}$ ferrocenyl carbons of dppf resonate as doublets (J = 9.42 and 7.41 Hz respectively) due to coupling with phosphorus whilst the C_g carbon is observed as a singlet at δ 131.0.

Table 3.21: $^{13}C\{^{1}H\}$ NMR chemical shifts for selected carbons of compounds **30**-**32**

Compound number	C-S (ppm, J = Hz)	C=N (ppm, J = Hz)	NCH_2N (ppm, J = Hz)	PCH_2N (ppm, J = Hz)	Aromatic carbons (ppm)
30	171.5 (d, J = 12.1)	152.5 (s)	-	-	75.8 (d, J = 7.41, C_i); 76.2 (d, J = 9.42, C_h).
31	167.8 (s)	154.8 (s)	72.2 (d, J = 12.8)	51.5 (d, J = 18.2)	119.9 (C_i); 136.1 (C_h).
32	167.2 (s)	156.0 (s)	-	-	119.8 (C_i); 136.0 (C_h)

For **31** and **32**, the quaternary carbons (C_h) of the aromatic spacer are observed as a singlet at *ca.* δ 136.0 while the remaining aromatic carbons (C_i) are observed as a singlet at *ca.* δ 119.8. As observed with other PTA containing complexes, the PTA carbons of **31** resonate as doublets due to coupling with phosphorus. The NCH_2N carbons are observed at δ 72.2, with the PCH_2N carbons being observed at δ 51.5 (Table 3.21). For compounds **30** and **32**, the phenyl carbons are observed in the range δ 128.1-134.4.

^{31}P NMR spectroscopy

For compound **30**, a peak is observed at δ 22.0, which is upfield from the signal observed at δ -17.8 for free dppf. For the palladium-precursors, *cis*-$PdCl_2(PTA)_2$ and $PdCl_2(PPh_3)_2$, a peak is observed at δ -20.4 and δ 23.6 respectively. Upon formation of compounds **31** and **32**, the peak in the ^{31}P NMR spectra shifts upfield in the case of **31** (δ -32.0) and downfield for **32** (δ 27.8). These values are comparable to those seen for the binuclear complexes (**28** and **29**) in Section 3.2.3.a.

Infrared (IR) spectroscopy

In the IR spectra of compounds **30**-**32**, two absorption bands are observed in the range 1572-1602 cm^{-1}, which corresponds to the two imine bonds. The absorption band at the lower wavenumber corresponding to the C=N bond coordinated to the metal (Table 3.22).

Table 3.22: The absorption bands observed in the IR spectra of compounds **30**-**32**

Compound number	C=N *ν* (cm^{-1})
30	1602, 1587
31	1593, 1576
32	1598, 1572

Mass spectrometry

The ESI^+-mass spectra was recorded for compounds **30** and **31**. For **30**, the peak observed at *m/z* 1412 (3 %) and 1375 (30 %) corresponds to the $[M+H]^+$ and $[M+2H-Cl]^+$ ions respectively (see appendix, pg. 137). For compound **31**, the molecular ion peak is observed at *m/z* 1244 (10 %). For compound **32**, the peak observed at 1457 (3 %) and 692 (100 %) corresponds to the $[M+H]^+$ and $[M-Cl]^{2+}$ ions respectively.

3.3. Cyclic voltammetry

Electrochemical studies were carried out as a preliminary investigation to determine the effect of phosphorus-containing ligands (PTA, PPh_3 and dppf) on the ferrocenyl moiety through the palladium metal centre. These electrochemical studies were conducted in order to possibly compare the electronic effects with the antiplasmodial activity of the compounds. There is evidence which suggests that the oxidation of the ferrocenyl moiety could produce, via Fenton-like reactions, reactive oxygen species (hydroxyl radicals) which disrupts lipid membranes.[33-35] In principle, compounds containing more electron-donating groups would favour the oxidation process of the Fc/Fc^+ couple i.e. hydroxyl radicals will form easily resulting in antiplasmodial activity.

Table 3.23: Cyclic voltammetry of selected compounds (**16**, **28**, **29**)

Compound	E_{pa} (mV)[a]	E_{pc} (mV)[b]	$E_{1/2}$ (mV)[c]
Fc	283	217	250
16	384	328	356
28	402	344	373
29	391	326	359
30	364, 791	297	331

[a] E_{pa}: Anodic potential
[b] E_{pc}: Cathodic potential
[c] $E_{1/2}$: Half wave potential [$(E_{pa} + E_{pc})/2$]

In this study, the effects of the thiosemicarbazone moiety, as well as palladium and the P-donor ligand will be investigated. The synthesis of compounds **16**, **28**, **29** and **30** were described in Sections 3.2.3.a. and 3.2.3.b.[17] The voltammograms of compounds **16**, **28** and **29** show a full reversible one electron redox event, which corresponds to the Fc/Fc^+ couple (Table 3.23).[36] On the other hand, from the cyclic voltammogram of compound **30** the redox cycle the two ferrocenyl moieties of the thiosemicarbazone unit was fully reversible, whereas only the oxidation peak was observed for the ferrocenyl moiety of the 1,1'-bis(diphenylphosphino)ferrocene. An irreversible redox process was also observed for free dppf.

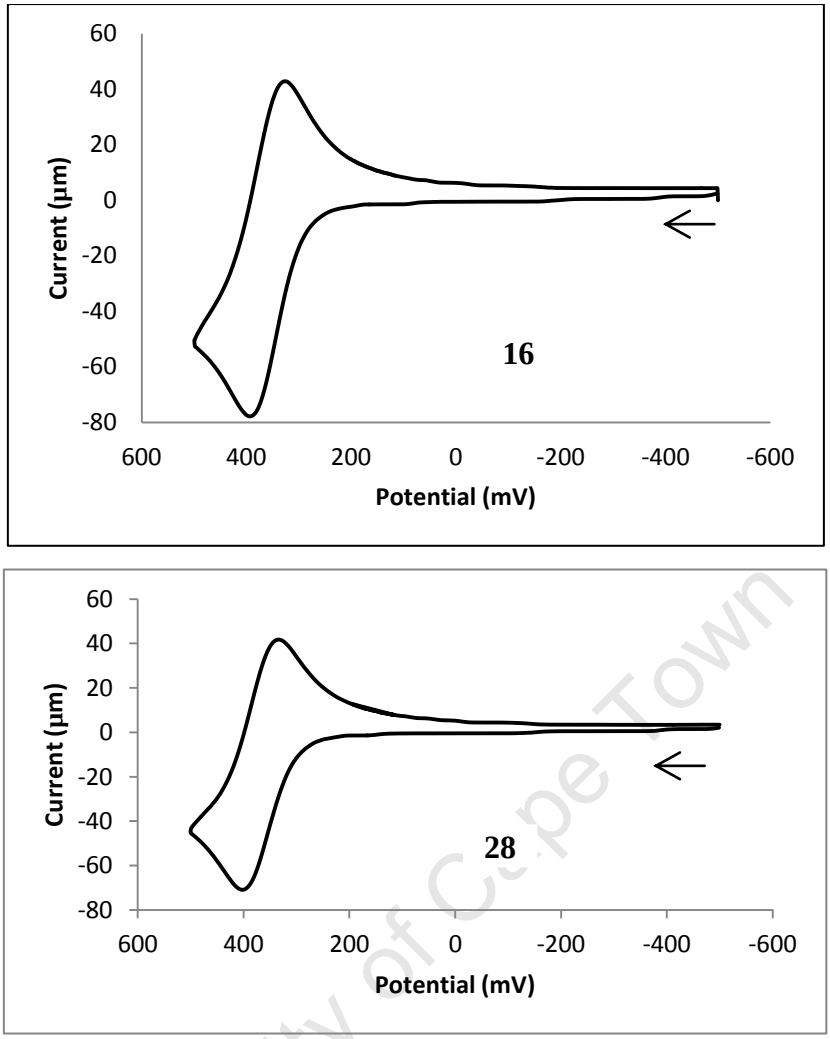

Figure 3.3: Cyclic voltammograms of compounds **16** and **28**.

The half wave potential ($E_{1/2}$) could indicate the ease with which the ferrocenyl moiety is oxidized compared to ferrocene.[36] Therefore, an $E_{1/2}$ value larger than that observed for ferrocene suggests a system which is more difficult to oxidize. In comparison to free ferrocene ($E_{1/2}$ = 250 mV), the ferrocenyl moiety of the tested compounds (**16**, **28**-**30**) are more difficult to oxidize due the presence of the thiosemicarbazone unit, palladium and the phosphorus ligands (Fig. 3.3). However, compounds **16** and **29** have comparable $E_{1/2}$ values (356 mV and 359 mV respectively), while compound **28** has an $E_{1/2}$ value of 373 mV showing the poorest electron-donating effect (Table 3.23). Therefore, from the $E_{1/2}$ values it can be deduced that the ferrocenyl moiety in compound **28** is more difficult to oxidize. The PPh_3 ligand displayed a greater electron-donating effect than PTA, which resulted in a lower $E_{1/2}$ value.

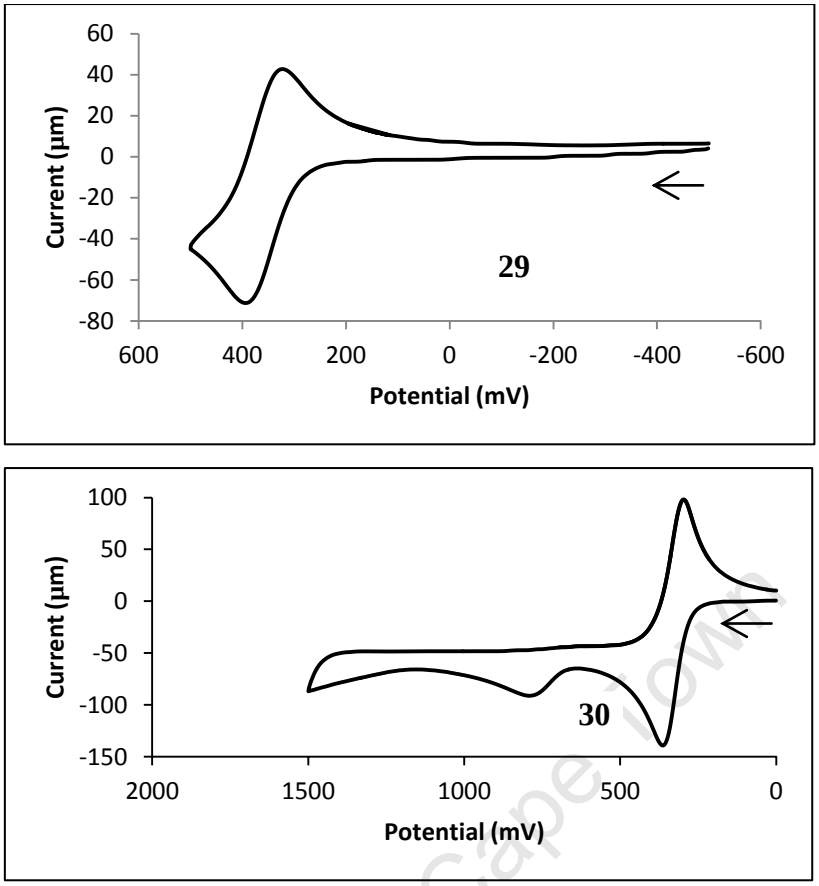

Figure 3.4: Cyclic voltammograms of compounds **29** and **30**.

As mentioned above, the Fc/Fc^+ redox cycle of the dppf group in compound **30** was irreversible (Fig. 3.4). Free dppf was analysed, and the voltammogram displayed the oxidation signal of free dppf at 1068 mV. The cyclic voltammogram of **30** displayed an oxidation signal at 791 mV which suggest that the palladium thiosemicarbazone units have an electron-donating effect on dppf, resulting in an easily oxidized ferrocenyl moiety. However, an $E_{1/2}$ value of 331 mV suggests that the ferrocenyl moieties of the thiosemicarbazone unit were easy to oxidize when compared to the compounds **28** and **29** (Table 3.23).

3.4. Summary

The ferrocenyl-derived thiosemicarbazone compounds (**16** and **18**) were synthesized, and reacted with the ruthenium-dimers **19-21** to yield heterobimetallic compounds **22-26**. These compounds (**22-26**) were isolated as cationic ruthenium(II) complexes, and characterized using NMR spectroscopy, infrared spectroscopy and mass spectrometry (ESI^+). The ruthenium(II) complexes containing the *p*-cymene and phenoxyethanol rings were generally more air-stable than their benzene-containing complex. The binuclear ruthenium(II) complex

(**24**) was isolated as an air-stable hexafluorophosphate salt, while this was not the case for tetranuclear complex.

The ferrocenyl-derived compound **16** was also reacted with potassium tetrachloropalladate to synthesize the chloro-bridged compound, **27**. Compound **27** was used in subsequent reactions with P-donor ligands, PTA, PPh_3 and dppf, to prepare binuclear complexes **28** and **29** and pentanuclear complex **30** respectively. Compound **18** was reacted with palladium-precursors to synthesize tetranuclear palladium(II)-complexes (**31** and **32**) containing P-donor ligands, PTA and PPh_3. As opposed to the cationic ruthenium(II) complexes, the neutral palladium(II) complexes (**28**-**32**) were air-stable compounds. The palladium(II) complexes (**27**-**32**) were characterized using NMR spectroscopy, infrared spectroscopy and mass spectrometry (EI^+ and ESI^+). The crystal structure of compound **28** was determined using single-crystal X-ray diffraction, and found to have a slightly distorted square planar geometry.

Preliminary electrochemical studies were carried out on selected ferrocenyl-derived palladium complexes to determine which ferrocenyl moiety is more easily oxidized. The cyclic voltammograms revealed that compound **28** was the most difficult to oxidize, whereas compound **30** was oxidized more easily. Compound **30** displayed a greater electron-donating effect compared to compounds **28** and **29**, while the PTA ligand displayed a weaker electron-donating effect when compared to the PPh_3 ligand.

3.5. References

1. C. Biot, G. Glorian, L. A. Maciejewski and J. S. Brocard, *J. Med. Chem.*, 1997, **40**, 3715.
2. M. A. L. Blackie, P. Beagley, K. Chibale, C. Clarkson, J. R. Moss and P. J. Smith, *J. Organomet. Chem.*, 2003, **688**, 144.
3. C. Biot, J. Dessolin, I. Ricard and D. Dive, *J. Organomet. Chem.*, 2004, **689**, 4678.
4. C. Biot, F. Dubar, J. Khalife and C. Slomianny, *Metallomics*, 2012, **4**, 780.
5. Quirante, F. Dubar, A. González, C. Lopez, M. Cascante, R. Cortés, I. Forfar, B. Pradines and C. Biot, *J. Organomet. Chem.*, 2011, **696**, 1011.
6. X. Wu, E. R. T. Tiekink, I. Kostetski, N. Kocherginsky, A. L. C. Tan, S. B. Khoo, P. Wilairat, M.-L. Go, *Eur. J. Pharm. Sci.*, 2006, **27**, 175.
7. C. Biot, L. Delhaus, L. A. Maciejewski, M. Mortuaire, D. Camus, D. Dive and J. S. Brocard, *Eur. J. Med. Chem.*, 2000, **35**, 707.

8. L. Delhaus, C. Biot, L. Berry, L. A. Maciejewski, D. Camus, J. S. Brocard and D. Dive, *Bioorg. Med. Chem.*, 2000, **8**, 2739.
9. M. Navarro, W. Castro and C. Biot, *Organometallics*, 2012, **31**, 5715.
10. C. Biot, D. Taramelli, I. Forfar-Bares, L. A. Maciejewski, M. Boyce, G. Nowogrocki, J. S. Brocard, N. Basilico, P. Olliaro and T. J. Egan, *Mol. Pharm.*, 2005, **2**, 185.
11. C. Biot and D. Dive, *Top Organomet. Chem.*, 2010, **32**, 155.
12. M. Christlieb, H. S. R. Struthers, P. D. Bonnitcha, A. R. Crowley and J. R. Dilworth, *Dalton Trans.*, 2007, 5043.
13. T. S. Lobana, G. Bawa, G. Hundal and M. Zeller, *Z. Anorg. Allg. Chem*., 2008, **634**, 931.
14. F. Bellot, F. Coslédan, L. Vendier, J. Brocard, B. Meunier and A. Robert, *J. Med. Chem.*, 2010, **53**, 4103.
15. X. Wu, E. R. T. Tiekink, I. Kostetski, N. Kocherginsky, A. L. C. Tan, S. B. Khoo, P. Wilairat, M.-L. Go, *Eur. J. Pharm. Sci*., 2006, **27**, 175.
16. C. Biot, B. Pradines, M. H. Sergeant, J. Gut, P. J. Rosenthal and K. Chibale, *Bioorg. Med. Chem. Lett*., 2007, **17**, 6434.
17. M. Mariño, E. Gayoso, J. M. Antelo, L. A. Adrio, J. J. Fernández and J. M. Vila, *Polyhedron*, 2006, **25**, 1449.
18. X. Du, C. Guo, E. Hansell, P. S. Doyle, C. R. Caffrey, T. P. Holler, J. H. McKerrow and F. E. Cohen, *J. Med. Chem.*, 2002**, 45**, 2695.
19. T. S. Lobana, A. Sánchez, J. S. Casas, A. Castiñeiras, J. Sordo, M. S. García-Tasende and E. M. Vázquez-López, *J. Chem. Soc*., *Dalton Trans*., 1997, 4289.
20. T. S. Lobana, G. Bawa, G. Hundal and M. Zeller, *Organometallics.* 2008, **27**, 175.
21. T. S. Lobana, G. Bawa, G. Hundal, R. J. Butcher, A. Castineiras, *Z. Anorg. Allg. Chem.*, 2009, **635**, 1447.
22. G. Socrates, in *Infrared and Raman characteristic group frequencies: tables and charts*, John Wiley and Sons, West Sussex, 3rd edn, 2001, pg. 8.
23. M. A. Bennett and A.K. Smith, *J. Chem. Soc. Dalton Trans.*, 1974, **2**, 233.
24. J. Soleimannejad and C. White, *Organometallics*, 2005, **24**, 2538.
25. R. A. Zelonka and M. C. Baird, *Can. J. Chem.*, 1972, **50**, 3063.
26. D. M. P. Mingos and A. L. Rohl, *Inorg. Chem.*, 1991, **30**, 3769.
27. T. Stringer, B. Therrien, D. T. Hendricks, H. Guzgay and G. S. Smith, *Inorg. Chem. Commun.*, 2011, **14**, 956.
28. T. Stringer, D. T. Hendricks, H. Guzgay and G. S. Smith, *Polyhedron*, 2012, **31**, 486.

29. P. Chellan, S. Nasser, L. Vivas, K. Chibale and G. S. Smith, *J. Organomet. Chem.*, 2010, **695**, 2225.
30. H. Weiss and F. Mohr, *J. Organomet. Chem.*, 2011, **696**, 3150.
31. L. Adrio, G. Alberdi, A. Amoedo, D. Lata, A. Fernández, J. Martínez, M. T. Pereira and J. M. Vila, *Z. Anorg. Allg. Chem.*, 2005, **631**, 2197.
32. A. M. M. Meij, S. Otto and A. Roodt, *Inorg. Chim. Acta.*, 2005, **358**, 1005.
33. N. Chavain, H. Vezin, D. Dive, N. Touati, J. F. Paul, E. Buisine and C. Biot, *Mol. Pharm.*, 2008, **5**, 710.
34. F. Dubar, S. Bohic, C. Slomianny, J. C. Morin, P. Thomas, H. Kalamou, Y. Guérardel, P. Cloetens, J. Khalife and C. Biot, *Chem. Commun.*, 2012, **48**, 910.
35. C. Biot, W. Castro, C. Y. Botte and M. Navarro, *Dalton Trans.*, 2012, **41**, 6335.
36. R. G. Compton and C. E. Banks, in *Understanding voltammetry*, Imperial College Press, London, 2nd edn., 2011.

CHAPTER 4

Antiplasmodial evaluation of aryl- and ferrocenyl-derived transition metal thiosemicarbazone complexes

4.1. Introduction

Thiosemicarbazones have been evaluated for antiplasmodial activity against *P. falciparum* strains.[1-3] Several mechanisms have been proposed to explain the activity of thiosemicarbazones against *P. falciparum.* An important process for parasite survival involves the degradation of host haemoglobin in the food vacuole of the parasite to derive amino acids.[4] It is believed that thiosemicarbazones may either inhibit cysteine proteases which are involved in haemoglobin degradation, or chelate to endogenous metals such as Fe(III) which may be required for the function of certain metal dependent enzymes.[1,5]

A variety of organometallic compounds have been evaluated as antimalarial agents.[6-9] As previously mentioned thiosemicarbazones are favourable ligands for coordination compounds due to the supply of electron-donating atoms such as oxygen, nitrogen and sulfur which are able to chelate to a range of metals. As part of this MSc study, the metals of interest are palladium and ruthenium. It has been stated in Chapter 1 that ruthenium was chosen due to its' ability to mimic iron as well as the low toxicity generally observed for ruthenium(II) complexes.[10] On the other hand, platinum and palladium resemble each other in a given oxidation state, and toxicity problems have been reported for platinum complexes.[11] Therefore, palladium complexes were synthesized to determine if they were more biologically active and a suitable alternative.

Reports of complexes so far studied include metals such as palladium(II), platinum(II), gold(I), gold(III), copper(II), nickel(II) and iron(II) ions.[12-17] The biological activity of thiosemicarbazone complexes is believed to be attributed to either the generation of reactive oxygen species or a synergistic effect whereby the thiosemicarbazone ligand dissociates from the metal upon entering the cell to allow chelation of endogenous metals.[1,18] In earlier studies, an enhancement of activity has been observed upon complexation as opposed to the free ligand, as well as an enhancement with an increase in metal centres.[19-20] Therefore, in this study the antiplasmodial activity of the free ligands synthesized as well as the polynuclear complexes will be evaluated to determine if the presence of a metal and/or several metals enhances biological activity.

4.2. The antiplasmodial activity of aryl-derived thiosemicarbazone cyclopalladated complexes containing N- and P-donor ligands

A biological evaluation of selected aryl-derived thiosemicarbazones (**1** and **2**) and their corresponding palladium(II) complexes (**7**-**15**) described in Chapter 2 was undertaken. These compounds were evaluated for antiplasmodial activity against the *P. falciparum* strains, NF54 (chloroquine-sensitive) and Dd2 (chloroquine-resistant). The control drug used in the experiment was chloroquine diphosphate (CQDP) for both the NF54 and the Dd2 strains.

Compounds **1** and **2** (Fig. 4.1) exhibited better activity against the Dd2 strain than the NF54 strain, with the lowest IC_{50} value of 4.46 ± 0.74 μM being observed for compound **2** (Table 4.1). The observation that the compound containing an ethyl group (on the imine carbon) has better activity over those containing methyl groups have been reported in literature.[21] For the tetranuclear complexes **7** and **8** (Fig. 4.1), both complexes were inactive against the NF54 and Dd2 strains, which may be attributed to poor solubility at the highest tested concentrations (100 000 ng/mL).

The thiosemicarbazone ligands (**1** and **2**) and complexes (**7** and **8**) have previously been tested against different strains, namely the CQS (3D7) and CQR (K1) strains.[12] In these strains, the ligands exhibited moderate activity against 3D7, but were inactive (> 20 μM) against the K1 strain.[12] When tested against the 3D7 and K1 strains, complex **7** exhibited moderate activity while **8** was inactive at the tested concentration.[12] Perhaps different modes of action are responsible for the activity in the different strains.

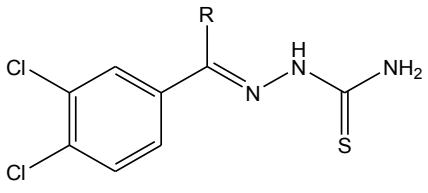

R = CH_3 (**1**), CH_2CH_3 (**2**)

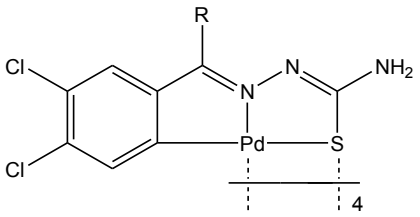

R = CH_3 (**7**), CH_2CH_3 (**8**)

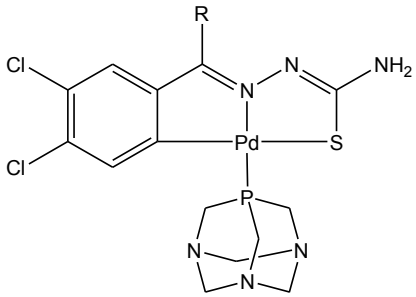

R = CH_3 (**9**), CH_2CH_3 (**10**)

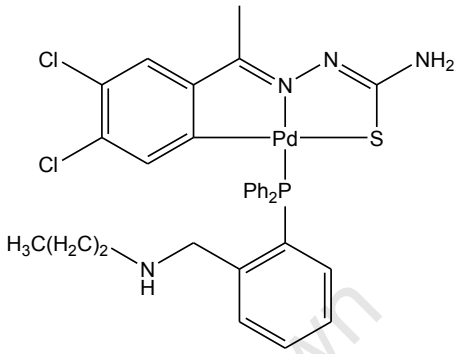

11

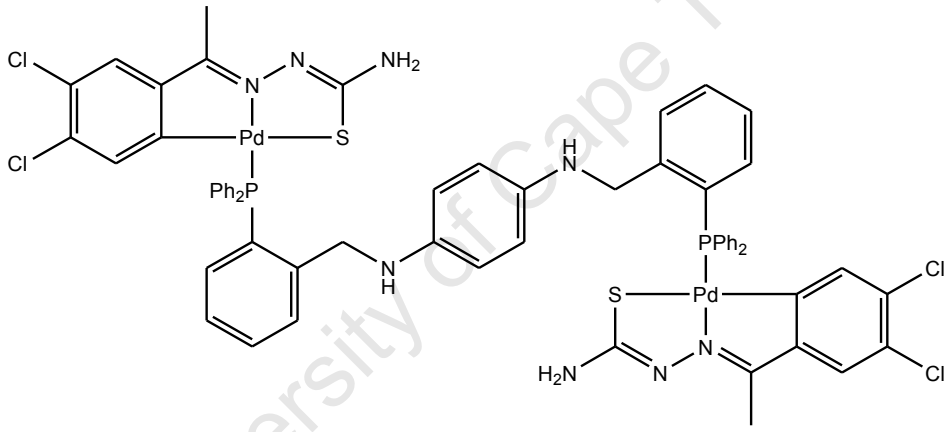

12

Figure 4.1: The cyclopalladated complexes evaluated for antiplasmodial activity.

The mononuclear complexes containing P-donor ligands exhibited activity against the NF54 and Dd2 strains. A comparison between compounds **9** and **10** (Fig. 4.1, containing the P-donor ligand PTA), shows that compound **10** (containing the ethyl chain on the imine carbon) exhibits better inhibitory activity against the Dd2 strain (IC_{50} = 1.73 ± 0.16 μM) than **9** (IC_{50} = 2.69 ± 0.22 μM).[21] However, it appears that incorporation of an aminophosphine ligand may contribute more to the lipophilic properties of the compound. Compound **11** (Fig. 4.1) is slightly more active than compounds **9** and **10**, with the best inhibitory effect displayed against the Dd2 strains (IC_{50} = 1.59 ± 0.053 μM). Compounds **9**-**11** exhibit comparable inhibitory activity against the NF54 strain with IC_{50} values of 1.93 ± 0.04 μM, 1.81 ± 0.11 μM and 1.76 ± 0.074 μM respectively (Table 4.1). An enhancement of activity is observed

for the mononuclear complexes (**9-11**) compared to the free monothiosemicarbazone ligands (**1** and **2**).

Table 4.1: IC_{50}[a] values for compounds **1-15** against the *P. falciparum* strains NF54 (CQS) and Dd2 (CQR).

Compound	NF54 (μM)	Dd2 (μM)	RI[b]
1	14.1 ± 0.34	9.82 ± 0.78	0.70
2	19.0 ± 2.18	4.46 ± 0.74	0.23
7	Inactive	Inactive	ND[c]
8	Inactive	Inactive	ND
9	1.93 ± 0.04	2.69 ± 0.22	1.39
10	1.81 ± 0.11	1.73 ± 0.16	0.96
11	1.76 ± 0.074	1.59 ± 0.053	0.90
12	Inactive	54.56 ± 3.83	ND
13	86.8 ± 9.99	7.11 ± 0.068	0.082
14	ND	0.191 ± 0.0013	ND
15	63.71 ± 6.49	Inactive	ND
CQDP	0.031 ± 0.006	0.22 ± 0.016	7.10

[a] IC_{50}: Compound concentration causing 50 % inhibition of parasitaemia *in vitro*
[b] RI : Resistance index = [IC_{50} (Dd2)]/[IC_{50} (NF54)]
[c] ND : Not determined

As previously stated, the rationale behind the synthesis of polynuclear complexes is to determine if an enhancement of activity will be observed for an increased number of metal centres. However, compound **12** (Fig. 4.1) which contains a dimeric aminophosphine ligand, allowing for the synthesis of a binuclear complex, exhibits only moderate activity (IC_{50} = 54.56 ± 3.83 μM) against the Dd2 strain in comparison to the mononuclear complexes **9-11** (IC_{50} = *ca.* 1.83 μM). Against the NF54 strain, compound **12** is inactive at the tested concentration (>100 000 ng/mL, Table 4.1), which may be due to poor solubility in the assay. However, based on the data available for the Dd2 strain, the proposed enhancement of activity is not observed moving from the mononuclear complexes (**9-11**) to the binuclear complex (**12**).

An RI value <1 or as small as possible would suggest that there is no evidence of cross-resistance occurring and that the compounds are likely to be active against resistant strains

and do not display cross-resistance with chloroquine.[22] The RI values of the tested compounds are determined relative to chloroquine, and are calculated by dividing the IC_{50} values for the CQR strain (Dd2) by that of the CQS strain (NF54). The RI values were calculated for the aryl-derived compounds, and found to be lower than the value for chloroquine diphosphate. Comparing the RI values of compounds **1**-**12**, only compound **9** is susceptible to cross-resistance.

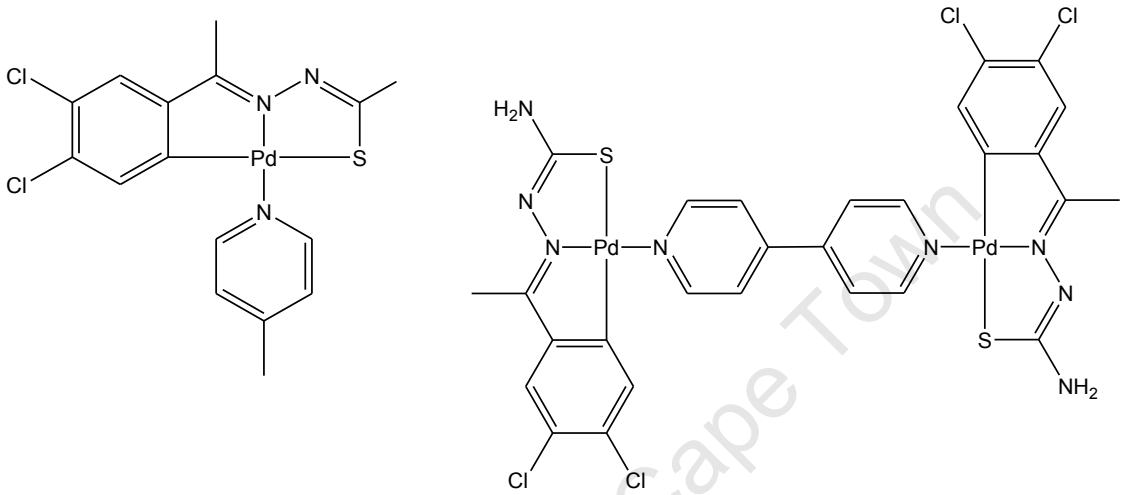

13

14

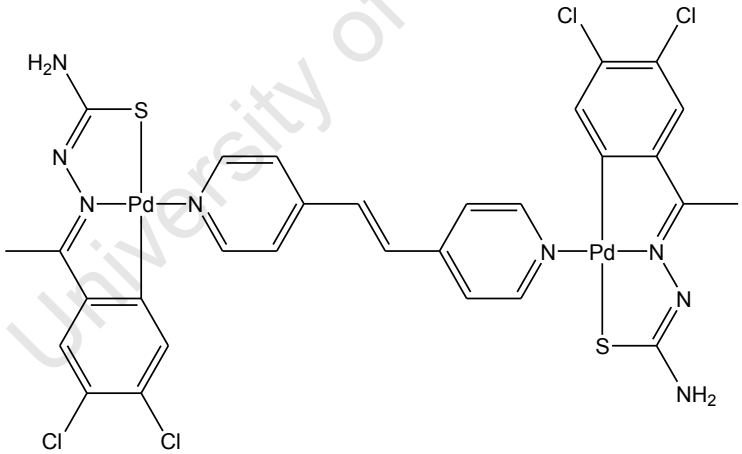

15

Figure 4.2: The cyclopalladated complexes evaluated for antiplasmodial activity.

Cyclopalladated complexes containing N-donor ligands have also been evaluated for antiplasmodial activity. Against the Dd2 strain, compounds **13** and **14** (Fig. 4.2) exhibited moderate activity with IC_{50} values of 7.11 ± 0.068 μM and 0.191 ± 0.0013 μM respectively. Compound **15** (Fig. 4.2) was inactive at the tested concentration (>10 000 ng/mL). However, against the NF54 strain compounds **13** and **15** exhibits moderate activity, whilst compound **14** was not tested (Table 4.1). Compound **13** exhibits a 12-fold (IC_{50} = 7.11 ± 0.068 μM)

increase in activity against the Dd2 in comparison to the NF54 strain. Compound **14** exhibited the highest activity with an IC_{50} value of 0.191 ± 0.0013 μM against the Dd2 strain (Table 4.1).

There is no obvious trend observed for the complexes containing N-donor ligands (**13**-**15**) when comparing their activity to the free ligand, as well as the activity between the mono- and binuclear complexes. Against the Dd2 strain, the mononuclear complex **13** exhibited a slight enhancement of activity compared to the free ligand (**1**). Moving from the mononuclear complex to the binuclear complex (**14**) there is a significant enhancement of activity compared to both the free ligand and the mononuclear complex. It appears that a trend is evident when considering the Dd2 strain. However, for the NF54 strain there is a loss of activity for **13** (IC_{50} = 86.8 ± 9.9 μM) compared to the free ligand (IC_{50} = 14.1 ± 0.34 μM), and a slight enhancement of activity moving from **13** to the binuclear complex **15** (IC_{50} = 63.71 ± 6.49 μM).

The calculated RI value for the aryl-derived complex **13** (RI = 0.082) was lower than the value for chloroquine diphosphate, suggesting that **13** is more active against the Dd2 strain and is less likely to be susceptible to cross-resistance. A comparison of the RI values of compounds **1**-**13**, shows that compound **13** is the least susceptible (Table 4.1).

4.3. The antiplasmodial activity of *N,S*-chelated ferrocenylthiosemicarbazone ruthenium(II)-arene complexes

The ferrocenyl-derived thiosemicarbazone (**16**) and related ruthenium(II) complexes (**22**-**24**) described in Chapter 3 were screened for antiplasmodial activity against the *P. falciparum* strains, NF54 and Dd2. The control drug used in the experiment was once again chloroquine diphosphate (CQDP).

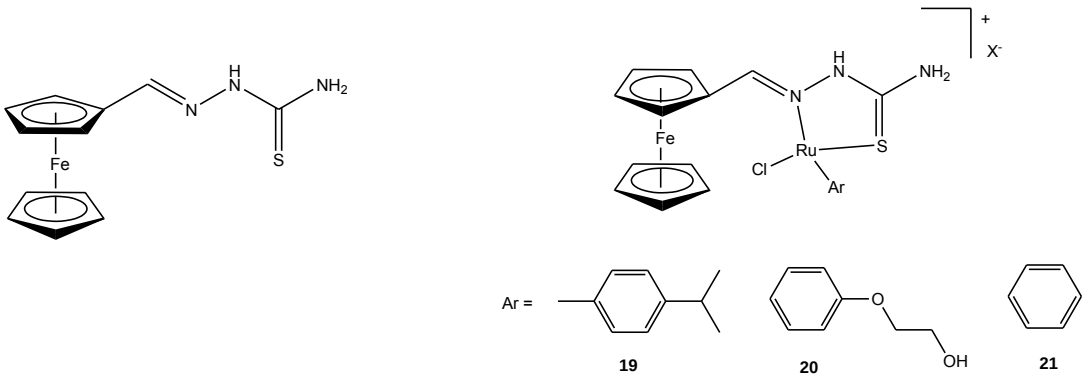

22 (Ar = **19**), X = Cl
23 (Ar = **20**), X = Cl
24 (Ar = **21**), X = PF_6

Figure 4.3: The ferrocenylthiosemicarbazone ruthenium complexes evaluated for antiplasmodial activity.

Compound **16** (Fig. 4.3) exhibited moderate activity against the NF54 and Dd2 strains with IC_{50} values of 3.43 ± 0.36 μM and 6.40 ± 0.088 μM respectively. When evaluated against the Dd2 strain, the ruthenium(II) complexes **22** and **23** (Fig. 4.3) exhibited activity (IC_{50} = 6.59 ± 0.31 and 6.61 ± 0.29 μM respectively) comparable to that of the free ligand (**16**, IC_{50} = 6.40 ± 0.088 μM), whereas compound **24** was 2-fold less active (IC_{50} = 14.1 ± 0.88 μM) than both the free ligand and compounds **22** and **23** (Table 4.2). While compound **16** appears to exhibit higher activity against the NF54 strain, the same cannot be said for the complexes. There was a decrease in activity when the ruthenium(II)-arene complexes **22-24** were tested against the NF54 strain, exhibiting only moderate activity. Once again compounds **22** and **23** exhibited comparable activity (IC50 = 8.63 ± 0.60 and 9.71 ± 1.97 μM respectively) to each other, whilst compound **24** was significantly less active (IC_{50} = 16.5 ± 1.02 μM, Table 4.2). The arene ring is present in order to stabilize the metal, as well as possibly altering the lipophilicity of the complex, either to assist with membrane crossing or retaining the complex within the active site.[23] Perhaps the complexes containing the *p*-cymene and phenoxyethanol rings are more favourable than the benzene (**24**), due to the lipophilic properties contributed to whichever mode of action is being followed.

The calculated RI values for the free ligand (**16**) as well as the ruthenium(II) complexes (**22-24**) are significantly lower than chloroquine diphosphate (RI = 7.10). However, it is apparent that only the free ligand is prone to cross-resistance, whereas compounds **22-24** have RI values of <1 and are therefore not susceptible to cross-resistance (Table 4.2).

Table 4.2: IC_{50}[a] values for compounds **16** and **22-24** against the *P. falciparum* strains NF54 (CQS) and Dd2 (CQR).

Compound	NF54 (µM)	Dd2 (µM)	RI[b]
16	3.43 ± 0.36	6.40 ± 0.088	1.87
22	8.63 ± 0.60	6.59 ± 0.31	0.76
23	9.71 ± 1.97	6.61 ± 0.29	0.68
24	16.5 ± 1.02	14.1 ± 0.88	0.85
CQDP	0.031 ± 0.006	0.22 ± 0.016	7.10

[a] IC_{50}: Compound concentration causing 50 % inhibition of parasitaemia *in vitro*
[b] RI : Resistance index = [IC_{50} (Dd2)]/[IC_{50} (NF54)]

4.4. The antiplasmodial activity of *N,S*-chelated ferrocenylthiosemicarbazone palladium(II) complexes containing P-donor ligands

The synthesis of palladium(II) complexes containing ferrocenyl-derived thiosemicarbazones were described in Chapter 3. The ferrocenyl-derived thiosemicarbazones (**16** and **18**) and the corresponding palladium(II) complexes (**28**-**31**) were screened for antiplasmodial activity against the NF54 and Dd2 strains, with chloroquine diphosphate (CQDP) as the control drug used in the experiment.

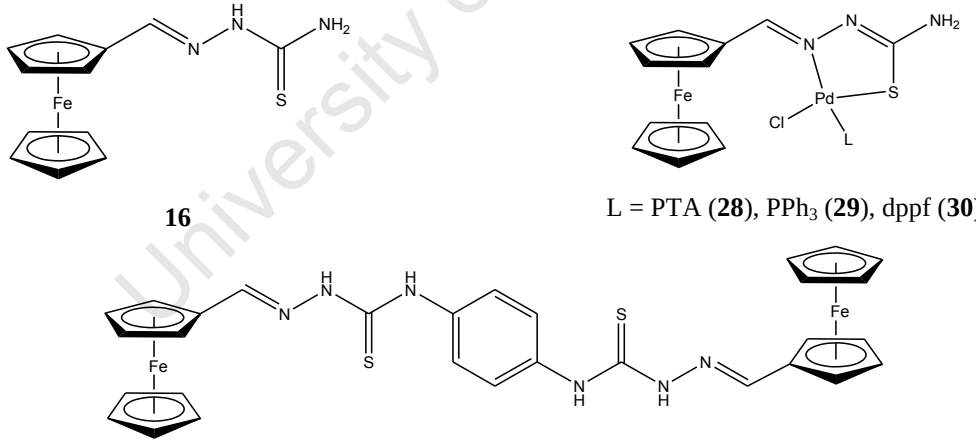

16

L = PTA (**28**), PPh_3 (**29**), dppf (**30**)

18

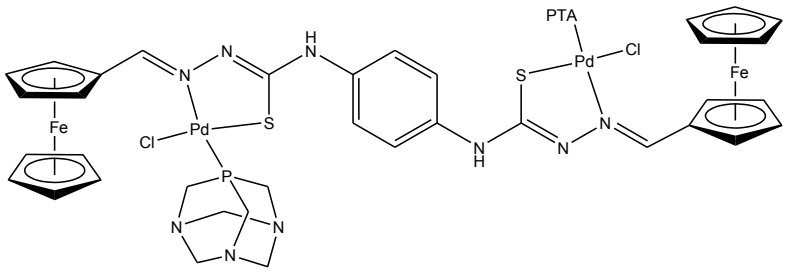

31

Figure 4.4: The ferrocenylthiosemicarbazone palladium complexes evaluated for antiplasmodial activity.

The heterobimetallic binuclear complexes (**28** and **29**) exhibited moderate activity against both strains, whilst the heterobimetallic pentanuclear complex (**30**) exhibited moderate activity (IC_{50} = 5.56 ± 0.26 μM) against the NF54 strain but was inactive (>10 000 ng/mL) against the Dd2 strain. Compound **29** (Fig. 4.4)**,** which contains the triphenylphosphine ligand, is more active than compound **28** (PTA, Fig. 4.4) against both the NF54 and Dd2 strains with IC_{50} values of 3.89 ± 0.53 μM and 4.94 ± 0.41 μM respectively. When compared to the free ligand, the activity of compound **29** (IC_{50} = 3.89 ± 0.53 μM) is similar against the NF54 strain and more active (IC_{50} = 4.94 ± 0.41 μM) than compound **16** against the CQR (Dd2) strain (Table 4.3).

Compound **28** (IC_{50} = 9.29 ± 0.51 μM) was more active against the Dd2 strain than the NF54, but no enhancement of activity is observed compared to the free ligand (IC_{50} = 6.40 ± 0.088 μM). As mentioned before, compound **30** (Fig.4.4) was inactive against the Dd2 strain at the tested concentration. An IC_{50} value of 5.56 ± 0.26 μM was obtained when **30** was tested against the NF54 strain. The pentanuclear complex (**30**), containing three ferrocenyl moieties and two palladium centres, exhibited good activity. However, this activity was not higher than that of the binuclear complex (**29**).

Table 4.3: IC_{50}[a] values for compounds **16**, **18** and **28**-**31** against the *P. falciparum* strains NF54 (CQS) and Dd2 (CQR).

Compound	NF54 (μM)	Dd2 (μM)	RI[b]
16	3.43 ± 0.36	6.40 ± 0.088	1.86
28	14.98 ± 0.32	9.29 ± 0.51	0.62
29	3.89 ± 0.53	4.94 ± 0.41	1.27
30	5.56 ± 0.26	Inactive	ND[c]
18	Inactive	Inactive	ND
31	Inactive	Inactive	ND
CQDP	0.031 ± 0.006	0.22 ± 0.016	7.10

[a] IC_{50}: Compound concentration causing 50 % inhibition of parasitaemia *in vitro*
[b] RI : Resistance index = [IC_{50} (Dd2)]/[IC_{50} (NF54)]
[c] ND : Not determined

The observation that a complex containing PPh_3 is more active than one containing PTA (Fig. 4.5) has previously been reported in the literature by Chellan *et al.*[14] The complexes were tested against the CQS (D10) and CQR (Dd2) strains. The complex containing the PPh_3

ligand exhibited higher activity than those containing PTA, with IC_{50} values of 19.93 ± 3.74 μM and 14.47 ± 1.98 μM for D10 and Dd2 respectively.[14] The complexes containing PTA exhibited IC_{50} values of 21.42 ± 1.22 and 24.90 ± 3.24 μM against D10 and Dd2 respectively.[14]

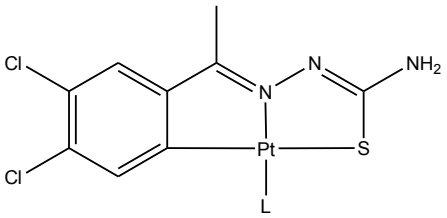

L = PTA, PPh_3

Figure 4.5: Cycloplatinated complexes containing the P-donor ligands PTA and PPh_3.[14]

Both the ferrocenyldithiosemicarbazone (**18**) and the palladium(II) complex (**31**) were inactive at the tested concentration against the CQS (NF54) and CQR (Dd2) strains. The resistance index values were calculated for compounds **28**-**29** (Table 4.3). A comparison of the RI values suggests that compound **28**, which is the least active against both strains, has the lowest RI value.

As seen in Chapter 3 (Section 3.3), preliminary cyclic voltammetry studies were carried out to determine if the activity of the compounds could be related to the generation of reactive oxygen species. There is evidence which suggests that the oxidation of the ferrocenyl moiety could produce, via Fenton-like reactions, reactive oxygen species (hydroxyl radicals) which disrupts lipid membranes.[7,18,24]

From the electrochemical studies, it was found that compounds **16** and **29** had comparable $E_{1/2}$ values of 356 mV and 359 mV, respectively. Compound **28** had an $E_{1/2}$ value of 373 mV, whereas compound **30** had a value of 331 mV. If it is easier to oxidise the iron in the ferrocenyl moiety (lower $E_{1/2}$ value) then more electrons would be available for radical generation. Therefore, examining the $E_{1/2}$ values it is expected that compounds **16** and **29** would have similar activity. As stated before compounds **16** and **29** have comparable IC_{50} values against the NF54 strain, whilst compound **28** is the least active (Table 4.3). It is expected that compound **30** would have the best activity, whereas compound **28** would be the least active. The proposal that compound **30** has the best activity is not observed in this study, but it does exhibit better activity than compound **28**.

4.5. Summary

Selected aryl- and ferrocenyl derived ligands, as well as palladium and ruthenium compounds were evaluated for antiplasmodial activity against the chloroquine-sensitive (NF54) and the chloroquine-resistant (Dd2) strains of *P. falciparum*. For the aryl-derived series (**1**-**15**) it was found that of the palladium(II) complexes containing P-donor ligands, the mononuclear complex **11** containing the aminophosphine ligand, was the most active against both strains. For the compounds containing the N-donor ligands the binuclear complex **14** was the most active against the Dd2 strain. Overall, the mononuclear complexes containing P-donor ligands (**9**-**11**) exhibited an enhancement of activity compared to the free ligands (**1** and **2**). However, this trend was not observed moving to the binuclear complex (**12**), which was less active than the ligands as well as the mononuclear complexes.

There was no clear overall correlation between the ligand, the number of metal centres and the biological activity observed. Against the Dd2 strain, the trend appears to hold as an enhancement of activity is observed moving from the free ligand (**1**) to the mononuclear complex (**13**) to the binuclear complex (**14**). Considering the activity exhibited against the NF54 strain, a slight enhancement of activity moving from **13** to the binuclear complex **15**, whereas both are significantly less active than the free ligand.

In the second series, which focuses on ferrocenyl-derived ruthenium(II) complexes, the free ligand **16** and the heterobimetallic binuclear complexes (**22**-**24**) were tested. There was no obvious beneficiary effect observed due to the incorporation of a ruthenium(II) ion as the IC_{50} values were either similar to that of the free ligand or exhibited lower activity.

The third series of compounds synthesized centred around ferrocenyl-derived palladium(II) complexes (**28**-**31**) which contain P-donor ligands. Compounds **28**-**30** exhibited activity against both strains, with compound **29** which contains the triphenylphosphine ligand, exhibiting the best activity. The free ferrocenyldithiosemicarbazone (**18**) and the corresponding palladium(II) complex (**31**) which contains PTA were both inactive against the NF54 and Dd2 strains at the tested concentrations.

Against the NF54 strain, the activity observed for the free ligand and the binuclear complex (**29**) is comparable whereas the binuclear complex **28** is less active. The pentanuclear complex (**30**) is both more active (**28**) and less active (**29**) than the binuclear complexes.

Therefore, the expected enhancement of activity cannot ultimately be ruled out for this series of compounds. The preliminary data from electrochemical studies for certain compounds suggest a correlation between the ease of oxidation and the IC_{50} values.

4.6. References

1. D. C. Greenbaum, Z. Mackey, E. Hansell, P. Doyle, J. Gut. C. R. Caffrey, J. Lehrman, P. J. Rosenthal, J. H. McKerrow and K. Chibale, *J. Med. Chem.*, 2004, **47**, 3212.
2. R. B. de Oliveira, E. M. de Souza-Fagundes, R. P. P. Soares, A. A. Andrade, A. U. Krettli and C. L. Zani, *Eur. J. Med. Chem.*, 2008, **43**, 1983.
3. A. Chipeleme, J. Gut, P.J. Rosenthal and K. Chibale, *Bioorg. Med. Chem.*, 2007, **15**, 273.
4. I. W. Sherman, in *Malaria: Parasite biology, pathogenesis and protection*, American Society for Microbiology, Washington, 1998, chap. 10.
5. I. Chiyanzu, E. Hansell, J. Gut, P. J. Rosenthal, J. H. McKerrow and K. Chibale, *Bioorg. Med. Chem. Lett.*, 2003, **13**, 3527.
6. R. A. Sánchez-Delgado, M. Navarro, H. Pérez and J. A. Urbina, *J. Med. Chem.*, 1996, **39**, 1095.
7. C. Biot, W. Castro, C. Y. Botte and M. Navarro, *Dalton Trans.*, 2012, **41**, 6335.
8. M. Navarro, W. Castro and C. Biot, *Organometallics*, 2012, DOI: 10.1021/om300296n.
9. S. D. Khanye, J. Gut, P. J. Rosenthal, K. Chibale and G. S. Smith, *J. Organomet. Chem.*, 2011, **696**, 3296.
10. C. S. Allardyce and P. J. Dyson, *Platinum Met. Rev.*, 2001, **45**, 62.
11. E. Wong and C. M. Giandomenico, *Chem. Rev.*, 1999, **99**, 2451.
12. P. Chellan, S. Nasser, L. Vivas, K. Chibale and G. S. Smith, *J. Organomet. Chem.*, 2010, **695**, 2225.
13. P. Chellan, N. Shunmoogam-Gounden, D. T. Hendricks, J. Gut, P. J. Rosenthal, C. Lategan, P. J. Smith, K. Chibale and G. S. Smith, *Eur. J. Inorg. Chem.*, 2010, **22**, 3520.
14. P. Chellan, K. M. Land, A. Shokar, A. Au, S. H. An, C. M. Clavel, P. J. Dyson, C. de Kock, P. J. Smith, K. Chibale and G. S. Smith, *Organometallics*, 2012, **31**, 5791.
15. S. D. Khanye, G. S. Smith, C. Lategan, P. J. Smith, J. Gut, P. J. Rosenthal and K. Chibale, *J. Inorg. Biochem.*, 2010, **104**, 1079.
16. S. D. Khanye, B. Wan, S. G. Franzblau, J. Gut, P. J. Rosenthal, G. S. Smith and K. Chibale, *J. Organomet. Chem.*, 2011, **696**, 3392.
17. J. P. Scovill, D. L. Klayman and C. F. Franchino, *J. Med. Chem.*, 1982, **25**, 1261.

18. N. Chavain, H. Vezin, D. Dive, N. Touati, J. F. Paul, E. Buisine and C. Biot, *Mol. Pharm.*, 2008, **5**, 710.
19. R. A. Sánchez-Delgado, M. Navarro, H. Pérez and J. A. Urbina, *J. Med. Chem.*, 1996, **39**, 1095.
20. S. D. Khanye, J. Gut, P. J. Rosenthal, K. Chibale and G. S. Smith, *J. Organomet. Chem.*, 2011, **696**, 3296.
21. X. Du, C. Guo, E. Hansell, P. S. Doyle, C. R. Caffrey, T. P. Holler, J. H. McKerrow and F. E. Cohen, *J. Med. Chem.*, 2002**, 45**, 2695.
22. C. Herrmann, P. F. Salas, J. F. Cawthray, C. de Kock, B. O. Patrick, P. J. Smith, M. J. Adam and C. Orvig, *Organometallics*, DOI: 10.1021/om300354x.
23. L. Glans, A. Ehnbom, C. De Kock, A. Martínez, J. Estrada, P. J. Smith, M. Haukka, R. A. Sánchez-Delgado and E. Nordlander, *Dalton Trans.*, 2012, **41**, 2764.
24. F. Dubar, S. Bohic, C. Slomianny, J. C. Morin, P. Thomas, H. Kalamou, Y. Guérardel, P. Cloetens, J. Khalife and C. Biot, *Chem. Commun.*, 2012, **48**, 910.

CHAPTER 5

Overall conclusion and future outlook

5.1. Overall conclusion

The first series focuses on aryl-derived cyclopalladated thiosemicarbazone complexes. Aryl-derived monothiosemicarbazone ligands were prepared and characterized using spectroscopic techniques such as NMR and infrared (IR) spectroscopy. When the thiosemicarbazone ligands were reacted with $K_2[PdCl_4]$/$Na_2[PdCl_4]$, the thiosemicarbazone chelated in a tridentate *C,N,S*-donor fashion to afford the tetranuclear complexes. The tetranuclear complexes were characterized using NMR and infrared (IR) spectroscopy, and used in subsequent reactions with P- and N-donor ligands.

Monomeric and dimeric imino- and aminophosphine ligands were prepared by reacting the aldehyde with the appropriate amine, and the further reduction of the iminophosphine using sodium borohydride to synthesize the aminophosphine ligands. The ligands were characterized using various spectroscopic and analytical techniques such as NMR and IR spectroscopies, and mass spectrometry.

P-donor ligands, including the aforementioned aminophosphine ligands, were used to prepare three mononuclear complexes and one binuclear complex. One mononuclear and two binuclear complexes were prepared as additional set of cyclopalladated complexes which contain N-donor ligands. These complexes were characterized using NMR and IR spectroscopies, and mass spectrometry. In addition to their spectroscopic and analytical characterization, the molecular structures of two mononuclear cyclopalladated complexes (**10** and **11**) have been determined using single-crystal X-ray diffraction, and found to have a slightly distorted square-planar geometry around the palladium(II) centre.

Ferrocenyl-derived thiosemicarbazones have been prepared and characterized using NMR, infrared (IR) spectroscopy and mass spectrometry. The ferrocenyl-derived thiosemicarbazones were used in the preparation of a second and third series of compounds.

Heterobimetallic ruthenium(II) complexes make up the second series, wherein the ferrocenyl-derived thiosemicarbazones chelate in a *N,S*-chelated mode. Three ruthenium dimers $[Ru(Ar)(\mu\text{-}Cl)Cl]_2$ (Ar = *p*-$^{i}PrC_6H_4CH_3$, $C_6H_5O(CH_2)_2OH$, C_6H_6) were reacted with

ferrocenyl-derived thiosemicarbazones to prepare three binuclear and two tetranuclear ruthenium(II)-arene complexes. These complexes were characterized using NMR and IR spectroscopies, and mass spectrometry.

The third series focuses on the synthesis of *N*,*S*-chelated ferrocenyl-derived palladium(II) complexes. A binuclear chloro-bridged complex, prepared by reacting the monomeric ferrocenyl-derived thiosemicarbazone with $K_2[PdCl_4]$, is used in subsequent reactions with P-donor ligands. Two binuclear complexes, two tetranuclear complexes and one pentanuclear complex were synthesized and characterized using NMR and IR spectroscopies, and mass spectrometry. The molecular structure of a binuclear complex, containing the water-soluble P-donor ligand 1,3,5-triaza-7-phosphaadamantane, was elucidated using single-crystal X-ray diffraction.

Selected ligands and metal complexes were evaluated for antiplasmodial activity against *Plasmodium falciparum* strains, NF54 (chloroquine-sensitive) and Dd2 (chloroquine-resistant). The ligands and complexes exhibited moderate inhibitory effects in the low micromolar range, with the first series of compounds containing the cyclopalladated complexes exhibiting better inhibitory effects than series two and three.

5.2. Future outlook

This project has revealed that there is merit in the use of these thiosemicarbazone palladium and ruthenium complexes as biological agents. Better inhibitory effects may be observed if changes are made to the structures presented in this study. Perhaps varying the aryl rings of the thiosemicarbazone ligand, the terminal amine group or even the metal centre will favourably change the properties of the compounds, allowing for an enhancement of biological activity.

β-hematin studies carried out by Chellan *et al.* with cycloplatinated complexes revealed that there was no interaction between the *β*-hematin and the thiosemicarbazone complexes.[1] It is believed that the interaction between thiosemicarbazone ligands and cysteine proteases leads to the observed biological activity.[2] However the mode of action for the complexes is believed to be via synergistic effects. Therefore, additional studies would need to be carried out in order to elucidate possible mechanisms of action for thiosemicarbazone complexes.

Further ROS studies would need to be conducted on the ferrocenyl-derived palladium complexes to determine if there is a connection between the cyclic voltammetry data and the biological data.

5.3. References

1. P. Chellan, K. M. Land, A. Shokar, A. Au, S. H. An, C. M. Clavel, P. J. Dyson, C. de Kock, P. J. Smith, K. Chibale and G. S. Smith, *Organometallics*, 2012, **31**, 5791.
2. D. C. Greenbaum, Z. Mackey, E. Hansell, P. Doyle, J. Gut, C. R. Caffrey, J. Lehrman, P. J. Rosenthal, J. H. McKerrow and K. Chibale, *J. Med. Chem.*, 2004, **47**, 3212.

CHAPTER 6

Experimental procedures

6.1. General remarks

All reagents and solvents were purchased from commercial suppliers. All reagents were purchased from Aldrich and used without further purification. $PdCl_2$ and $Na_2PdCl_4.nH_2O$ and $RuCl_3.nH_2O$ were received as a generous donation from the Anglo American South Africa. $K_2[PdCl_4]$, $PdCl_2(PPh_3)_2$ and $PdCl_2(PTA)_2$ was prepared according to published literature procedures.[1-2] Nuclear magnetic resonance (NMR) spectra were recorded on either a Varian Mercury XR300 MHz (^{1}H: 300.08 MHz, ^{13}C: 75.46 MHz, ^{31}P: 121.47 MHz), Varian Mercury XR400 MHz (^{1}H: 399.95 MHz) or Bruker Biospin GmbH (^{1}H: 400.22 MHz, ^{13}C: 100.65 MHz, ^{31}P: 162.00 MHz) spectrometer at ambient temperature. ^{1}H and ^{13}C{^{1}H} NMR chemical shifts are referenced to the deuterated solvent. Infrared (IR) spectra were determined using a Perkin–Elmer Spectrum 100 FT-IR spectrometer, and were recorded using KBr pellets or NaCl solution cell (dichloromethane). Elemental analyses (C, H, S and N) were recorded on a Thermo Flash 1112 Series CHNS-O Analyser. Mass spectrometry was carried out at the University of Cape Town on a JEOL GCmateII and data were recorded using Electron Impact (EI) mode. Mass spectrometry was carried out at the University of Stellenbosch on a Waters API Quattro Micro triple quadrupole mass spectrometer and samples injected into a stream of 50% acetonitrile and 0.1% formic acid. Data were recorded using Electrospray Ionisation (ESI) mass spectrometry in the positive mode. Melting points were determined on the Büchi Melting Point apparatus B-540. Single-crystal X-ray diffraction data were collected on a Bruker KAPPA APEX II DUO diffractometer using graphite-monochromated Mo-Kα radiation (χ = 0.71073 Å).

6.2. Aryl-derived cyclopalladated thiosemicarbazone complexes

6.2.1. Synthesis of monothiosemicarbazone, imino- and aminophosphine ligands (1-6)

Synthesis of 3,4-dichloroacetophenone thiosemicarbazone (**1**)[3]

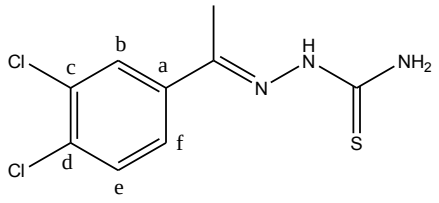

3,4-Dichloroacetophenone (0.708 g, 3.75 mmol) and thiosemicarbazide (0.342 g, 3.75 mmol) was added to ethanol (30.0 mL). While stirring, excess acetic acid (~ 2 mL) was added to the reaction. The reaction mixture was refluxed in air at 85 ˚C for 3 hrs, which produced a white solid upon cooling. The white crystalline solid, **1** (0.504 g, 51 %), was collected by suction filtration, washed with ethanol (20.0 mL) and diethyl ether (20.0 mL), and dried *in vacuo*. Melting point: 194.8-197.9 ˚C (lit. m.p. 196.0-197.9 ˚C). ^{1}H NMR (400.22 MHz, DMSO-d_6): δ (ppm) = 10.24 (s, 1H, CNNH); 8.31 (br s, 1H, NH_2); 8.25 (d, $^{4}J_{HH}$ = 2.00 Hz, 1H, H_b); 8.14 (br s, 1H, NH_2); 7.88 (dd, $^{4}J_{HH}$ = 2.00, $^{3}J_{HH}$ = 8.40 Hz, 1H, H_f); 7.61 (d, $^{3}J_{HH}$ = 8.40 Hz, 1H, H_e); 2.28 (s, 3H, CH_3). Elemental analysis for $C_9H_9Cl_2N_3S$: Found C 41.3, H 3.54, N 15.7, S 12.3 %; Calculated C 41.2, H 3.46, N 16.0, S 12.2 %. FT-IR (KBr, cm^{-1}): ν = 3422 (s, N-H); 3187 (w, N-H); 3141 (w, N-H); 1594 (s, C=N); 817 (m, C=S).

Synthesis of 3,4-dichloropropiophenone thiosemicarbazone (**2**)[3]

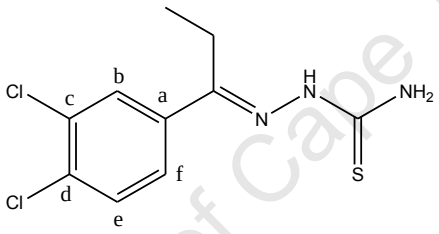

3,4-Dichloropropiophenone (0.515 g, 2.54 mmol) and thiosemicarbazide (0.232 g, 2.54 mmol) was added to ethanol (30.0 mL). While stirring, excess acetic acid (~ 3 mL) was added to the reaction. The reaction mixture was refluxed in air at 85 ˚C for 2 days and stirred overnight, which produced a white solid. The white crystalline solid, **2** (0.379 g, 54 %), was collected by suction filtration, and washed with ethanol (20.0 mL) and diethyl ether (10.0 mL), and dried *in vacuo*. Melting point: 186.6-188.1 ˚C (lit. m.p. 185.6-186.4 ˚C). ^{1}H NMR (400.22 MHz, DMSO-d_6) : δ (ppm) = 10.36 (s, 1H, CNNH); 8.31 (br s, 1H, NH_2); 8.23 (d, $^{4}J_{HH}$ = 2.00 Hz, 1H, H_b); 8.13 (br s, 1H, NH_2); 7.86 (d, $^{4}J_{HH}$ = 2.00, $^{3}J_{HH}$ = 8.80 Hz, 1H, H_f); 7.60 (d, $^{3}J_{HH}$ = 8.80 Hz, 1H, H_e); 2.86 (q, $^{3}J_{HH}$ = 7.60 Hz, 2H, CH_2); 0.99 (t, $^{3}J_{HH}$ = 7.60 Hz, 3H, CH_3). Elemental analysis for $C_{10}H_{11}Cl_2N_3S$: Found C 44.1, H 4.04, N 15.4, S 11.6 %; Calculated C 43.5, H 4.01, N 15.2, S 11.6 %. FT-IR (KBr, cm^{-1}): ν = 3387 (m, N-H); 3261 (w, N-H); 3175 (m, N-H); 1596 (s, C=N); 822 (s, C=S).

Synthesis of (E)-N-(2-(diphenylphosphino)benzylidene)propan-1-amine (**3**)[4]

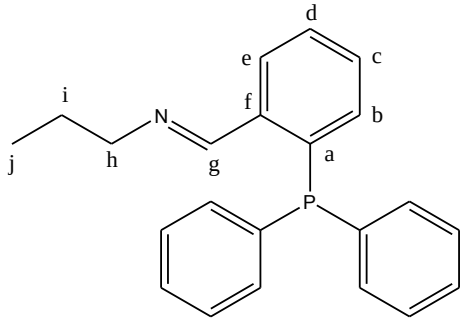

2-(Diphenylphosphino)benzaldehyde (0.147 g, 0.507 mmol) was dissolved in dry toluene (30.0 mL), followed by the addition of *n*-propylamine (0.0500 mL, 0.609 mmol). The reaction mixture was stirred over anhydrous $MgSO_4$, at ambient temperature for 24 hrs. The anhydrous $MgSO_4$ was filtered by gravity, and the solvent removed to yield an oil. The oil was redissolved in chloroform (20.0 mL) and extracted with water (40.0 mL x 6), after which the organic layer was collected. The organic layer was dried over anhydrous $MgSO_4$, the anhydrous $MgSO_4$ filtered, and the solvent removed. An orange oil, **3** (0.149 g, 90 %), was isolated and dried *in vacuo*. ^{1}H NMR (300.08 MHz, $CDCl_3$): δ (ppm) = 8.87 (d, $^4J_{HP}$ = 4.77 Hz, 1H, H_g); 7.98 (m, 1H, H_e); 7.31 (m, 12H, H_c & H_d & PPh_2); 6.88 (dd, J_{HH} = 7.51, 4.48 Hz, 1H, H_b); 3.44 (t, $^3J_{HH}$ = 6.83 Hz, 2H, H_h); 1.51 (m, 2H, H_i); 0.75 (t, $^3J_{HH}$ = 7.38 Hz, 3H, H_j). ^{31}P NMR (121.47 MHz, $CDCl_3$): δ (ppm) = -13.9. FT-IR (solution, CH_2Cl_2, cm^{-1}): ν = 1637 (s, C=N).

Synthesis of N-(2-(diphenylphosphino)benzyl)propan-1-amine (**4**)

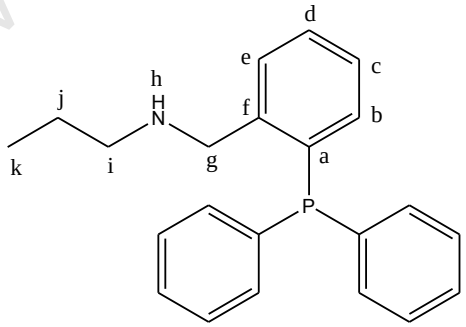

Compound **3** (0.0635 g, 0.192 mmol) was dissolved in dry methanol (20.0 mL), followed by the slow addition of sodium borohydride (0.0127 g, 0.336 mmol). The reaction mixture was stirred at ambient temperature for 3 hrs. The solvent was removed, the contents of the flask quenched with water (20.0 mL), and extracted with dichloromethane (3 x 20.0 mL). The organic layer was collected, washed with water (2 x 15.0 mL), and dried over anhydrous $MgSO_4$. The solvent was removed to afford a yellow oil, **4** (0.0583 g, 91 %), which was dried

in vacuo. ^{1}H NMR (399.95 MHz, $CDCl_3$): δ (ppm) = 7.58 (m, 1H, H_e); 7.40 (m, 1H, H_d); 7.23 (m, 10H, PPh_2); 7.09 (t, $^{3}J_{HH}$ = 7.64 Hz, 1H, H_c); 6.83 (dd, J_{HH} = 7.32, 4.39 Hz, 1H, H_b); 3.90 (s, 2H, H_g); 2.39 (t, $^{3}J_{HH}$ = 7.40 Hz, 2H, H_i); 1.72 (br s, 1H, H_h); 1.26 (m, 2H, H_j); 0.73 (t, $^{3}J_{HH}$ = 7.44 Hz, 3H, H_k). ^{13}C NMR (75.46 MHz, $CDCl_3$): δ (ppm) = 144.6 (d, $^{2}J_{CP}$ = 24.1 Hz, C_f); 136.6 (d, $^{1}J_{CP}$ = 10.1 Hz, C_{Ph}); 135.6 (d, $^{1}J_{CP}$ = 13.5 Hz, C_a); 133.9 (d, $^{2}J_{CP}$ = 20.1 Hz, C_{Ph}); 133.6 (C_e); 129.3 (d, $^{2}J_{CP}$ = 5.20 Hz, C_b); 128.8 (C_d); 128.7 (C_{Ph}); 128.5 (d, $^{3}J_{CP}$ = 6.87 Hz, C_{Ph}); 127.1 (C_c); 52.7 (d, $^{3}J_{CP}$ = 20.7 Hz, C_g); 51.4 (C_i); 23.2 (C_j); 11.9 (C_k). ^{31}P NMR (121.47 MHz, $CDCl_3$): δ (ppm) = -16.1. FT-IR (solution, CH_2Cl_2, cm^{-1}): ν = 3405 (w, N-H).

Synthesis of N^1,N^4-bis(2-(diphenylphosphino)benzylidene)benzene-1,4-diamine (**5**)

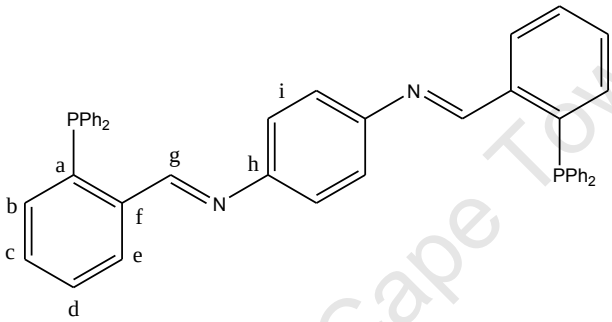

2-(Diphenylphosphino)benzaldehyde (0.101 g, 0.346 mmol) was added to methanol (15.0 mL), followed by the addition of *p*-phenylenediamine (0.0186 g, 0.172 mmol). The reaction mixture was refluxed at 68 ˚C for 6 hrs, and stirred overnight at ambient temperature to yield a yellow suspension. A light yellow powder, **5** (0.0985 g, 88 %), was collected by suction filtration, washed with hexane (5.00 mL), and dried *in vacuo*. Melting point: 206.4-210.4 ˚C. ^{1}H NMR (399.95 MHz, $CDCl_3$): δ (ppm) = 9.06 (d, $^{4}J_{HP}$ = 5.10 Hz, 2H, H_g); 8.19 (m, 2H, H_e); 7.45 (t, $^{3}J_{HH}$ = 7.80 Hz, 2H, H_d); 7.33 (m, 22H, PPh_2 & H_c); 6.94 (m, 2H, H_b); 6.88 (s, 4H, H_i). ^{31}P NMR (162.00 MHz, $CDCl_3$): δ (ppm) = -22.2. FT-IR (KBr, cm^{-1}): ν = 3435 (w, N-H); 1610 (m, C=N). MS-EI^{+}: *m/z* 653 ([M]$^{+}$, 40 %); 652 ([M-H]$^{+}$, 94 %).

Synthesis of N^1,N^4-bis(2-(diphenylphosphino)benzyl)benzene-1,4-diamine (**6**)

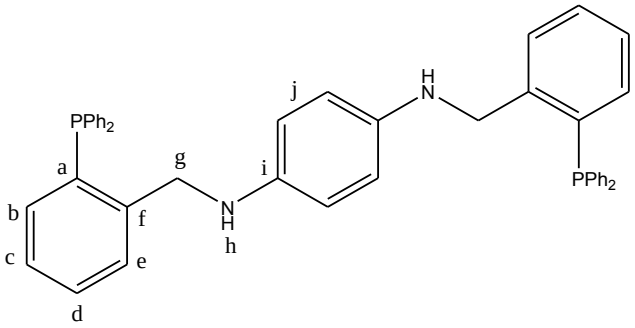

Compound **5** (0.0572 g, 0.0876 mmol) was dissolved in dry dichloromethane:methanol (75:25 % V/V, 20.0 mL), followed by the slow addition of sodium borohydride (0.0157g, 0.415 mmol). The reaction mixture was stirred at ambient temperature for 6 hrs. The solvent was removed, the contents redissolved in dichloromethane (25.0 mL), extracted using water (20.0 mL), and the organic layer was collected. The organic layer was washed with water (4 x 20.0 mL), and once again collected, and dried over anhydrous $MgSO_4$. The solvent was reduced to precipitate a yellow powder, **6** (0.0543 g, 94 %), which was collected by suction filtration, washed with hot hexane and dried *in vacuo*. Melting point: 194.8-198.5 ˚C. ^{1}H NMR (399.95 MHz, DMSO-d_6): δ (ppm) = 7.60 (m, 4H, H_e); 7.41 (m, 12H, PPh_2); 7.31 (t, $^3J_{HH}$ = 7.80 Hz, 2H, H_d); 7.24 (m, 8H, PPh_2); 7.17 (t, $^3J_{HH}$ = 7.60 Hz, 2H, H_c); 6.76 (dd, J_{HH} = 7.51, 4.76 Hz, 2H, H_b); 6.14 (s, 4H, H_j); 5.30 (br s, 2H, H_h); 4.19 (br s, 4H, H_g). ^{13}C NMR (100.65 MHz, DMSO-d_6): δ (ppm) = 144.1 (d, $^2J_{CP}$ = 22.0 Hz, C_f); 139.7 (C_i); 135.7 (d, $^1J_{CP}$ = 10.3 Hz, C_{Ph}); 134.4 (d, $^1J_{CP}$ = 14.7 Hz, C_a); 133.5 (d, $^2J_{CP}$ = 19.8 Hz, C_{Ph}); 132.2 (C_e); 131.3 (d, $^2J_{CP}$ = 9.46 Hz, C_b); 129.0 (C_d); 128.8 (d, $^3J_{CP}$ = 6.60 Hz, C_{Ph}); 127.0 (d, $^4J_{CP}$ = 4.40 Hz, C_{Ph}); 126.7 (C_c); 113.5 (C_j); 46.1 (d, $^3J_{CP}$ = 25.7 Hz, C_g). ^{31}P NMR (162.00 MHz, $CDCl_3$): δ (ppm) = - 16.9. FT-IR (KBr, cm^{-1}): ν = 3427 (w, N-H); 1517 (s, C=C). MS-EI$^+$: *m/z* 656 ([M]$^+$, 40 %); 655 ([M-H]$^+$, 100 %).

6.2.2. Synthesis of *C,N,S*-chelated thiosemicarbazone tetranuclear cyclopalladated complexes (7, 8)

Synthesis of [Pd(3,4-dichloroacetophenone thiosemicarbazone)]$_4$ (**7**)[5]

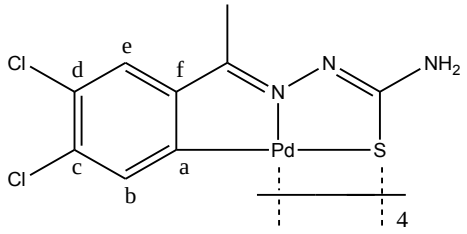

Potassium tetrachloropalladate (0.629 g, 1.93 mmol) was dissolved in water (5.00 mL). Ethanol (25.0 mL) was added to the solution, followed by the addition of compound **1** (0.502 g, 1.93 mmol), while stirring. The reaction mixture was stirred in air, at ambient temperature, for 2 days to produce a yellow solid. The solid was purified using diethyl ether and hexane. The yellow powder, **7** (0.945 g, 34 %), was collected by suction filtration, washed with ethanol (30.0 mL), and dried *in vacuo*.

The reaction with sodium tetrachloropalladate was carried out using a similar method to the reaction with potassium tetrachloropalladate. Sodium tetrachloropalladate (0.701 g, 2.01 mmol) was dissolved in water (5.00 mL). Ethanol (30.0 mL) was added to the solution, followed by the addition of compound **1** (0.622 g, 2.37 mmol), while stirring. The reaction mixture was stirred at ambient temperature for 3 days to produce a brown solid. The brown solid was recrystallised using diethyl ether and hexane. The yellow powder, **7** (0.383 g, 44 %), was collected by suction filtration, washed with hexane (30.0 mL), and dried *in vacuo*. Melting point: 313.2-318.3 ˚C (Decomposition without melting). ^{1}H NMR (399.95 MHz, DMSO-d_6): δ (ppm) = 7.37 (s, 1H, H_b); 7.07 (s, 2H, NH_2); 6.72 (s, 1H, H_e); 2.00 (s, 3H, CH_3). Elemental analysis for $C_{36}H_{28}Cl_8N_{12}Pd_4S_4$: Found C 29.3, H 2.20, N 10.62, S 8.28 %; Calculated C 29.5, H 1.92, N 11.5, S 8.75 %. FT-IR (KBr, cm^{-1}): ν = 3473 (w, N-H); 3352 (w, N-H); 1600 (m, C=N); 1560 (s, C=C).

Synthesis of [Pd(3,4-dichloropropiophenone thiosemicarbazone)]$_4$ (**8**)[5]

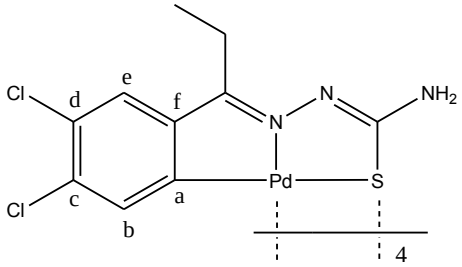

Potassium tetrachloropalladate (0.352 g, 1.08 mmol) was dissolved in water (5.00 mL), followed by the addition of ethanol (20.0 mL). Compound **2** (0.296 g, 1.07 mmol) was added to the flask while stirring. The reaction mixture was stirred at ambient temperature for 2 days to produce a yellow solid. The yellow powder, **8** (0.408 g, 25 %), was collected by suction filtration, washed with ethanol (20.0 mL) and diethyl ether (10.0 mL), and dried *in vacuo*. Melting point: 322-327 ˚C (Decomposition without melting). ^{1}H NMR (400.22 MHz, DMSO-d$_6$): δ (ppm) = 7.34 (s, 1H, H$_b$); 7.16 (s, 2H, NH$_2$); 6.65 (s, 1H, H$_e$); 2.86 (q, $^3J_{HH}$ = 7.68, 12.7 Hz, 1H, CH$_2$); 1.79 (q, $^3J_{HH}$ = 7.44, 12.5 Hz, 1H, CH$_2$); 1.06 (t, $^3J_{HH}$ = 7.00 Hz, 3H, CH$_3$). Elemental analysis for $C_{40}H_{36}Cl_8N_{12}Pd_4S_4$: Found C 31.9, H 2.64, N 10.4, S 8.10 %; Calculated C 31.6, H 2.38, N 11.0, S 8.42 %. FT-IR (KBr, cm^{-1}): ν = 3472 (w, N-H); 3376 (w, N-H); 1595 (s, C=N); 1562 (m, C=C).

6.2.3. Synthesis of *C,N,S*-chelated thiosemicarbazone cyclopalladated complexes containing P-donor ligands

a. Mononuclear *C,N,S*-chelated thiosemicarbazone cyclopalladated complexes (9-11)

Synthesis of [Pd(3,4-dichloroacetophenone thiosemicarbazone)(PTA)] (**9**)

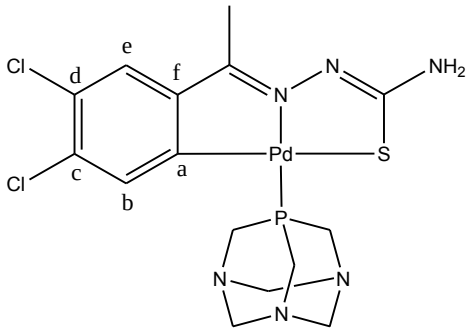

Compound **7** (0.300 g, 0.205 mmol) was suspended in acetone (30.0 mL), followed by the addition of 1,3,5-triaza-7-phosphaadamantane (0.123 g, 0.781 mmol) to the reaction flask. The reaction mixture was refluxed at 60 ˚C for 3 hrs, and cooled to ambient temperature. The yellow powder, **9** (0.383 g, 94 %), was collected by suction filtration, washed with acetone (15.0 mL) and diethyl ether (5.00 mL), and dried *in vacuo*. Melting Point: 243.0-248.4 °C.

^{1}H NMR (399.95 MHz, DMSO-d_6): δ (ppm) = 7.27 (s, 1H, H_e); 7.10 (d, $^{4}J_{HP}$ = 3.42 Hz, 1H, H_b); 7.02 (s, 2H, NH_2); 4.59 (d, J_{HP} = 12.4 Hz, 3H, N-$CH_{2(eq)}$-N); 4.44 (d, J_{HP} = 13.2 Hz, 3H, N-$CH_{2(ax)}$-N); 4.27 (s, 6H, PCH_2N); 2.21 (s, 3H, CH_3). ^{13}C NMR (100.65 MHz, DMSO-d_6): δ (ppm) = 177.2 (C-S); 163.7 (C=N); 163.6 (C_a); 153.2 (C_f); 136.4 (C_c); 130.6 (C_d); 127.2 (C_b); 127.1 (C_e); 72.4 (d, $^{3}J_{CP}$ = 7.40 Hz, NCH_2N); 51.5 (d, $^{1}J_{CP}$ = 15.5 Hz, PCH_2N); 13.6 (CH_3). ^{31}P NMR (162.00 MHz, DMSO-d_6): δ (ppm) = -49.5. Elemental analysis for $C_{15}H_{19}Cl_2N_6PdPS$: Found C 35.0, H 3.46, N 16.4, S 5.91%; Calculated C 34.4, H 3.66, N 16.0, S 6.12 %. FT-IR (KBr, cm^{-1}): ν = 3414 (m, N-H); 1624 (m, C=N); 1574 (w, C=N); 1488 (w, C=C aromatics). MS-EI^{+}: *m/z* 524 ($[M]^{+}$, 4 %).

Synthesis of [Pd(3,4-dichloropropiophenone thiosemicarbazone)(PTA)] (**10**)

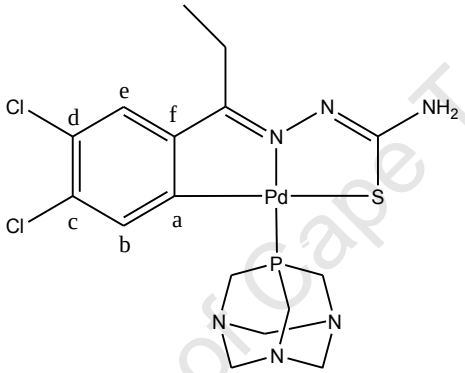

Compound **8** (0.253 g, 0.166 mmol) was suspended in acetone (30.0 mL). PTA (0.109 g, 0.693 mmol) was then added to the reaction flask while stirring. The reaction mixture was refluxed at 60 ˚C for 3 hrs, and cooled to ambient temperature. The yellow powder, **10** (0.265 g, 74 %), was collected by suction filtration, washed with acetone (15.0 mL) and diethyl ether (10.0 mL), and dried *in vacuo*. Melting Point: 235.9-239.4 °C. ^{1}H NMR (399.95 MHz, DMSO-d_6): δ (ppm) = 7.27 (br s, 1H, H_e); 7.11 (br s, 1H, H_b); 7.05 (s, 2H, NH_2); 4.58 (d, J_{HP} = 12.8 Hz, 3H, N-$CH_{2(eq)}$-N); 4.44 (d, J_{HP} = 12.8 Hz, 3H, N-$CH_{2(ax)}$-N); 4.26 (s, 6H, PCH_2N); 2.70 (q, $^{3}J_{HH}$ = 7.60 Hz, 2H, CH_2); 1.02 (t, $^{3}J_{HH}$ = 7.60 Hz, 3H, CH_3). ^{13}C NMR (100.65 MHz, DMSO-d_6): δ (ppm) = 177.4 (C-S); 168.3 (C=N); 164.2 (C_a); 151.9 (C_f); 136.6 (C_c); 130.6 (C_d); 127.2 (C_b); 127.0 (C_e); 72.4 (d, $^{3}J_{CP}$ = 7.40 Hz, NCH_2N); 51.5 (d, $^{1}J_{CP}$ = 15.5 Hz, PCH_2N); 20.0 (CH_2); 11.5 (CH_3). ^{31}P NMR (162.00 MHz, DMSO-d_6): δ (ppm) = -49.6. Elemental analysis for $C_{16}H_{22}Cl_2N_6PdPS$: Found C 35.8, H 4.14, N 16.1, S 5.48 %; Calculated C 35.7, H 4.12, N 15.6, S 5.95 %. FT-IR (KBr, cm^{-1}): ν = 3440 (br, N-H); 1641 (w, C=N); 1559 (w, C=N); 1497 (w, C=C aromatics). MS-EI^{+}: *m/z* 538 ($[M]^{+}$, 2.4 %).

Synthesis of [Pd (3,4-dichloroacetophenone thiosemicarbazone)(N-(2-(diphenylphosphino)benzyl)propan-1-amine)] (**11**)

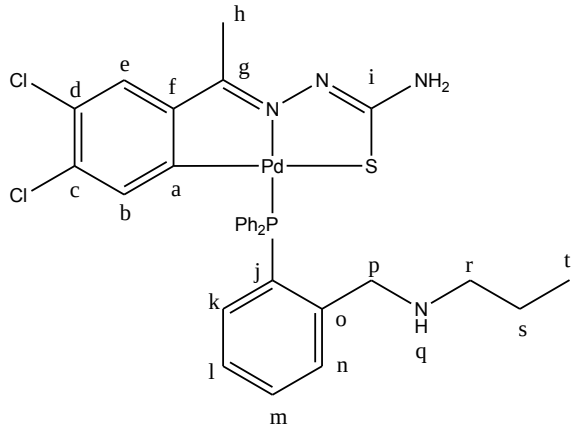

Compound **4** (0.131 g, 0.393 mmol) was dissolved in dry acetone (20.0 mL), followed by the addition of compound **7** (0.143 g, 0.0973 mmol). The reaction mixture was stirred at ambient temperature for 3 hrs. The volume of the solution was reduced, and the solid precipitated with the addition of hexane. The solid was purified using column chromatography (silica, Ethyl acetate: hexane, 1:1). The yellow powder, **11** (0.108 g, 40 %) was collected by suction filtration, and washed with diethyl ether (10.0 mL). Melting point: 179.7-184.1 ˚C. ^{1}H NMR (399.95 MHz, DMSO-d$_6$): δ (ppm) = 7.74 (m, 1H, H$_n$); 7.49 (m, 11H, H$_k$ & PPh$_2$); 7.32 (t, $^{3}J_{HH}$ = 7.70 Hz, 1H, H$_l$); 7.23 (s, 1H, H$_e$); 7.00 (m, 1H, H$_m$); 6.90 (br s, 2H, NH$_2$); 6.13 (d, $^{4}J_{HP}$ = 3.85 Hz, H$_b$); 4.13 (s, 2H, H$_p$); 2.28 (m, 2H, H$_s$); 2.26 (s, 3H, H$_h$); 0.71 (t, $^{3}J_{HH}$ = 7.28 Hz, 3H, H$_t$). ^{13}C NMR (100.65 MHz, DMSO-d$_6$): δ (ppm) = 177.2 (d, $^{3}J_{CP}$ = 9.43 Hz, C-S); 172.4 (C=N); 163.7 (C$_a$); 163.6 (d, $^{2}J_{CP}$ = 4.70 Hz, C$_o$); 153.2 (C$_f$); 145.2 (d, $^{3}J_{CP}$ = 11.4 Hz, C$_n$); 135.9 (d, $^{1}J_{CP}$ = 8.10 Hz, C$_j$); 135.0 (d, $^{1}J_{CP}$ = 12.8 Hz, *i*-C); 132.6 (C$_k$); 131.7 (C$_m$); 131.3 (C$_d$); 130.8 (C$_c$); 130.7 (d, $^{2}J_{CP}$ = 8.10 Hz, PPh$_2$); 130.1 (d, $^{4}J_{CP}$ = 3.40 Hz, PPh$_2$); 129.3 (d, $^{2}J_{CP}$ = 10.1 Hz, C$_b$); 127.2 (d, $^{3}J_{CP}$ = 8.10 Hz, PPh$_2$); 127.0 (C$_l$); 126.7 (C$_e$); 56.2 (C$_r$); 52.8 (d, $^{3}J_{CP}$ = 12.8 Hz, C$_p$); 51.5 (C$_s$); 13.7 (C$_h$); 12.0 (C$_t$). ^{31}P NMR (162.00 MHz, DMSO-d$_6$): δ (ppm) = 29.5. Elemental analysis for $C_{31}H_{31}Cl_2N_4PdPS \cdot H_2O \cdot 2C_3H_6O \cdot ½n\text{-}C_6H_{14}$: Found C 50.8, H 5.17, N 5.92, S 3.59 %; Calculated C 50.7, H 4.94, N 6.39, S 3.66 %. FT-IR (KBr, cm^{-1}): ν = 3435 (w, N-H); 3318 (w, N-H); 1618 (m, C=N); 1582 (w, C=N). MS-ESI^{+}: *m/z* 700 ([M]$^{+}$, 45 %); 701 ([M+H]$^{+}$, 100 %).

b. Binuclear *C,N,S*-chelated thiosemicarbazone cyclopalladated complex (12)

Synthesis of [Pd_2(3,4-dichloroacetophenone thiosemicarbazone)$_2$(N^1,N^4-bis(2-(diphenylphosphino)benzyl)benzene-1,4-diamine)] (**12**)

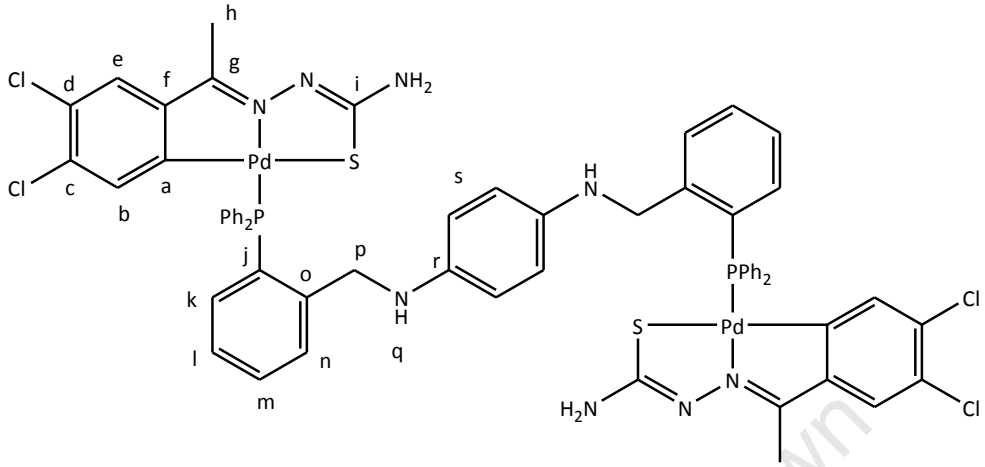

Compound **6** (0.0413 g, 0.0629 mmol) was suspended in an acetone: dichloromethane (80:20 % V/V, 10.0 mL) mixture, followed by the addition of compound **7** (0.0459 g, 0.0313 mmol). The reaction mixture was stirred at ambient temperature for 5 hrs. The yellow powder, **12** (0.0507 g, 58 %), was collected by suction filtration, washed with hexane (10.0 mL) and diethyl ether, and dried *in vacuo*. Melting point: 246.5-249.3 ˚C. ^{1}H NMR (399.95 MHz, DMSO-d_6): δ (ppm) = 7.50 (m, 24H, H_k & H_n & PPh_2); 7.35 (t, $^{3}J_{HH}$ = 7.50 Hz, 1H, H_l); 7.21 (s, 1H, H_e); 7.08 (m, 1H, H_m); 6.91 (br s, 2H, NH_2); 6.18 (d, $^{4}J_{HP}$ = 3.70 Hz, H_b); 5.87 (s, 4H, H_s); 5.32 (br s, 2H, H_q); 4.65 (br s, 2H, H_p); 2.24 (s, 3H, H_h). ^{13}C NMR (100.65 MHz, DMSO-d_6): δ (ppm) = 177.1 (d, $^{3}J_{CP}$ = 10.1 Hz, C-S); 164.0 (C=N); 163.5 (d, $^{2}J_{CP}$ = 4.71 Hz, C_o); 163.3 (C_a); 153.3 (C_f); 144.6 (d, $^{3}J_{CP}$ = 11.4 Hz, C_n); 140.0 (C_r); 135.7 (d, $^{1}J_{CP}$ = 7.40 Hz, C_j); 135.0 (d, $^{1}J_{CP}$ = 12.1 Hz, C_{Ph}); 133.0 (d, $^{2}J_{CP}$ = 3.40 Hz, C_k); 131.8 (C_m); 130.8 (C_d); 130.3 (C_c); 130.1 (d, $^{4}J_{CP}$ = 3.89 Hz, C_{Ph}); 129.3 (d, $^{2}J_{CP}$ = 10.4 Hz, C_{Ph}); 128.6 (d, $^{3}J_{CP}$ = 8.17 Hz, C_b); 127.0 (d, $^{3}J_{CP}$ = 10.8 Hz, C_{Ph}); 126.8 (C_l); 126.5 (C_e); 114.0 (C_s); 47.9 (d, $^{3}J_{CP}$ = 14.8 Hz, C_p); 13.8 (C_h). ^{31}P NMR (162.00 MHz, DMSO-d_6): δ (ppm) = 29.0. Elemental analysis for $C_{62}H_{52}Cl_4N_8Pd_2P_2S_2 \cdot ½H_2O$: Found C 53.6, H 4.13, N 7.52, S 3.92 %; Calculated C 53.2, H 3.75, N 8.01, S 4.58 %. FT-IR (KBr, cm^{-1}): ν = 3483 (w, N-H); 3380 (w, N-H); 1597 (m, C=N); 1574 (w, C=N). MS-ESI^{+}: *m/z* 1391 ($[M+H]^{+}$, 12 %); 1390 ($[M]^{+}$, 10 %).

6.2.4. Synthesis of *C,N,S*-chelated thiosemicarbazone cyclopalladated complexes containing N-donor ligands (13-15)

Synthesis of [Pd(3,4-dichloroacetophenone thiosemicarbazone)(4-picoline)] (**13**)

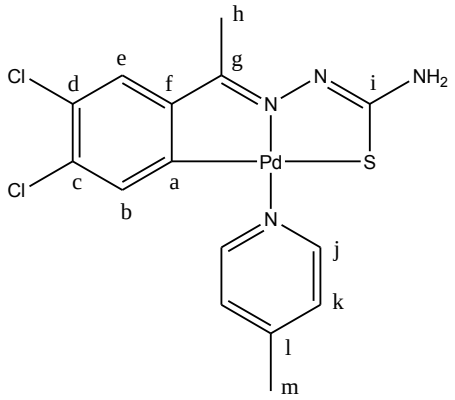

Compound **7** (0.100 g, 0.0682 mmol) was suspended in toluene (30.0 mL), followed by the addition of excess 4-picoline (~ 2 mL). The reaction mixture was refluxed in air at 135 ˚C for 9 days. The solvent was removed in order to precipitate an orange solid. The orange powder, **13** (0.0546 g, 43 %), was collected by suction filtration, washed with ethanol (20.0 mL) and dried *in vacuo*.

Compound **13** was synthesized via another method. Compound **8** (0.303 g, 0.207 mmol) was suspended in acetone (20.0 mL), followed by the addition of excess 4-picoline (~ 1 mL). The reaction mixture was refluxed in air at 70 ˚C for 5 days. The yellow powder, **13** (0.263 g, 69 %), was collected by suction filtration, washed with diethyl ether (20.0 mL) and dried *in vacuo*.

Melting point: 311.0 ˚C (Decomposition without melting). ^{1}H NMR (300.08 MHz, DMSO-d_6): δ (ppm) = 8.41 (d, $^{3}J_{HH}$ = 5.86 Hz, 2H, H_j); 7.38 (s, 1H, H_b); 7.20 (d, $^{3}J_{HH}$ = 4.90 Hz, 2H, H_k); 7.08 (br s, 2H, NH_2); 6.73 (s, 1H, H_e); 2.31 (s, 3H, H_m); 2.00 (s, 3H, H_h). ^{13}C NMR (100.65 MHz, DMSO-d_6): δ (ppm) = 166.8 (C-S); 165.1 (C=N); 164.0 (C_a); 149.6 (C_j, C_k); 149.1 (C_f); 146.5 (C_l); 132.8 (C_c); 125.8 (C_d); 125.6 (C_e); 124.4 (C_b); 20.2 (C_m); 13.3 (CH_3). FT-IR (KBr, cm^{-1}): ν = 3427 (w, N-H); 3289 (m, N-H); 1617 (s, C=N); 1568 (w, C=N); 1559 (w, C=N); 1493 (s, C=C aromatics). MS-EI^{+}: *m/z* 459 ([M]$^{+}$, 2.2 %).

Synthesis of [Pd_2(3,4-dichloroacetophenone thiosemicarbazone)$_2$(4,4'-dipyridyl)] (**14**)

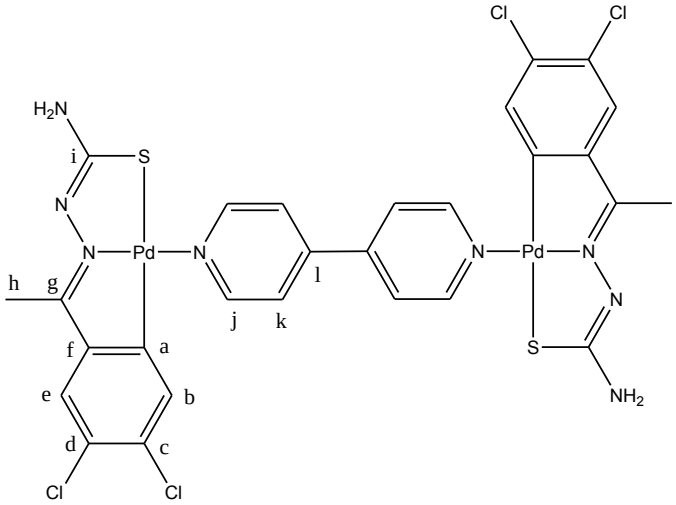

Compound **7** (0.184 g, 0.126 mmol) was suspended in dry toluene (30.0 mL), followed by the addition of 4,4'-dipyridyl (0.0390 g, 0.251 mmol). The reaction mixture was refluxed at 140 ˚C for 2 days, and stirred overnight. The brown powder, **14** (0.0761 g, 34 %), was collected by suction filtration, washed with dichloromethane (20.0 mL) and diethyl ether (10.0 mL), and dried *in vacuo*. Melting point: 287.8 ˚C (Decomposition without melting). ^{1}H NMR (399.95 MHz, DMSO-d_6): δ (ppm) = 8.73 (br s, 4H, H_j); 7.83 (br s, 4H, H_k); 7.37 (s, 2H, H_b); 7.18 (br s, 4H, NH_2); 6.72 (s, 2H, H_e); 2.00 (s, 3H, CH_3). ^{13}C NMR (100.65 MHz, DMSO-d_6): δ (ppm) = 167.5 (C-S); 165.8 (C=N); 164.8 (C_a); 151.1 (C_j, C_k); 150.4 (C_f); 133.6 (C_l); 129.7 (C_c); 126.5 (C_d); 126.4 (C_e); 121.8 (C_b); 14.1 (CH_3). Elemental analysis for $C_{28}H_{22}Cl_4N_8Pd_2S_2.H_2O$: Found C 36.8, H 2.45, N 11.8, S 7.07 %; Calculated C 37.1, H 2.44, N 12.4, S 7.07 %. FT-IR (KBr, cm^{-1}): ν = 3456 (w, N-H); 3384 (w, N-H); 1643 (m, C=N); 1624 (w, C=N); 1593 (m, C=N); 1522 (s, C=C aromatics). MS-ESI$^+$: *m/z* 838 ($[M+2H-ClN]^+$, 5 %); 409 ($[M-2Cl]^{2+}$, 100 %).

Synthesis of [Pd_2(3,4-dichloroacetophenone thiosemicarbazone)$_2$(1,2-bis(4-pyridyl)ethylene)] (**15**)

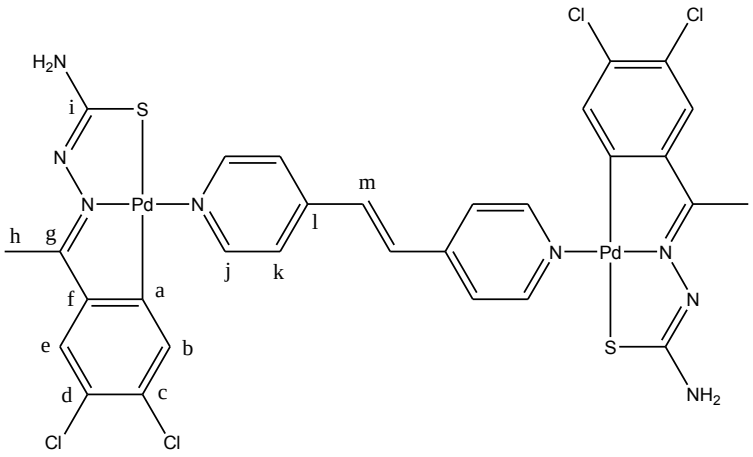

Compound **7** (0.201 g, 0.136 mmol) was suspended in acetone (20.0 mL). 1,2-Bis(4-pyridyl)ethylene (0.0502 g, 0.275 mmol) was added to the suspension while stirring. The reaction mixture was refluxed in air at 80˚C for 3 days. The yellow powder, **15** (0.0387 g, 15 %), was collected by suction filtration, washed with acetone (15.0 mL) and dried *in vacuo*. Melting point: 274.6 ˚C (Decomposition without melting). ^{1}H NMR (300.08 MHz, DMSO-d_6): δ (ppm) = 8.59 (d, $^{3}J_{HH}$ = 5.86 Hz, 4H, H_j); 7.59 (d, $^{3}J_{HH}$ = 5.86 Hz, 4H, H_k); 7.50 (s, 2H, H_d); 7.38 (s, 2H, H_b); 7.08 (br s, 4H, NH_2); 6.72 (s, 2H, H_e); 2.00 (s, 3H, CH_3). ^{13}C NMR (100.65 MHz, DMSO-d_6): δ (ppm) = 167.5 (C-S); 165.8 (C=N); 164.8 (C_a); 150.7 (C_j, C_k); 150.4 (C_f); 133.6 (C_l); 131.1 (C_m); 129.7 (C_c); 126.5 (C_d); 126.4 (C_e); 121.8 (C_b); 14.1 (CH_3). Elemental analysis for $C_{30}H_{24}Cl_4N_8Pd_2S_2$: Found C 39.1, H 2.76, N 10.8, S 6.18 %; Calculated C 39.4, H 2.64, N 12.2, S 7.01%. IR (KBr, cm^{-1}): ν = 3453 (br, N-H); 1628 (w, C=N); 1611 (w, C=N); 1596 (w, C=N). MS-ESI^{+}: *m/z* 916 ([M+H]$^{+}$, 5 %); 915 ([M]$^{+}$, 4 %).

6.3. Ferrocenyl-Derived Ruthenium(II) and Palladium(II) Thiosemicarbazone Complexes

6.3.1. Synthesis of mono- and dimeric ferrocenylthiosemicarbazones (16, 18)

Synthesis of ferrocenylthiosemicarbazone (**16**)[6]

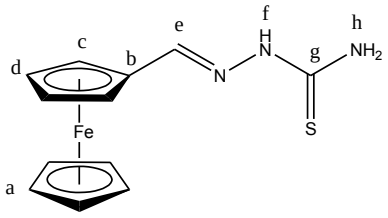

Thiosemicarbazide (0.204 g, 2.24 mmol) was suspended in water (40.0 mL), to which HCl (5 drops) was added. Ferrocenecarboxaldehyde (0.481 g, 2.25 mmol) was added to the suspension, and the reaction mixture was stirred at ambient temperature for 4.5 hrs. The solid was purified using dichloromethane and hexane. The orange powder, **16** (0.533 g, 83 %), was collected by suction filtration, washed with hexane, and dried *in vacuo*.

Compound **16** was also synthesized using a method similar to that of the ligands synthesized in section 5.2.1.

Thiosemicarbazide (0.216 g, 2.37 mmol) was suspended in ethanol (30.0 mL), to which ferrocenecarboxaldehyde (0.509 g, 2.38 mmol) was added. The suspension was refluxed at 81˚C for 5 hrs, and stirred overnight. The solid was purified using dichloromethane/hexane to yield an orange powder, **16** (0.582 g, 85 %), which was collected by suction filtration, and dried *in vacuo*.

Melting point: 150.4 ˚C (Decomposition without melting). ^{1}H NMR (399.95 MHz, DMSO-d_6): δ (ppm) = 11.12 (s, 1H, H_f); 7.96 (s, 1H, H_h); 7.88 (s, 1H, H_e); 7.55 (s, 1H, H_h); 4.71 (t, $^{3}J_{HH}$ = 1.60 Hz, 2H, H_c); 4.39 (t, $^{3}J_{HH}$ = 1.60 Hz, 2H, H_d); 4.18 (s, 5H, H_a). ^{13}C NMR (100.65 MHz, DMSO-d_6): δ (ppm) = 176.9 (C=S); 143.3 (C=N); 78.8 (C_b); 69.9 (C_d); 68.8 (C_c); 67.5 (C_a). Elemental analysis for $C_{12}H_{13}FeN_3S$: Found C 50.1, H 4.66, N 15.0, 8.71 %; Calculated C 50.2, H 4.56, N 14.6, S 11.2 %. FT-IR (KBr, cm^{-1}): ν = 3419 (m, N-H); 3246 (m, N-H); 3154 (m, N-H); 1599 (s, C=N); 818 (m, C=S). MS-EI^{+}: *m/z* 287 ([M]$^{+}$, 100 %).

Synthesis of benzene-1,4-dithiosemicarbazide (**17**)[7]

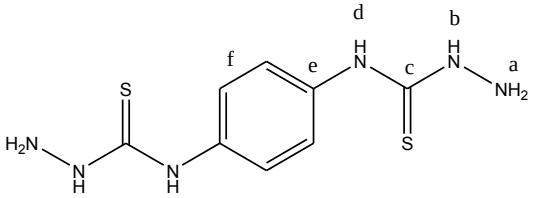

Hydrazine hydrate (0.720 mL, 25.0 mmol) dissolved in water (0.500 mL) was added dropwise to a suspension of 1,4-phenyldiisothiocyanate (0.240 g, 1.23 mmol) in ethanol (20.0 mL). The reaction mixture was refluxed at 81 ˚C for 1 hr, and the white suspension was collected by suction filtration. The white powder, **17** (0.270 g, 84 %), was washed with cold water (15.0 mL), cold ethanol (10.0 mL) and cold diethyl ether (10.0 mL). Melting point: 198.6-199.3 ˚C. ^{1}H NMR (300.08 MHz, DMSO-d_6): δ (ppm) = 8.94 (s, 2H, H_d); 7.54 (s, 4H, H_f); 4.79 (br s, 4H, H_a). ^{13}C NMR (100.64 MHz, DMSO-d_6): δ (ppm) = 179.4 (C=S); 135.4 (C_e); 123.2 (C_f). FT-IR (KBr, cm^{-1}): ν = 3333 (m, N-H); 3297 (m, N-H); 3237 (s, N-H); 3190 (s, N-H); 821 (m, C=S). MS-EI$^+$: *m/z* 256 ([M]$^+$, 23 %).

Synthesis of benzene-1,4-ferrocenyldithiosemicarbazone (**18**)

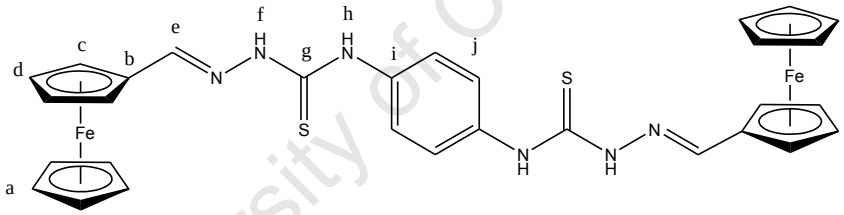

Compound **17** (0.199 g, 0.777 mmol) was suspended in ethanol (30.0 mL), followed by the addition of ferrocenecarboxaldehyde (0.332 g, 1.55 mmol). The reaction mixture was refluxed at 81 ˚C for 20 hr. The reddish-brown powder, **18** (0.434 g, 86 %), was collected by suction filtration, and washed with ethanol (10.0 mL) and diethyl ether (5.00 mL). Melting point: 208.1 ˚C (Decomposition without melting). ^{1}H NMR (399.95 MHz, DMSO-d_6): δ (ppm) = 11.55 (s, 2H, NH_f); 9.76 (s, 2H, NH_h); 8.02 (s, 2H, H_e); 7.59 (s, 4H, H_i); 4.84 (s, 4H, H_c); 4.46 (s, 4H, H_d); 4.25 (s, 10H, H_a). ^{13}C NMR (75.46 MHz, DMSO-d_6): δ (ppm) = 174.4 (C=S); 143.9 (C=N); 135.5 (C_i); 124.2 (C_j); 78.4 (C_b); 69.9 (C_d); 68.7 (C_a); 67.6 (C_c). Elemental analysis for $C_{30}H_{28}Fe_2N_6S_2 \cdot ½H_2O$: Found C 54.4, H 4.38, N 13.3, S 6.74 %; Calculated C 54.8, H 4.29, N 12.8, S 9.76 %. FT-IR (KBr, cm^{-1}): ν = 3440 (w, N-H); 3303 (w, N-H); 3154 (w, N-H); 1600 (s, C=N); 831 (m, C=S). MS-ESI$^+$: *m/z* 649 ([M+H]$^+$, 100 %).

6.3.2. Synthesis of heterometallic *N,S*-chelated ferrocenylthiosemicarbazone ruthenium(II)-arene complexes

Ruthenium(II)-precursors (**19-21**)

Synthesis of [Ru(η^6- p-^{i}PrC$_6$H$_4$CH$_3$)(μ-Cl)(Cl)]$_2$ (**19**)[8]

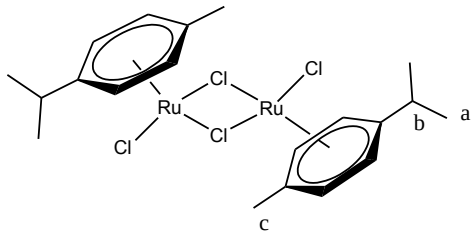

$RuCl_3 \cdot 3H_2O$ (1.00 g, 3.84 mmol) was dissolved in ethanol (30.0 mL), to which an excess of α-phellandrene (3.60 mL, 22.3 mL) was added. The reaction mixture was refluxed at 81 ˚C for 24 hrs. Half the solvent was removed, and diethyl ether was added to precipitate a red solid. The red solid, **19** (0.977 g, 83 %), was collected by suction filtration, and washed with cold ethanol (15.0 mL) and diethyl ether (10.0 mL). ^{1}H NMR (399.95 MHz, $CDCl_3$): δ (ppm) = 5.46 (d, 4H, *p*-cym), 5.33 (d, 4H, *p*-cym), 2.92 (m, 2H, H_b), 2.15 (s, 6H, H_c), 1.27 (d, 12H, H_a).

Synthesis of [Ru(η^6-C$_6$H$_5$OCH$_2$CH$_2$OH)(μ-Cl)(Cl)]$_2$ (**20**)[9]

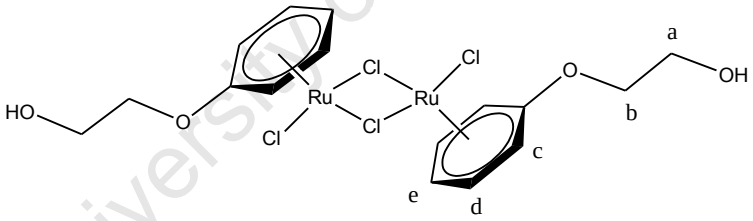

$RuCl_3 \cdot 3H_2O$ (0.999 g, 3.82 mmol) was dissolved in 1,2-ethanediol (15.0 mL), followed by the addition of an excess of 1-methoxy-1,4-cyclohexadiene (4.50 mL, 38.0 mmol). The reaction mixture was heated at 80 ˚C for 6 hrs, and left standing at ambient temperature to allow precipitation of a solid. The reddish-orange solid, **20** (0.469 g, 40 %), was collected by suction filtration and washed with methanol. Melting point: 153.1 ˚C (onset of decomposition without melting). ^{1}H NMR (399.95 MHz, DMSO-d_6): δ (ppm) = 6.14 (t, $^3J_{HH}$ = 5.60 Hz, 4H, H_c), 5.54 (d, $^3J_{HH}$ = 5.54 Hz, 4H, H_d), 5.38 (t, $^3J_{HH}$ = 5.20 Hz, 2H, H_e), 4.22 (t, $^3J_{HH}$ = 4.80 Hz, 4H, H_b), 3.73 (t, $^3J_{HH}$ = 4.80 Hz, 4H, H_a).

Synthesis of [Ru(η^6-C_6H_6)(μ-Cl)(Cl)]$_2$ (**21**)[10]

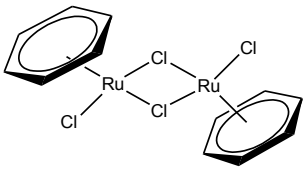

$RuCl_3 \cdot 3H_2O$ (0.975 g, 3.73 mmol) was dissolved in 90 % aqueous ethanol (50.0 mL), to which an excess of 1,3-cyclohexadiene (1.32 mL, 13.8 mmol) was added. The reaction mixture was heated at 45 ˚C for 5 hrs, and stirred overnight. The reddish-brown solid (0.877 g, 94 %) was collected by suction filtration, and washed with ethanol and diethyl ether. ^{1}H NMR (399.95 MHz, DMSO-d_6): δ (ppm) = 5.97 (br s, 12H, Ar-H).

a. Heterobimetallic binuclear *N,S*-chelated ferrocenyl-derived ruthenium(II)-arene complexes (22-24)

Synthesis of [Ru(η^6- p-^{i}Pr$C_6H_4CH_3$)(ferrocenylthiosemicarbazone)(Cl)]Cl (**22**)

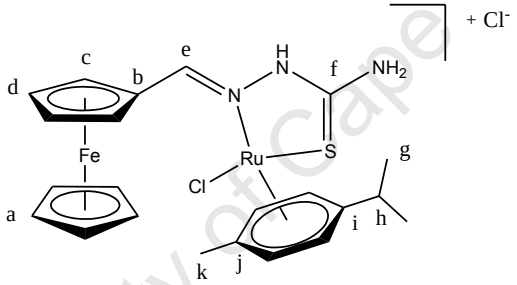

Ruthenium-dimer **19** (0.150 g, 0.245 mmol) was dissolved in dichloromethane (30.0 mL), followed by the addition of compound **16** (0.140 g, 0.490 mmol). The reaction mixture was stirred at ambient temperature for 24 hrs. The solution was filtered by gravity, and reduced to approximately 2 mL. The contents were added to a large volume (~ 70 mL) of stirring diethyl ether to precipitate an orange solid. The orange powder, **22** (0.268 g, 92 %), was collected by suction filtration, and washed with diethyl ether. Melting point: 162.1˚C (Decomposition without melting). ^{1}H NMR (399.95 MHz, Acetone-d_6): δ (ppm) = 8.74 (br s, 1H, H_e); 7.92 (s, 2H, NH_2); 6.02 (br s, 1H, H_c); 5.60 (d, $^3J_{HH}$ = 5.84 Hz, 1H, *p*-cym); 5.31 (d, $^3J_{HH}$ = 5.60 Hz, 1H, *p*-cym); 5.25 (d, $^3J_{HH}$ = 5.60 Hz, 1H, *p*-cym); 5.14 (d, $^3J_{HH}$ = 5.84 Hz, 1H, *p*-cym); 4.84 (br s, 1H, H_c); 4.64 (m, 2H, H_d); 4.21 (s, 5H, H_a); 2.57 (m, 1H, H_h); 1.99 (s, 3H, H_k); 1.06 (d, $^3J_{HH}$ = 6.96 Hz, 3H, H_g); 1.01 (d, $^3J_{HH}$ = 6.80 Hz, 3H, H_g). ^{13}C NMR (100.65 MHz, MeOD-d_4): δ (ppm) = 178.7 (C=S); 163.1 (C=N); 104.2 (C_i); 103.8 (C_j); 90.1 (*p*-cym); 89.2 (*p*-cym); 85.5 (*p*-cym); 83.9 (*p*-cym); 77.8 (C_b); 75.9 (C_c); 75.2 (C_d); 73.9 (C_d); 71.6 (C_a); 71.0 (C_c); 32.1 (C_h); 22.9 (C_g); 21.8 (C_g); 18.7(C_k). Elemental analysis for $C_{22}H_{27}Cl_2FeN_3RuS \cdot ¾H_2O$:

Found C 43.1, H 4.49, N 6.70, S 3.10 %; Calculated C 43.5, H 4.48, N 6.92, S 5.28 %. FT-IR (KBr, cm^{-1}): ν = 3435 (br, N-H); 3259 (w, N-H); 3093 (m, N-H); 1615 (w, C=N); 824 (w, C=S). MS-ESI^+: *m/z* 522 ($[M\text{-}Cl]^+$, 100 %).

Synthesis of [Ru(η^6- $C_6H_5OCH_2CH_2OH$)(ferrocenylthiosemicarbazone)(Cl)]Cl (**23**)

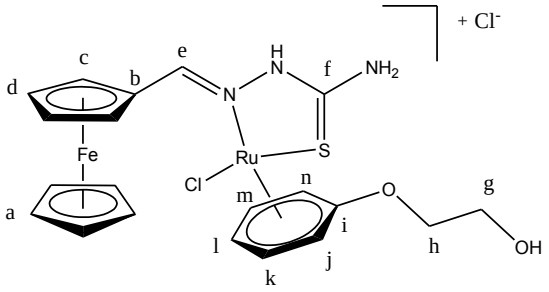

Ruthenium-dimer **20** (0.127 g, 0.205 mmol) was suspended in dichloromethane (20.0 mL), followed by the addition of compound **16** (0.121 g, 0.411 mmol). The reaction mixture was stirred at ambient temperature for 24 hrs. The solution was filtered by gravity to remove any unreacted **20**, and washed with methanol. The volume was reduced to approximately 2 mL, and added to a large volume of stirring diethyl ether, to precipitate a solid. The orange powder, **23** (0.164 g, 67 %), was collected by suction filtration, and washed with diethyl ether. Melting point: 155.1 ˚C (Decomposition without melting). ^{1}H NMR (400.22 MHz, MeOD-d_4): δ (ppm) = 8.48 (s, 1H, H_e); 6.06 (br s, 1H, H_c); 5.82 (t, $^3J_{HH}$ = 5.68 Hz, 1H, H_m); 5.72 (t, $^3J_{HH}$ = 5.95 Hz, 1H, H_k); 5.30 (d, $^3J_{HH}$ = 6.04 Hz, 1H, H_n); 5.26 (d, $^3J_{HH}$ = 6.41 Hz, 1H, H_j); 5.11 (t, $^3J_{HH}$ = 5.31 Hz, 1H, H_l); 4.30 (s, 5H, H_a); 4.15 (m, 2H, H_h); 3.87 (m, 2H, H_g). ^{13}C NMR (100.65 MHz, MeOD-d_4): δ (ppm) = 178.8 (C=S); 163.6 (C=N); 139.2 (C_i); 93.4 (C_m); 93.2 (C_k); 77.6 (C_b); 76.7 (C_l); 76.0 (C_c); 75.1 (C_d); 73.7 (C_d); 72.8 (C_h); 71.6 (C_a); 71.1 (C_c); 70.0 (C_n); 66.1 (C_j); 61.0 (C_g). Elemental analysis for $C_{20}H_{23}Cl_2FeN_3O_2RuS\cdot¼H_2O$: Found C 39.5, H 4.13, N 7.36, S 4.31 %; Calculated C 39.9, H 3.85, N 6.98, S 5.33 %. FT-IR (KBr, cm^{-1}): ν = 3401 (br, NH, OH); 3086 (w, N-H); 1615 (m, C=N); 833 (w, C=S). MS-ESI^+: *m/z* 526 ($[M\text{-}Cl]^+$, 100 %).

Synthesis of [Ru(η^6- C_6H_6)(ferrocenylthiosemicarbazone)(Cl)]PF_6 (**24**)

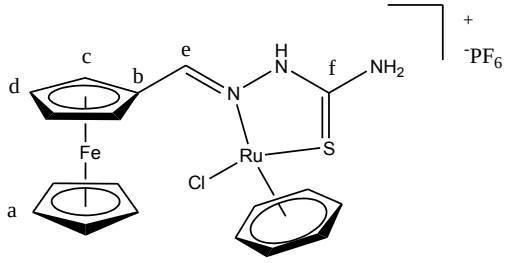

Ruthenium-dimer **19** (0.0520 g, 0.1039 mmol) was suspended in methanol (15.0 mL), followed by the addition of compound **16** (0.0598 g, 0.208 mmol). The reaction mixture was stirred at ambient temperature for 24 hrs in a flask covered in foil. The solution was filtered by gravity, sodium hexafluorophosphate (0.0446 g, 0.266 mmol) was added, and the soution was stirred at ambient temperature for 2 hrs. The resulting solution was added to a large volume of stirring diethyl ether, to precipitate a solid. The orange powder, **24**, (0.0933 g, 69 %) was collected by suction filtration, and washed with diethyl ether. Melting point: 173.8 °C (Decomposition without melting). ^{1}H NMR (399.95 MHz, MeOD-d_4): δ (ppm) = 8.50 (s, 1H, H_e); 6.08 (s, 1H, H_c); 5.69 (s, 6H, $H_{benzene}$); 4.34 (s, 5H, H_a). ^{13}C NMR (100.65 MHz, MeOD-d_4): δ (ppm) = 178.7 (C=S); 164.0 (C=N); 88.6 ($C_{benzene}$); 77.6 (C_b); 76.2 (C_c); 75.3 (C_d); 74.1 (C_d); 71.6 (C_a); 71.0 (C_c). ^{31}P NMR (162.00 MHz, MeOD-d_4): δ (ppm) = -144.6 (septet). Elemental analysis for $C_{18}H_{19}ClF_6FeN_3PRuS$: Found C 33.7, H 3.55, N 6.52, S 4.17 %; Calculated C 33.4, H 2.96, N 6.50, S 4.96 %. FT-IR (KBr, cm^{-1}): ν = 3405 (m, N-H); 3064 (m, N-H); 1617 (m, C=N); 843 (m, C=S). MS-ESI$^+$: *m/z* 466 ([M-Cl]$^+$, 100 %).

b. Heterobimetallic tetranuclear *N,S*-chelated ferrocenyl-derived ruthenium(II)-arene complexes (25, 26)

Synthesis of [Ru_2(p-^{i}$PrC_6H_4CH_3$)$_2$(ferrocenyldithiosemicarbazone)Cl_2]2PF_6 (**25**)

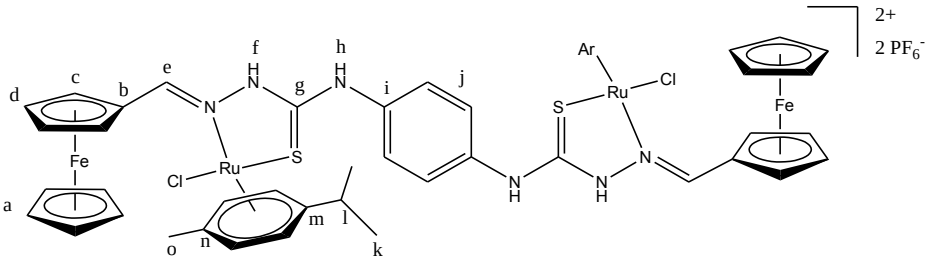

Compound **19** (0.0755 g, 0.123 mmol) and compound **18** (0.0801 g, 0.124 mmol) were suspended in a methanol: dichloromethane (75:25 % V/V, 20.0 mL) mixture. The red suspension was stirred at ambient temperature for 24 hrs in a foil-covered flask. The solvent

was filtered by gravity and the volume reduced. Sodium hexafluorophosphate (0.0427 g, 0.254 mmol) was added to the solution, and stirred at ambient temperature for 1 hr. The dark red powder, **25** (0.116 g, 64 %), was collected by suction filtration, washed with diethyl ether, and dried *in vacuo*. The solid was purified using ethanol/hexane. Melting point: 167.1 ˚C (Decomposition without melting). ^{1}H NMR (399.95 MHz, Acetone-d_6): δ (ppm) = 10.4 (br s, 2H, H_f); 9.14 (br s, 2H, H_h); 8.81 (br s, 2H, H_e); 7.53 (br s, 4H, H_j); 6.16 (d, $^{3}J_{HH}$ = 8.06 Hz, 2H, H_c); 5.78 (d, $^{3}J_{HH}$ = 6.23 Hz, 2H, *p*-cym); 5.44 (m, 4H, *p*-cym); 5.31 (br s, 2H, *p*-cym); 4.86 (br s, 2H, H_c); 4.77 (d, $^{3}J_{HH}$ = 7.69 Hz, 4H, H_d); 4.33 (s, 10H, H_a); 2.70 (m, 2H, H_l); 1.99 (s, 6H, H_o); 1.20 (m, 6H, H_k); 1.14 (m, 6H, H_k). ^{13}C NMR (100.65 MHz, Acetone-d_6): δ (ppm) = 176.6 (C=S); 164.2 (C=N); 136.9 (C_i); 126.4-126.6 (C_j); 104.3 (C_m); 103.7 (C_n); 89.9 (*p*-cym); 89.2 (*p*-cym); 85.4 (*p*-cym); 84.1 (*p*-cym); 78.0 (C_b); 75.8 (C_c); 74.9 (C_d); 73.7 (C_d); 71.4 (C_a); 71.2 (C_c); 31.7 (C_h); 23.1 (C_k); 22.1 (C_k); 18.8 (C_o). ^{31}P NMR (162.00 MHz, Acetone-d_6): δ (ppm) = -144.2 (septet). Elemental analysis for $C_{50}H_{56}Cl_2F_{12}Fe_2N_6P_2Ru_2S_2$: Found C 38.1, H 4.10, N 5.17, S 3.95 %; Calculated C 40.6, H 3.81, N 5.68, S 4.33 %. FT-IR (KBr, cm^{-1}): ν = 3435 (br, N-H); 3091 (w, N-H); 1611 (w, C=N); 841 (s, C=S). MS-ESI^{+}: *m/z* 559 ([M-2Cl]$^{2+}$, 100 %); 1153 ([M-HCl]$^{+}$, 2 %).

Synthesis of [Ru$_2$(η^6-C$_6$H$_5$O(CH$_2$)$_2$OH)$_2$(ferrocenyldithiosemicarbazone)Cl$_2$]2PF$_6$ (**26**)

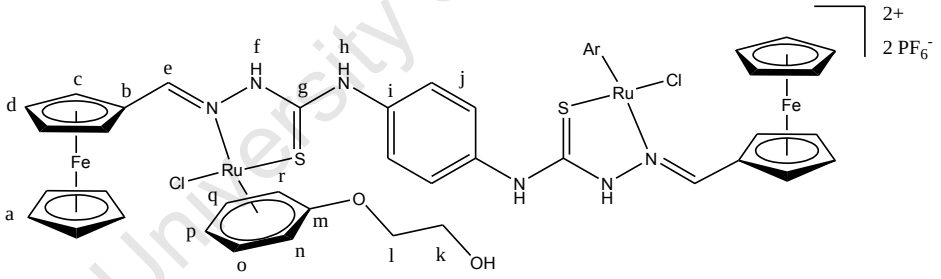

Compound **20** (0.0747 g, 0.120 mmol) and compound **18** (0.0779 g, 0.120 mmol) were suspended in a methanol: dichloromethane (75:25 % V/V, 20.0 mL) mixture. The red suspension was stirred at ambient temperature for 24 hrs in a foil-covered flask. The solvent was filtered by gravity and the volume reduced. Sodium hexafluorophosphate (0.0425 g, 0.253 mmol) was added to the solution, and stirred at ambient temperature for 2.5 hrs. The red-brown powder, **26** (0.160 g, 90 %), was collected by suction filtration, washed with diethyl ether, and dried *in vacuo*. Melting point: 120.6 ˚C (Decomposition without melting). ^{1}H NMR (300.07 MHz, MeOD-d_4): δ (ppm) = 8.71 (s, 2H, H_e); 7.56 (br s, 4H, H_j); 6.12 (br s, 2H, H_c); 5.88 (t, $^{3}J_{HH}$ = 6.00 Hz, 2H, H_q); 5.72 (t, $^{3}J_{HH}$ = 6.00 Hz, 2H, H_o); 5.35 (d, $^{3}J_{HH}$ = 6.22 Hz, 2H, H_r); 5.31 (d, $^{3}J_{HH}$ = 6.00 Hz, 2H, H_n); 5.18 (t, $^{3}J_{HH}$ = 5.70 Hz, 2H, H_p); 4.36 (m,

10H, H_a); 4.15 (m, 4H, H_l); 3.87 (m, 4H, H_k). ^{31}P NMR (162.00 MHz, MeOD-d_4): δ (ppm) = -144.6 (septet). Elemental analysis for $C_{46}H_{48}Cl_2F_{12}Fe_2N_6O_4P_2Ru_2S_2$: Found C 36.6, H 3.81, N 5.28, S 4.11 %; Calculated C 37.1, H 3.25, N 5.65, S 4.31 %. FT-IR (KBr, cm^{-1}): ν = 3418 (br, N-H); 3086 (w, N-H); 1611 (w, C=N); 841 (s, C=S). MS-ESI$^+$: *m/z* 563 ([M-2Cl]$^{2+}$, 70 %); 1198 ([M]$^+$, 2 %).

6.3.3. The synthesis of heterometallic *N,S*-chelated ferrocenylthiosemicarbazone palladium(II)-complexes containing P-donor ligands

Ferrocenylthiosemicarbazone palladium(II) precursor (27)

Synthesis of [Pd(ferrocenylthiosemicarbazone)(μ-Cl)$_2$ (**27**)

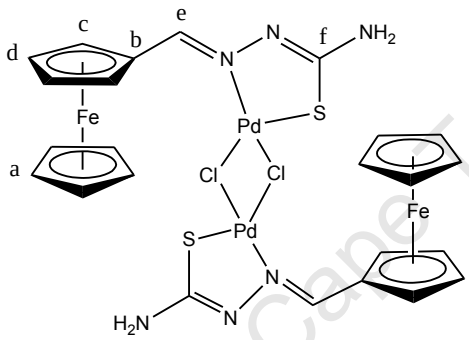

Potassium tetrachloropalladate (0.194 g, 0.596 mmol) was dissolved in distilled water (5.00 mL), followed by the addition of ethanol (20.0 mL), resulting in a brown suspension. Compound **16** (0.171 g, 0.595 mmol) was added to the suspension, and stirred at ambient temperature for 24 hrs in a foil-covered flask. The reddish-brown powder (0.242 g, 47 %) was collected by suction filtration, washed with water (10.0 mL), methanol (10.0 mL) and diethyl ether (20.0 mL) and dried *in vacuo*. ^{1}H NMR (400.22 MHz, DMSO-d_6): δ (ppm) = 7.44 (s, 2H, H_e); 6.91 (br s, 4H, NH_2); 5.04 (t, $^3J_{HH}$ = 1.60 Hz, 4H, H_c); 4.56 (t, $^3J_{HH}$ = 1.60 Hz, 4H, H_d); 4.22 (s, 10 H, H_a). ^{13}C NMR (100.65 MHz, DMSO-d_6): δ (ppm) = 169.9 (C-S); 155.2 (C=N); 73.2 (C_b); 73.0 (C_c); 69.4 (C_a); 69.1 (C_d). Elemental analysis for $C_{24}H_{24}Cl_2Fe_2N_6Pd_2S_2$: Found C 33.5, H 3.18, N 9.58, S 6.86 %; Calculated C 33.7, H 2.83, N 9.82, S 7.49 %. FT-IR (KBr, cm^{-1}): ν = 3431 (br, N-H); 3172 (w, N-H); 1602 (s, C=N). MS-ESI$^+$: *m/z* 854 ([M]$^+$, 5 %).

a. Heterobimetallic binuclear *N,S*-chelated ferrocenylthiosemicarbazone palladium(II)-complexes (28, 29)

Synthesis of [Pd(ferrocenylthiosemicarbazone)(PTA)Cl] (**28**)

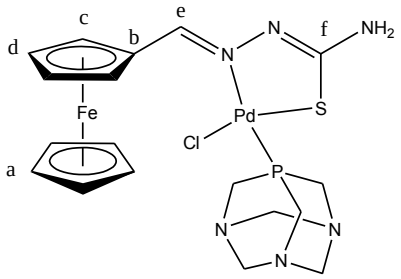

Compound **27** (0.108 g, 0.126 mmol) and PTA (0.0412 g, 0.262 mmol) was suspended in acetone (10.0 mL) and refluxed at 58 ˚C for 3 hrs. The red solid was purified by column chromatography (silica, ethyl acetate and eluted product with acetone), and purified using chloroform/hexane. The reddish-orange powder, **28** (0.0794 g, 52 %), was collected and dried *in vacuo*. Melting point: 241.3 ˚C (onset of decomposition without melting). ^{1}H NMR (399.95 MHz, DMSO-d_6): δ (ppm) = 7.87 (d, $^{4}J_{HP}$ = 3.66 Hz, 1H, H_e); 6.88 (br s, 2H, NH_2); 5.07 (t, $^{3}J_{HH}$ = 1.60 Hz, 2H, H_c); 4.54 (m, 5H, H_d & $NCH_{2(eq)}N$); 4.38 (d, $^{3}J_{HP}$ = 13.0 Hz, 3H, $NCH_{2(ax)}N$); 4.32 (s, 6H, PCH_2N); 4.17 (s, 5H, H_a). ^{13}C NMR (100.65 MHz, DMSO-d_6): δ (ppm) = 172.1 (d, $^{3}J_{CP}$ = 11.4 Hz, C-S); 151.6 (C=N); 73.8 (d, $^{4}J_{CP}$ = 4.71 Hz, C_b); 72.7 (C_c); 71.8 (d, $^{3}J_{CP}$ = 8.08 Hz, NCH_2N); 71.4 (C_d); 69.2 (C_a); 51.6 (d, $^{1}J_{CP}$ = 17.5 Hz, PCH_2N). ^{31}P NMR (162.00 MHz, DMSO-d_6): δ (ppm) = -33.5. Elemental analysis for $C_{18}H_{24}ClFeN_6PdPS$: Found C 36.6, H 4.26, N 14.0, S 5.46 %; Calculated C 36.9, H 4.13, N 14.3, S 5.48 %. FT-IR (KBr, cm^{-1}): ν = 3438 (w, N-H); 3164 (w, N-H); 1614 (w, C=N); 1598 (w, C=N). MS-EI^{+}: *m/z* 585 ($[M+H]^{+}$, 6.7 %).

Synthesis of [Pd(ferrocenylthiosemicarbazone)(PPh_3)Cl] (**29**)[6]

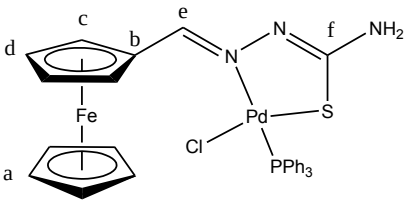

Compound **27** (0.0997 g, 0.116 mmol) and triphenylphoshine (0.0611 g, 0.233 mmol) was suspended in acetone (10.0 mL) and refluxed at 58 ˚C for 3 hrs. The solution was filtered by gravity, washed with acetone and the solvent reduced. Hexane was added to precipitate a red powder, **29** (0.121 g, 75 %), which was collected by suction filtration, washed with hexane and dried *in vacuo*. Melting point: 164.7 ˚C (onset of decomposition with melting). ^{1}H NMR

(399.95 MHz, DMSO-d_6): δ (ppm) = 8.14 (d, $^4J_{HP}$ = 4.00 Hz, 1H, H_e); 7.49-7.68 (m, 15H, PPh_3); 6.72 (br s, 2H, NH_2); 5.08 (t, $^3J_{HH}$ = 1.60 Hz, 2H, H_c); 4.53 (t, $^3J_{HH}$ = 1.60 Hz, 2H, H_d); 4.22 (s, 5H, H_a). ^{13}C NMR (100.65 MHz, DMSO-d_6): δ (ppm) = 171.6 (d, $^3J_{CP}$ = 11.5 Hz, C-S); 152.7 (C=N); 133.9 (d, J_{CP} = 10.8 Hz, C_{Ph}); 131.0 (C_{Ph}); 130.2 (C_{Ph}); 129.6 (C_{Ph}); 128.2 (d, J_{CP} = 10.8 Hz, C_{Ph}); 73.7 (d, $^4J_{CP}$ = 4.73 Hz, C_b); 72.7 (C_c); 71.4 (C_d); 69.2 (C_a). ^{31}P NMR (162.00 MHz, DMSO-d_6): δ (ppm) = 27.6. Elemental analysis for $C_{30}H_{27}ClFeN_3PdPS$: Found C 51.9, H 4.07, N 5.76, S 4.16 %; Calculated C 52.2, H 3.94, N 6.09, S 4.65 %. FT-IR (KBr, cm^{-1}): ν = 3457 (m, N-H); 3302 (m, N-H); 1607 (m, C=N); 1592 (w, C=N). MS-ESI$^+$: *m/z* 654 ([M-HCl]$^+$, 100 %).

b. Heterobimetallic tetra- and pentanuclear *N,S*-chelated ferrocenylthiosemicarbazone palladium(II)-complexes (30-32)

Synthesis of [Pd_2(ferrocenylthiosemicarbazone)$_2$(dppf)] (**30**)

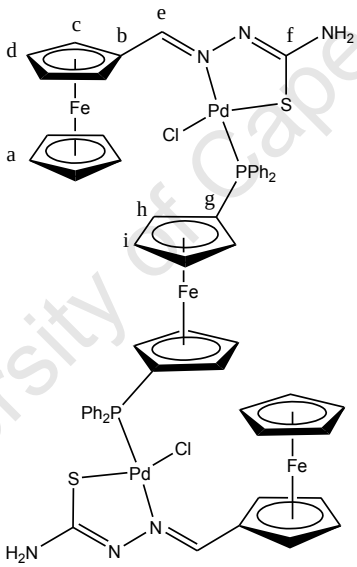

Compound **27** (0.0755 g, 0.0882 mmol) and dppf (0.0492 g, 0.0887 mmol) was suspended in acetone (10.0 mL) and refluxed at 58 ˚C for 3 hrs. The solution was filtered by gravity, the filtrate reduced and cold hexane added to yield a solid. The orange powder, **30** (0.0972 g, 78 %), was collected by suction filtration and dried *in vacuo*. Melting point: 200.0 ˚C (onset of decomposition without melting). ^{1}H NMR (399.95 MHz, DMSO-d_6): δ (ppm) = 8.19 (d, $^4J_{HP}$ = 4.03 Hz, 2H, H_e); 7.47-7.87 (m, 20H, PPh_3); 6.74 (br s, 4H, NH_2); 5.18 (br s, 4H, H_c); 5.07 (br s, 4H, H_h); 4.87 (br s, 4H, H_d); 4.51 (br s, 4H, H_i); 4.14 (s, 10H, H_a). ^{13}C NMR (100.65 MHz, DMSO-d_6): δ (ppm) = 171.5 (d, $^3J_{CP}$ = 12.1 Hz, C-S); 152.5 (C=N); 134.4 (C_{Ph}); 132.8 (d, J_{CP} = 10.8 Hz, C_{Ph}); 131.5 (C_{Ph}); 131.2 (C_{Ph}); 131.0 (C_g); 128.1 (d, J_{CP} = 10.8 Hz, C_{Ph}); 76.2 (d, J_{CP} = 9.42 Hz, C_h); 75.8 (d, J_{CP} = 7.41 Hz, C_i); 73.7 (d, $^4J_{CP}$ = 5.33 Hz, C_b); 72.8 (C_c);

71.4 (C_d); 69.2 (C_a). ^{31}P NMR (162.00 MHz, DMSO-d_6): δ (ppm) = 22.2. Elemental analysis for $C_{58}H_{52}Cl_2Fe_3N_6Pd_2P_2S_2$: Found C 49.8, H 4.03, N 5.29, S 4.38 %; Calculated C 49.4, H 3.72, N 5.96, S 4.55 %. FT-IR (KBr, cm^{-1}): ν = 3467 (m, N-H); 1602 (w, C=N); 1587 (w, C=N). MS-ESI$^+$: *m/z* 1412 ([M+H]$^+$, 3 %); 1375 ([M+2H-Cl]$^+$, 30 %); 669 ([M-2Cl]$^{2+}$, 70 %).

Synthesis of [Pd$_2$(ferrocenyldithiosemicarbazone)(PTA)$_2$Cl$_2$] (**31**)

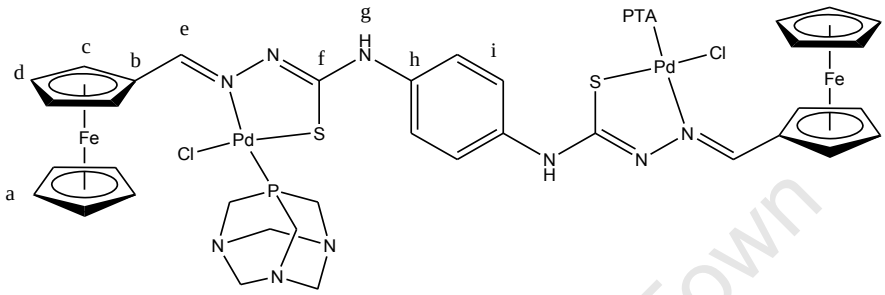

Compound **18** (0.0520 g, 0.0802 mmol) and $PdCl_2(PTA)_2$ (0.0787 g, 0.160 mmol) was suspended in ethanol:acetone (50 % V/V, 15.0 mL). The brown suspension was stirred at ambient temperature for 24 hrs, resulting in a red suspension. The reddish-orange powder, **31**, (0.0991 g, 99 %) was collected by suction filtration, and washed with water, ethanol and diethyl ether (25.0 mL). Melting point: 218.3 ˚C (Decomposition without melting). ^{1}H NMR (399.95 MHz, DMSO-d_6): δ (ppm) = 9.51 (s, 2H, H_g); 8.14 (d, $^4J_{HP}$ = 3.67 Hz, 2H, H_e); 7.59 (s, 4H, H_i); 5.01 (br s, 4H, H_c); 4.58 (d, $^3J_{HP}$ = 12.8 Hz, 6H, $NCH_{2(eq)}N$); 4.52 (br s, 4H, H_d); 4.41 (d, $^3J_{HP}$ = 13.4 Hz, 6H, $NCH_{2(ax)}N$); 4.38 (s, 12H, PCH_2P); 4.19 (s, 10H, H_a). ^{13}C NMR (100.65 MHz, DMSO-d_6): δ (ppm) = 167.8 (C-S); 154.8 (C=N); 136.1 (C_h); 119.9 (C_i); 73.1 (d, $^4J_{HP}$ = 4.04 Hz, C_b); 72.2 (d, $^3J_{HP}$ = 12.8 Hz, NCH_2N); 71.7 (C_c); 71.6 (C_d); 69.4 (C_a); 51.5 (d, $^1J_{CP}$ = 18.2 Hz, PCH_2N). ^{31}P NMR (162.00 MHz, DMSO-d_6): δ (ppm) = -32.0. Elemental analysis for $C_{42}H_{50}Cl_2Fe_2N_{12}Pd_2P_2S_2{\cdot}H_2O$: Found C 38.9, H 4.27, N 12.9, S 4.60 %; Calculated C 39.9, H 3.99, N 13.3, S 5.08 %. FT-IR (KBr, cm^{-1}): ν = 3401 (m, N-H); 1593 (w, C=N); 1576 (w**,** C=N). MS-ESI$^+$: *m/z* 1244 ([M]$^+$, 10 %); 622 ([M+2H-2Cl$_2$]$^+$, 35 %).

Synthesis of [Pd_2(ferrocenyldithiosemicarbazone)(PPh_3)$_2Cl_2$] (**32**)

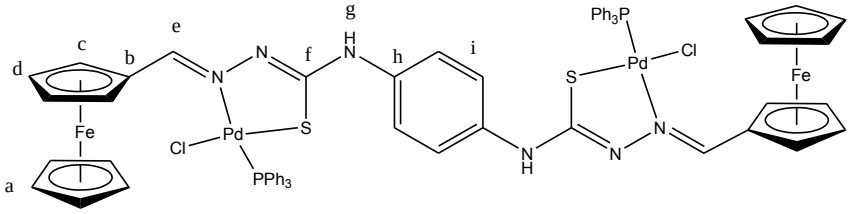

Compound **18** (0.0603 g, 0.0930 mmol) and $PdCl_2(PPh_3)_2$ (0.131 g, 0.186 mmol) was suspended in ethanol:acetone (50 % V/V, 15.0 mL). The brown suspension was stirred at ambient temperature for 24 hrs, resulting in a red suspension. The solid was purified using $CHCl_3$/THF/Hexane. The reddish-orange powder, **32**, (0.0941 g, 70 %) was collected by suction filtration, washed with diethyl ether (25.0 mL), and dried *in vacuo*. Melting point: 237.2 ˚C (onset of decomposition without melting). ^{1}H NMR (399.95 MHz, DMSO-d_6): δ (ppm) = 9.24 (s, 2H, H_g); 8.39 (d, $^4J_{HP}$ = 4.00 Hz, 2H, H_e); 7.47 (m, 34H, PPh_3 & H_i); 4.99 (br s, 4H, H_c); 4.52 (br s, 4H, H_d); 4.22 (s, 10H, H_a). ^{13}C NMR (100.65 MHz, DMSO-d_6): δ (ppm) = 167.2 (C-S); 156.0 (C=N); 136.0 (C_h); 134.0 (d, J_{CP} = 11.4 Hz, C_{Ph}); 131.2 (C_{Ph}); 130.2 (C_{Ph}); 129.6 (C_{Ph}); 128.4 (d, J_{CP} = 10.8 Hz, C_{Ph}); 119.8 (C_i); 72.3 (C_b); 72.1 (C_d); 69.4 (C_a); 66.9 (C_c). ^{31}P NMR (162.00 MHz, DMSO-d_6): δ (ppm) = 27.8. FT-IR (KBr, cm^{-1}): ν = 3440 (m, N-H); 1598 (m, C=N); 1572 (w**,** C=N). MS-ESI$^+$: *m/z* 1457 ($[M+H]^+$, 3 %); 692 ($[M-2Cl]^{2+}$, 100 %).

6.4. Single-crystal X-ray diffraction

Single-crystal X-ray diffraction data were collected on a Bruker KAPPA APEX II DUO diffractometer using graphite-monochromated Mo-Kα radiation (χ = 0.71073 Å). Data collection was carried out at 173(2) K. Temperature was controlled by an Oxford Cryostream cooling system (Oxford Cryostat). Cell refinement and data reduction were performed using the program SAINT.[11] The data were scaled and absorption correction performed using SADABS.[12] The structure was solved by direct methods using SHELXS-97[12] and refined by full-matrix least-squares methods based on F^2 using SHELXL-97[12] and using the graphics interface program X-Seed.[13-14] The programs X-Seed and POV-Ray[15] were both used to prepare molecular graphic images. All non-hydrogen atoms were refined anisotropically. All hydrogen atoms were placed at calculated positions with C-H distances ranging from 0.95 Å to 0.99 Å and N-H distance 0.88 Å and refined as riding on their parent atoms with U_{iso} (H) = 1.2 or 1.5 U_{eq} (C or N).

6.5. Cyclic voltammetry

Cyclic voltammograms were recorded at room temperature on a BAS 100W Electrochemical Analyzer with a one-compartment three-electrode cell system consisting of a platinum disk working electrode, a platinum wire auxiliary electrode and a $Ag/AgNO_3$ reference electrode (0.01 M $AgNO_3$ and 0.1 M [n-Bu_4N][ClO_4] in anhydrous acetonitrile). An IR compensation circuit was used for all measurements. A scan rate of 100 mV s^{-1} was used throughout, beginning from the most negative potential and initially scanning in the anodic direction. The half-wave potential of the ferrocene/ferrocenium couple in this cell never varied by more than 30 mV from a mean value of $E_{1/2}$ = 250 mV versus the $Ag/AgNO_3$ reference electrode, with a peak separation falling between ΔE_p = 59 and ΔE_p = 66 mV. Solutions were purged with argon and voltammograms were recorded under a blanket of argon. The platinum disk working electrode was polished between runs. The voltammograms of samples were recorded in dichloromethane solutions (1.5 μM).

6.6. Antiplasmodial testing

The test samples were tested in triplicate on one occasion against chloroquine sensitive (CQS) NF54 and chloroquine resistant (CQR) Dd2 strain of *Plasmodium falciparum*. Continuous *in vitro* cultures of asexual erythrocyte stages of *P. falciparum* were maintained using a modified method of Trager and Jensen.[16] Quantitative assessment of antiplasmodial activity *in vitro* was determined via the parasite lactate dehydrogenase assay using a modified method described by Makler *et al*.[17] The test samples were prepared to a 20 mg/ml stock solution in 100% DMSO and sonicated to enhance solubility. Samples were tested as a suspension if not completely dissolved. Stock solutions were stored at -20ºC. Further dilutions were prepared on the day of the experiment. Chloroquine diphosphate (CQDP) was used as the reference drug in the experiment. A full dose-response was performed for all compounds to determine the concentration inhibiting 50% of parasite growth (IC_{50} value). The samples were tested at a starting concentration of 100 000 ng/ml, which was then serially diluted 2-fold in complete medium to give 10 concentrations; with the lowest concentration being 2 ng/ml. The same dilution technique was used for all samples. The highest concentration of solvent to which the parasites were exposed to had no measurable effect on the parasite viability (data not shown). The IC_{50} values were obtained using a non-linear dose-response curve fitting analysis via Graph Pad Prism v.4.0 software.

6.7. References

1. M. G. Abdullaev, *Pharm. Chem. J*., 2001, **35**, 45.
2. A. M. M. Meij, S. Otto and A. Roodt, *Inorg. Chim. Acta.*, 2005, **358**, 1005.
3. X. Du, C. Guo, E. Hansell, P. S. Doyle, C. R. Caffrey, T. P. Holler, J. H. McKerrow and F. E. Cohen, *J. Med. Chem.*, 2002**, 45**, 2695.
4. C. A. Ghilardi, S. Midollini, S. Moneti, A. Orlandini and G. Scapacci, *J. Chem. Soc*., *Dalton Trans*., 1992, **1**, 3371.
5. P. Chellan, S. Nasser, L. Vivas, K. Chibale and G. S. Smith, *J. Organomet. Chem.*, 2010, **695**, 2225.
6. M. Mariño, E. Gayoso, J. M. Antelo, L. A. Adrio, J. J. Fernández and J. M. Vila, *Polyhedron*, 2006, **25**, 1449.
7. M. Christlieb, H. S. R. Struthers, P. D. Bonnitcha, A. R. Crowley and J. R. Dilworth, *Dalton Trans.*, 2007, 5043.
8. M. A. Bennett and A.K. Smith, *J. Chem. Soc. Dalton Trans.*, 1974, **2**, 233.
9. J. Soleimannejad and C. White, *Organometallics*, 2005, **24**, 2538.
10. R. A. Zelonka and M. C. Baird, *Can. J. Chem.*, 1972, **50**, 3063.
11. SAINT Version 7.60a, Bruker AXS Inc., Madison, WI, USA, 2006.
12. G. M. Sheldrick, SHELXS-97, SHELXL-97 and SADABS version 2.05, University of Göttingen, Germany, 1997.
13. L. J. Barbour, *J. Supramol. Chem.*, 2001, **1**, 189.
14. J. L. Atwood and L. J. Barbour, *Cryst. Growth Des*., 2003, **3**, 3.
15. http://www.povray.org.
16. W. Trager, J. B. Jensen, *Science*, 1976, **193**, 673.
17. M. T. Makler, J. M. Ries, J. A. Williams, J. E. Bancroft, R. C. Piper, B. L. Gibbins, D. J. Hinrichs, *Am. Soc. Trop. Med. Hyg*., 1993, **48**, 739.

Appendix

^{1}H NMR spectrum of compound **1** in DMSO-d_6

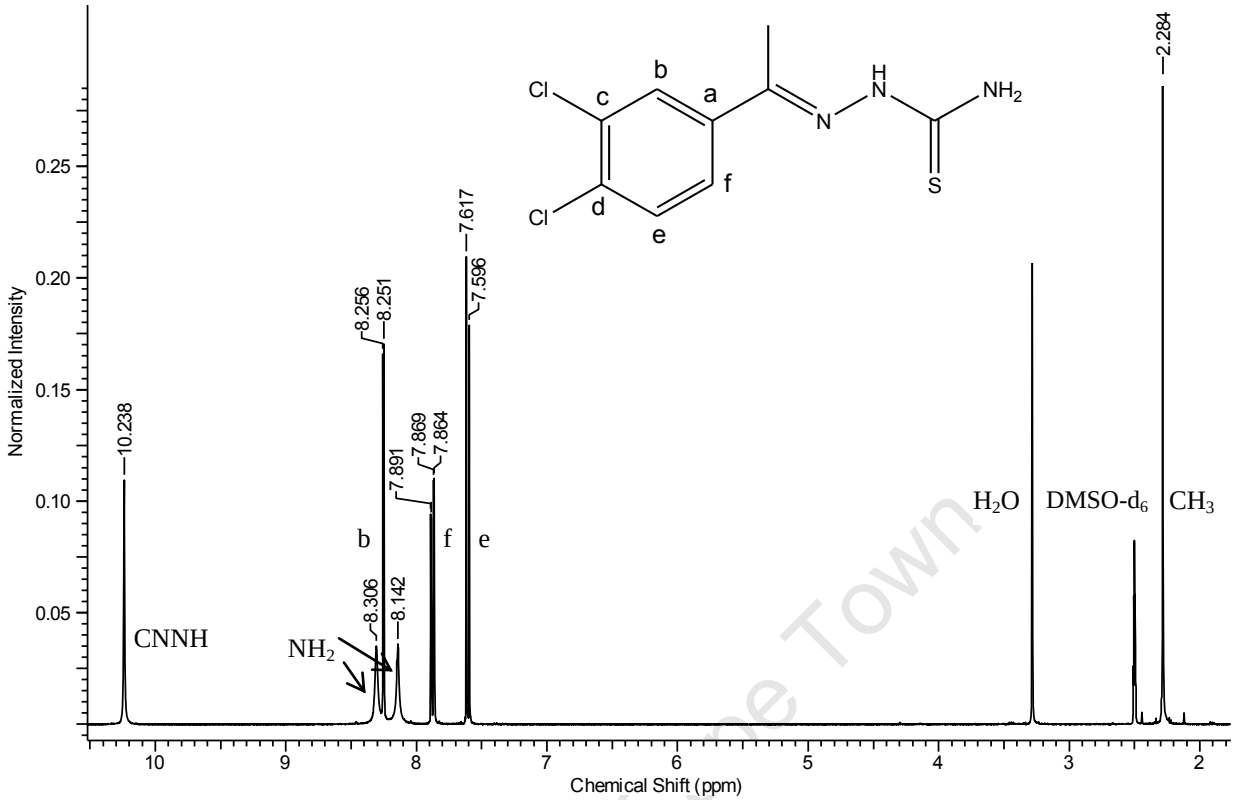

^{1}H NMR spectrum of compound **5** in $CDCl_3$

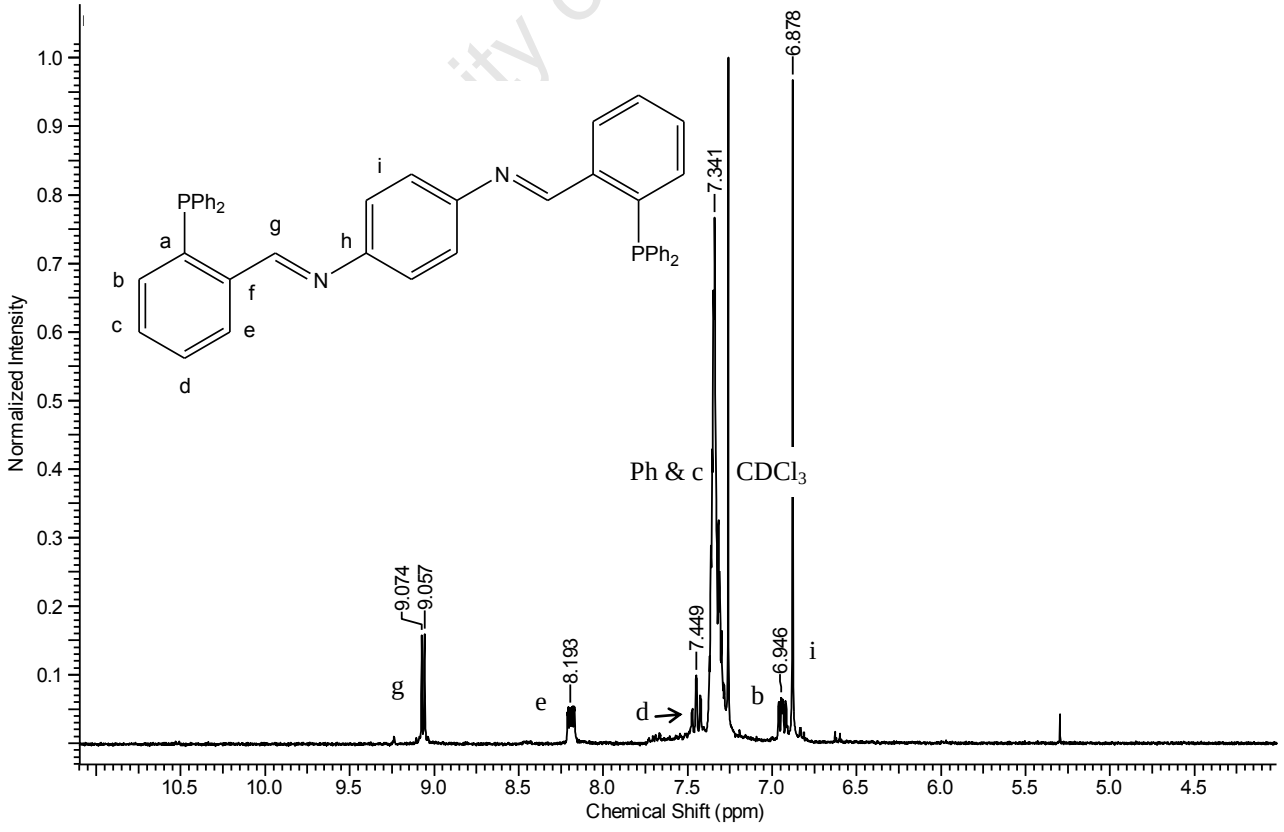

^{1}H NMR spectrum of compound **6** in DMSO-d_6

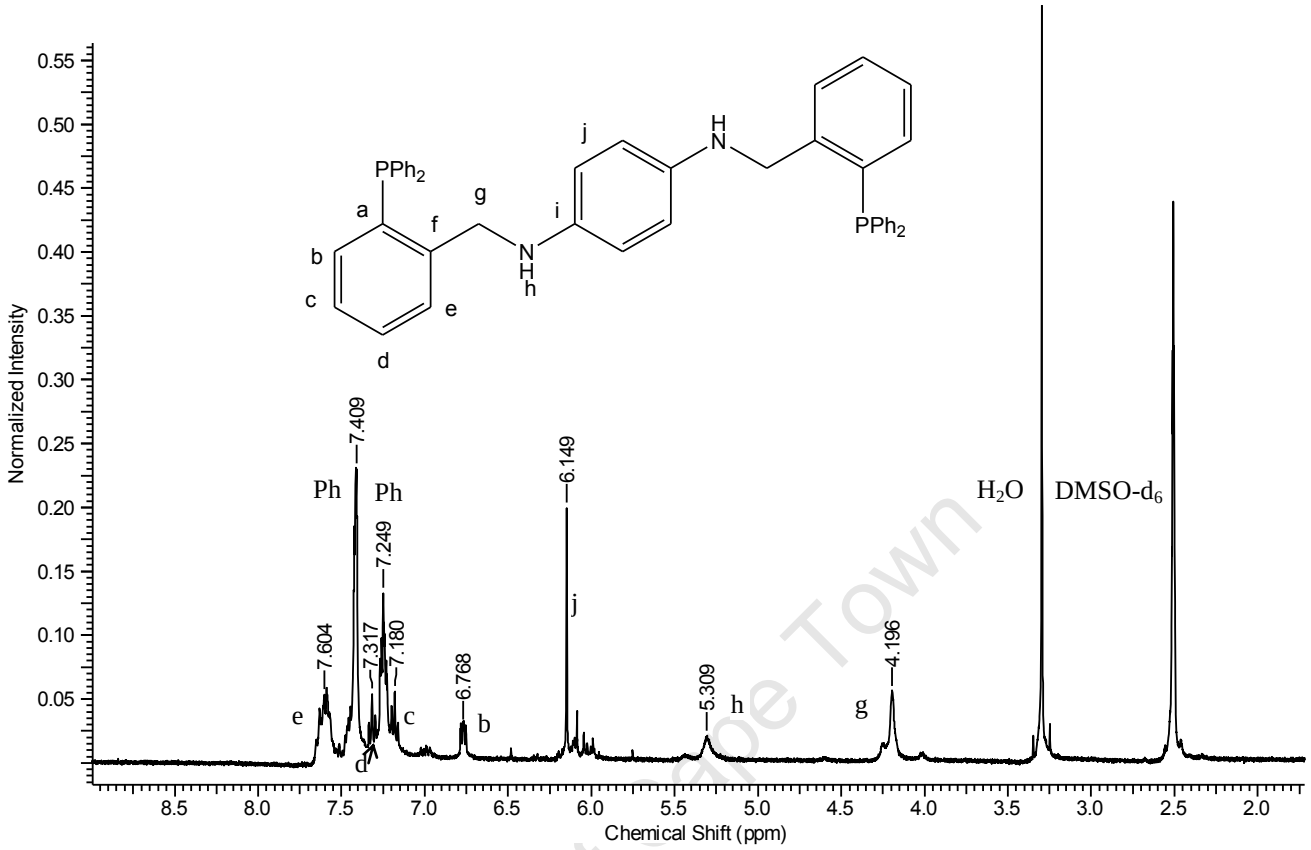

^{1}H NMR spectrum of compound **7** in DMSO-d_6

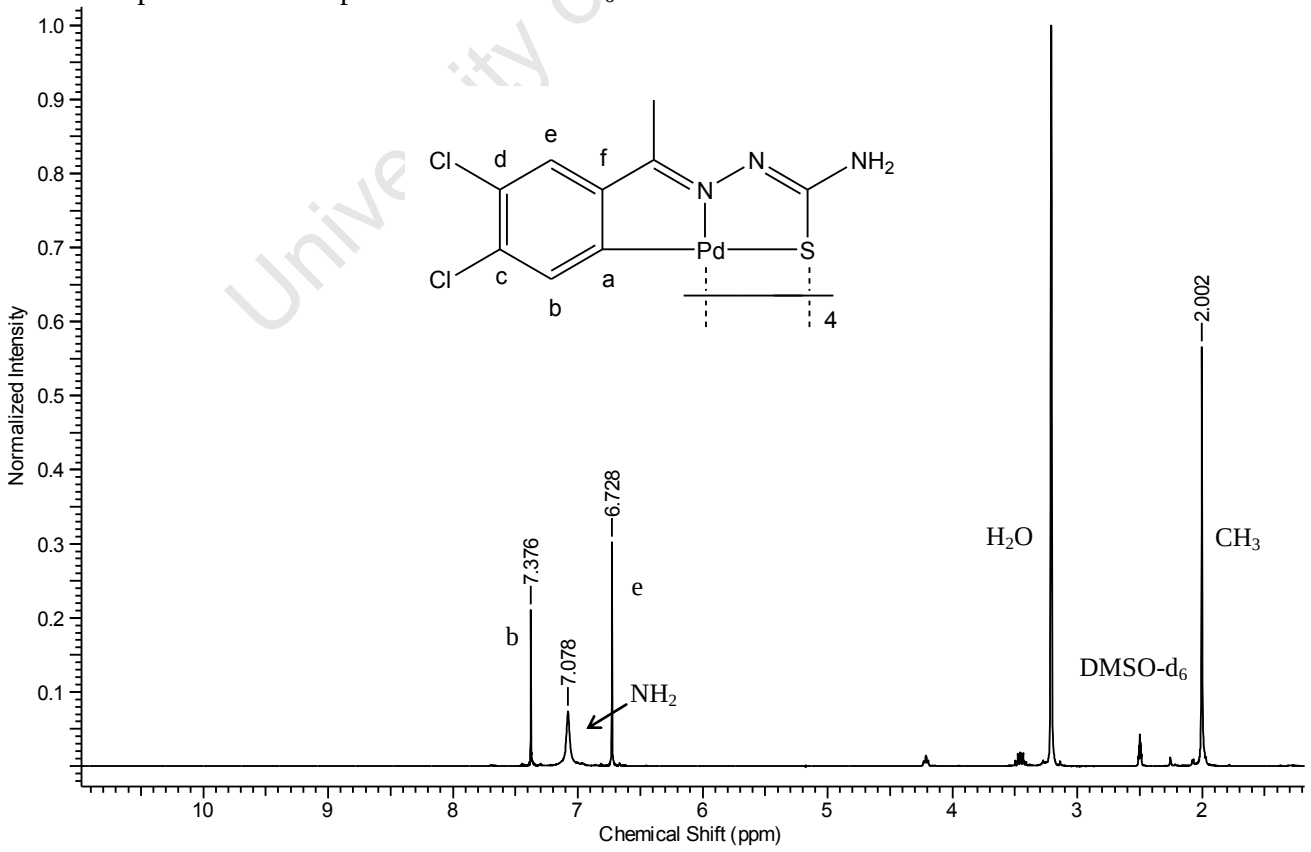

^{1}H NMR spectrum of compound **9** in DMSO-d_6

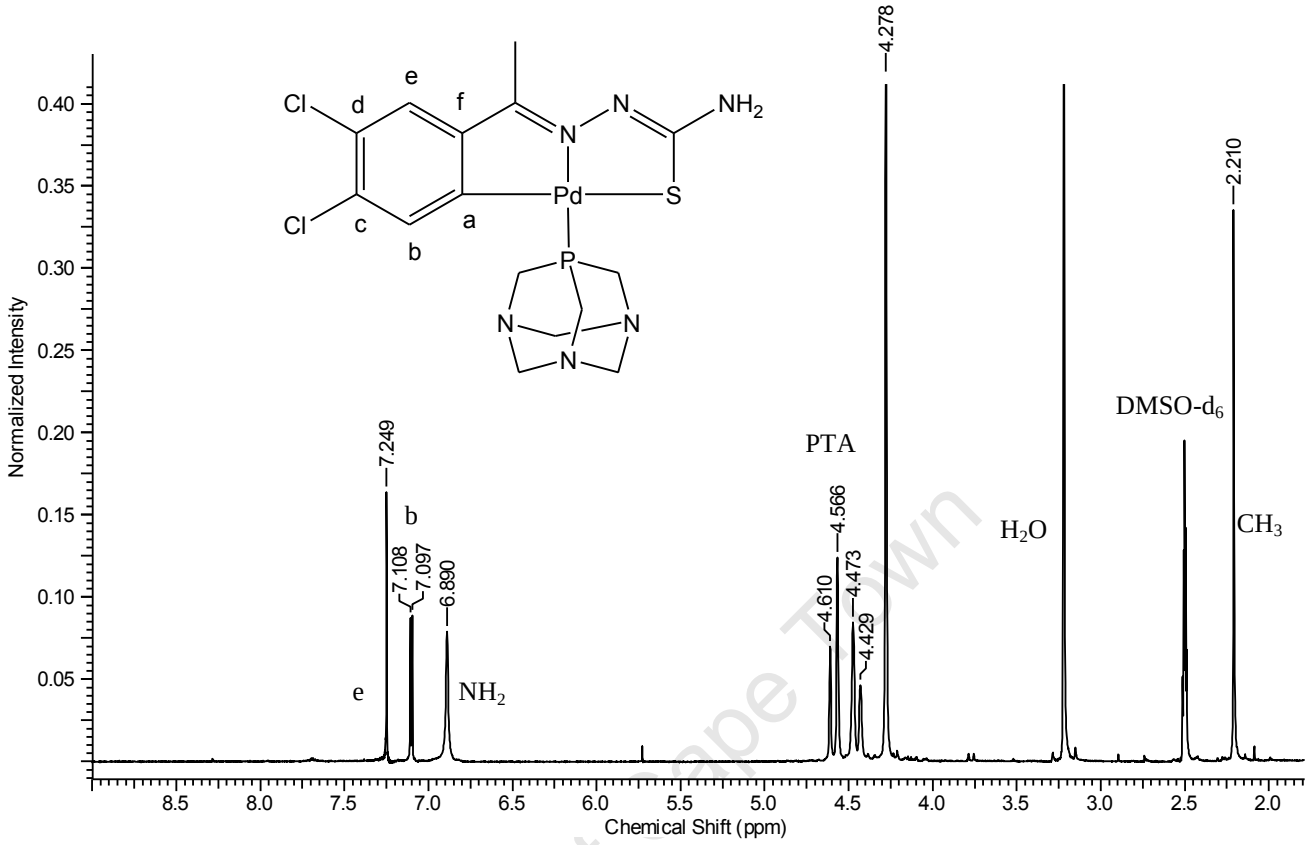

^{1}H NMR spectrum of compound **16** in DMSO-d_6

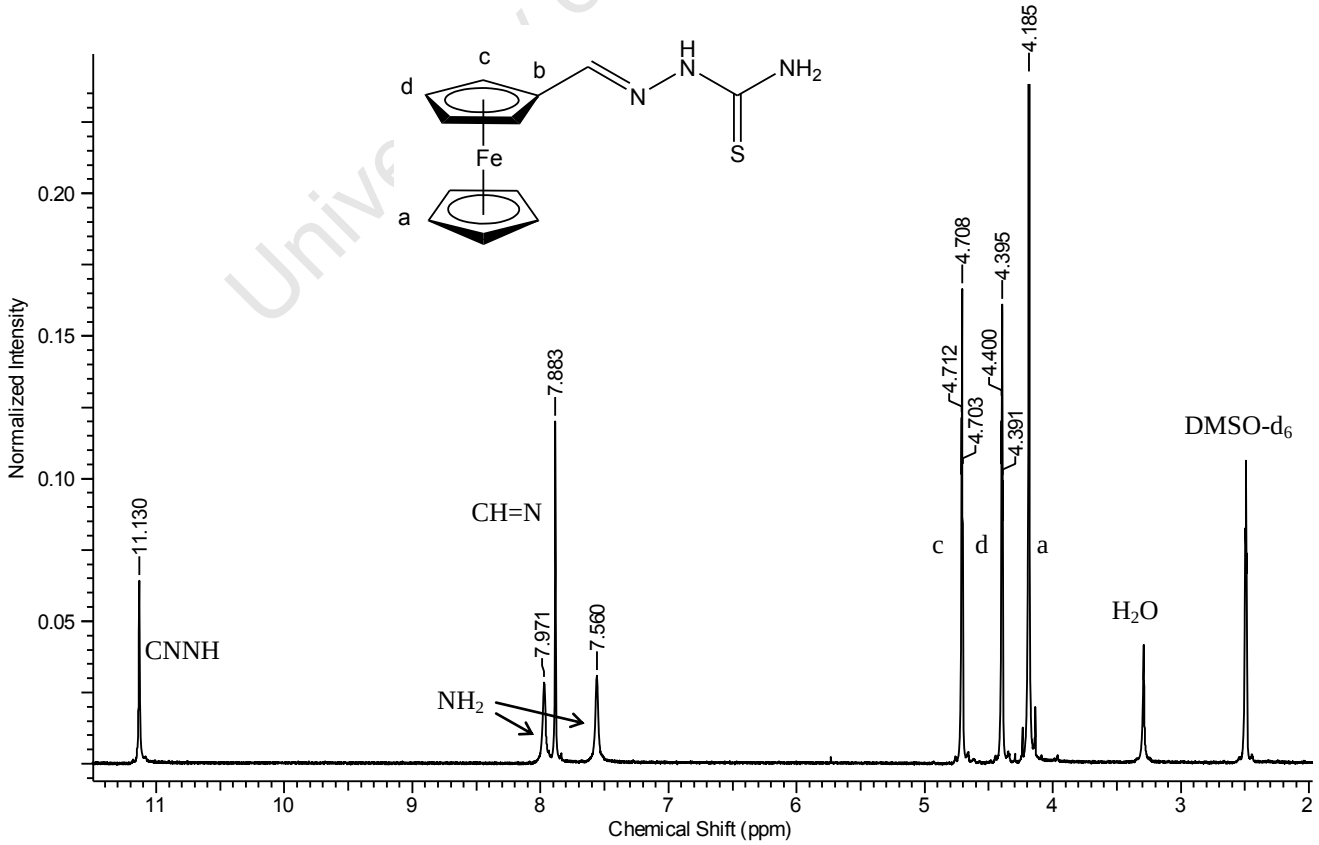

^{1}H NMR spectrum of compound **22** in Acetone-d_6

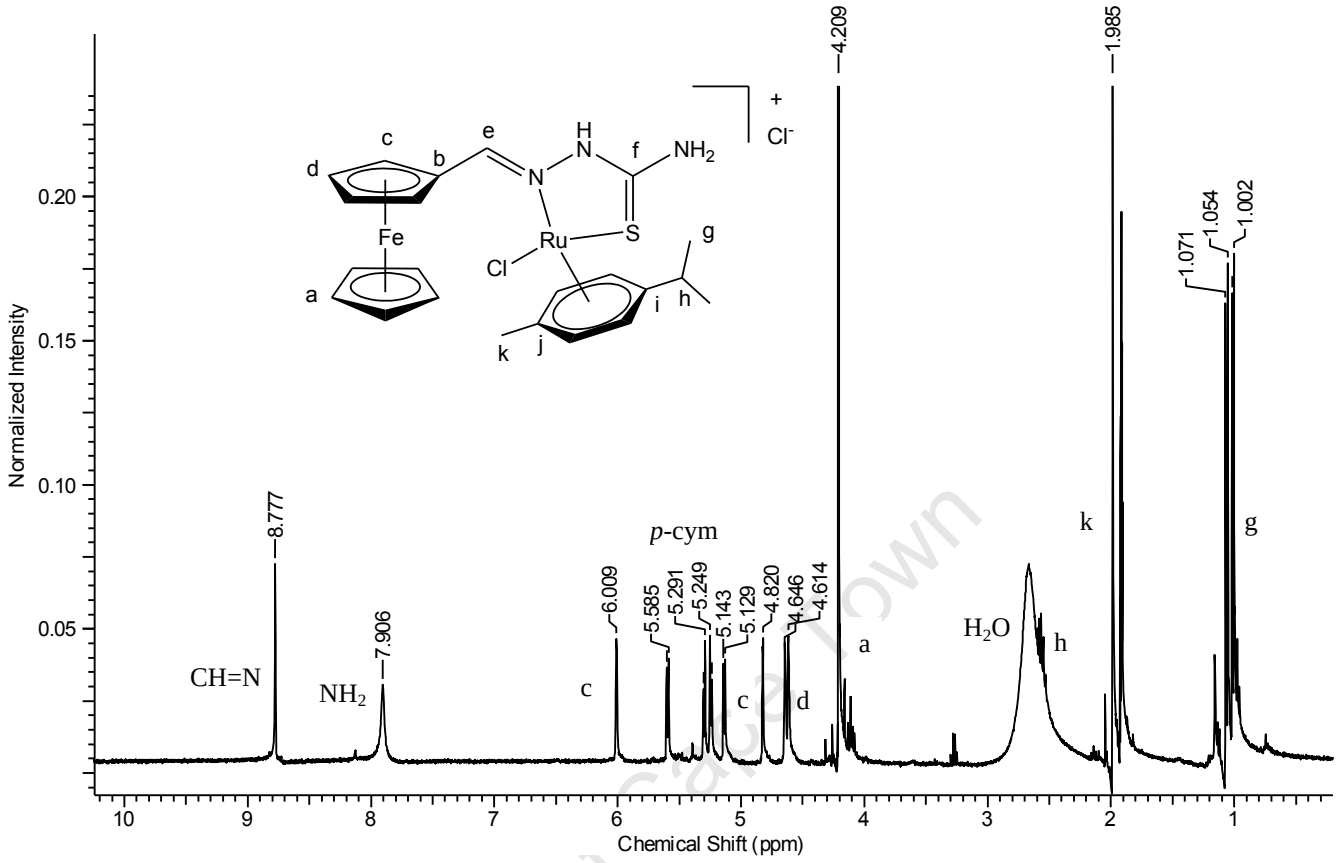

ESI^{+}-mass spectrum of compound **22**

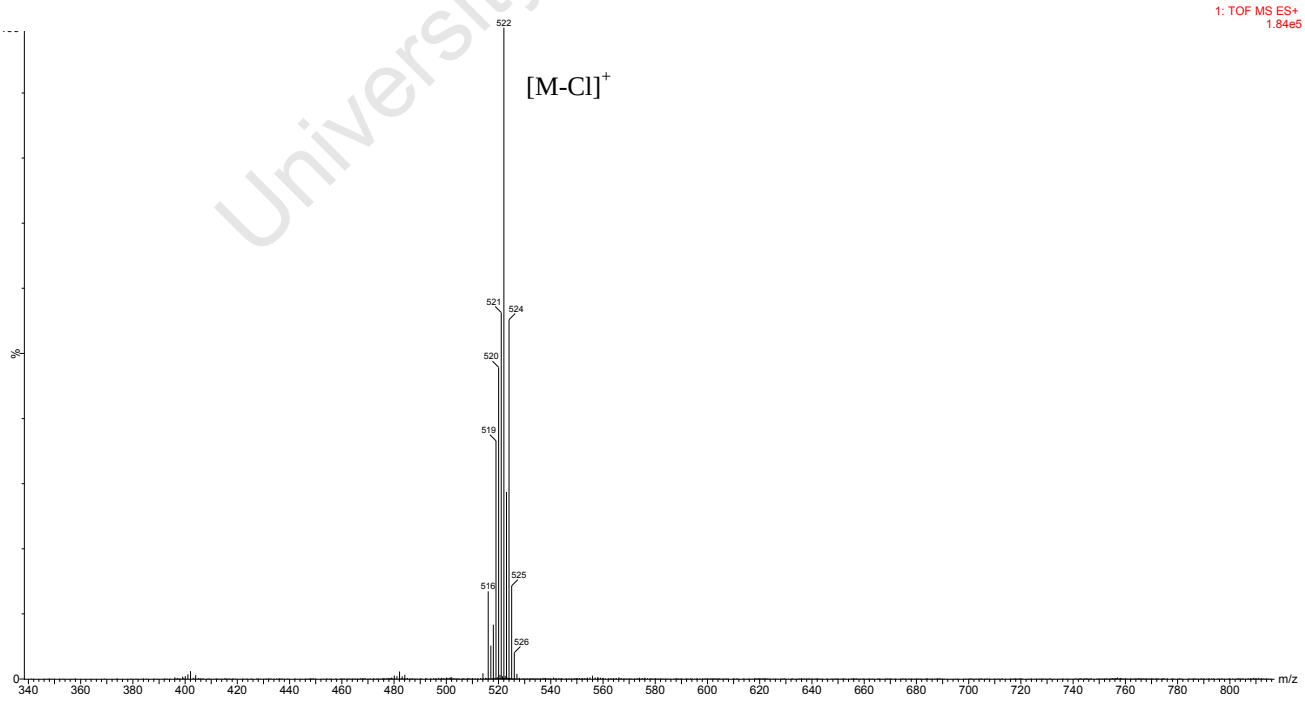

ESI$^+$-mass spectrum of compound **27**

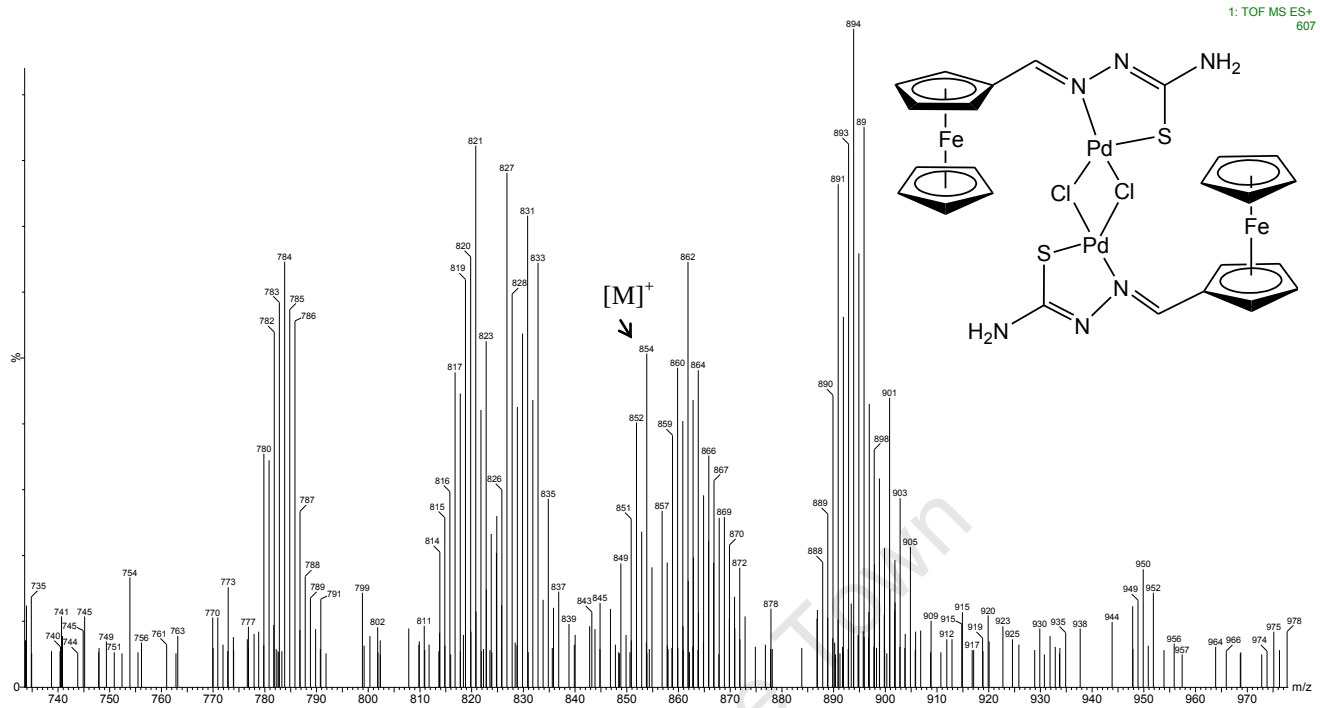

^{1}H NMR spectrum of compound **28** in DMSO-d$_6$

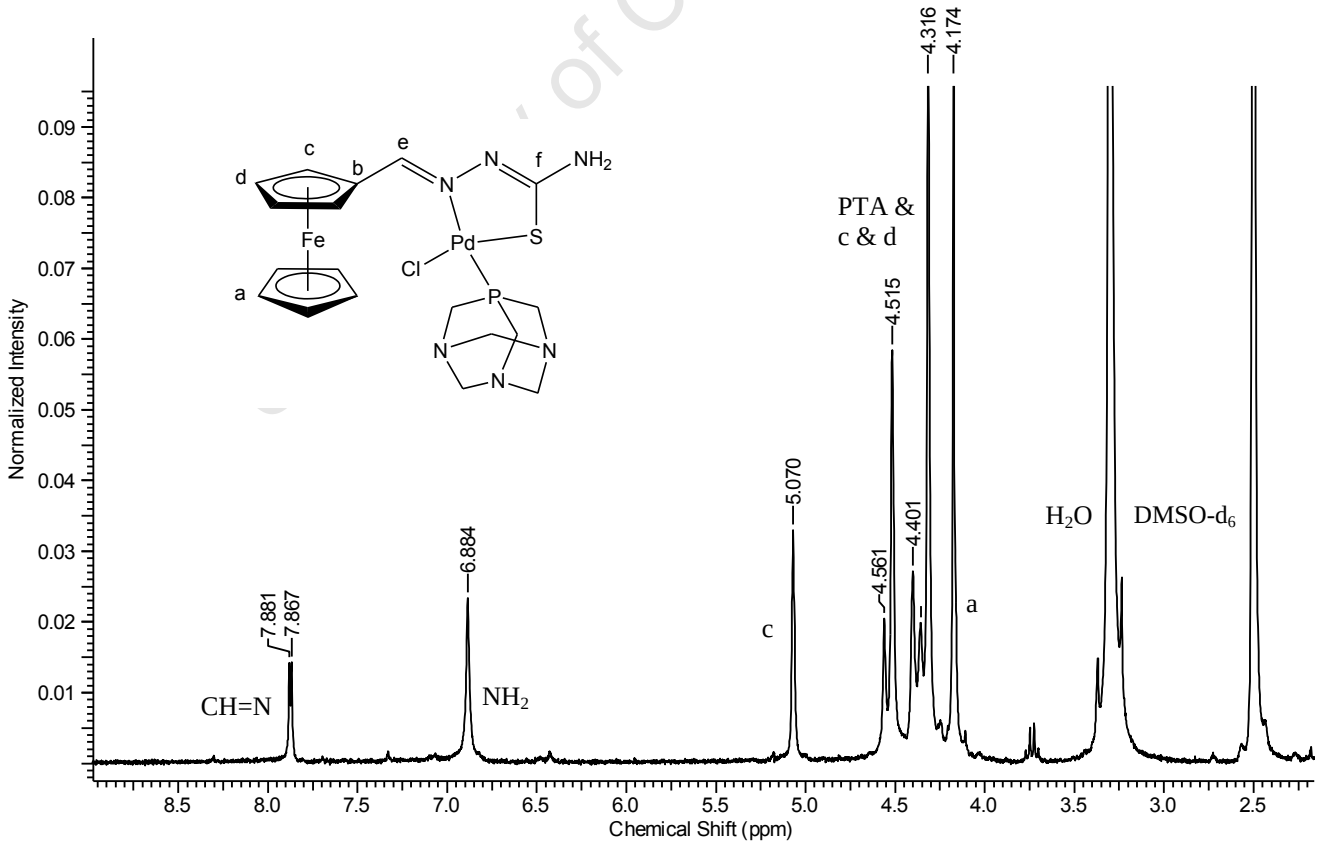

ESI$^+$-mass spectrum of compound **30**